DEPARTMENT OF PHYSICS
UNIVERSITY OF JYVÄSKYLÄ
RESEARCH REPORT No. 2/2011

DNA-BASED APPLICATIONS IN MOLECULAR ELECTRONICS

BY
VEIKKO LINKO

Academic Dissertation
for the Degree of
Doctor of Philosophy

To be presented, by permission of the
Faculty of Mathematics and Science
of the University of Jyväskylä,
for public examination in Auditorium FYS-1 of the
University of Jyväskylä on April 29, 2011
at 12 o'clock

Jyväskylä, Finland
April 2011

Preface

The work reviewed in this thesis has been carried out during the years 2006-2010 at the Nanoscience Center, Department of Physics, at the University of Jyväskylä.

First of all, I would like to thank my supervisor Doc. Jussi Toppari for his excellent guidance and scientific visions, as well as for his trust in me and encouragement throughout my Ph.D. studies. In addition, I thank Doc. Vesa Hytönen for his valuable biology-oriented comments and ideas, and Prof. Päivi Törmä for giving me an opportunity to start working in her brilliant group and therefore in the interesting field of nanoelectronics already in 2006.

It has been pleasant and extremely fruitful to work with Dr. Tommi Hakala, Dr. Anton Kuzyk, Mrs. Jenni Leppiniemi, Mr. Seppo-Tapio Paasonen, Mr. Boxuan Shen, Mr. Antti-Pekka Eskelinen, Mr. Kimmo Laitinen and Dr. Einari Niskanen, without their significant contribution I could not have reached this goal. Special mention is devoted to the staff of Nanoscience Center and especially to the following persons for collegial support, friendship and numerous fascinating discussions: Mr. Olli Herranen, Mr. Tero Isotalo, Dr. Andreas Johansson, Mr. Antti Juutilainen, Mr. Ville Kotimäki, Ms. Anna-Leena Latvala, Mr. Johan Lindgren, Mr. Lauri Nykänen, Mr. Mika Oksanen, Mr. Mikko Palosaari, Dr. Marcus Rinkiö and Dr. Sampo Tuukkanen.

Finally, I wish to thank my parents Eeva & Pentti, my brother Jaakko, my love Noora, and my dear friends for their support and empathy. You all are irreplaceable in my life.

Financial support from the Academy of Finland, National Doctoral Programme in Nanoscience (NGS-NANO), Finnish Academy of Science and Letters (Väisälä Foundation) and Finnish Cultural Foundation (Central Finland Regional Fund) are gratefully acknowledged.

Jyväskylä, April 2011

Veikko Linko

Abstract

Linko, Veikko
DNA-based applications in molecular electronics
Jyväskylä: University of Jyväskylä, 2011, 120 p.
(Research report/Department of Physics, University of Jyväskylä,
ISSN 0075-465X; 2/2011)
ISBN 978-951-39-425-5
diss.

This thesis is mainly focused on DNA molecules and especially on self-assembled DNA constructs and their potential applications in nanotechnology and molecular electronics. In the field of molecular electronics the conductivity of DNA is a crucial - yet open - question, and it is of great concern, since DNA is a very promising molecule in a context of bottom-up based nanodevices due to its superior self-assembly characteristics.

A key tool in all the experiments presented in this thesis is a dielectrophoretic trapping technique, which was exploited in spatial manipulation of individual DNA molecules, DNA constructs and also semiconducting quantum dots. In the case of DNA, the technique provides immobilization and connection of DNA molecules and constructs to nanoscale electrodes enabling characterization of the electrical properties at the single construct level, and on the other hand, bridging of the electrodes by growing DNA molecules locally from trapped oligonucleotides.

By exploiting dielectrophoresis phenomenon, two structurally distinct DNA constructs, DNA origamis and defined-sized TX tile complexes, were directed between lithographically fabricated nanoelectrodes. These structures could potentially serve as molecular scale circuit boards in nanoelectronics since they make controlled organization of wide range of materials possible. Thus, the electrical properties of a single rectangular origami and a TX tile construct were investigated by utilizing alternating current impedance spectroscopy with a full equivalent circuit modeling. The electrical measurements were carried out in high humidity conditions revealing that various environmental factors and in particular adsorbed water molecules surrounding the DNA had a significant influence to the observed conductance.

In addition, a high throughput field-induced lithography method for nanoobjects was introduced, and its feasibility was demonstrated using quantum dots in a proof-of-principle experiment. The method allows dynamic control over the

manipulation of any kinds of polarizable objects by dielectrophoresis and thus also over the formed pattern: one universal and reusable master stamp can be exploited in order to produce a desired multicomponent pattern on the specific target plate by recurrently trapping of certain components on the master followed by efficient mechanical transfer of the created pattern(s) to the target plate. The robust technique could be utilized in mass production and it is readily extendable to other nanoscale objects as well.

Moreover, a method to grow single double-stranded DNA molecules at certain locations on a chip is proposed and demonstrated. The technique is based on immobilization of single-stranded DNA molecules to the ends of a desired set of nanoelectrodes by dielectrophoresis, and further elongation of them by polymerase chain reaction. Finally, the extended single-strand molecules can form a complete double-stranded DNA by binding together via hybridization. By means of this method one can grow single DNA molecules at specific spatial positions on a substrate or bridge the neighboring electrodes by DNA, and therefore, it may be utilized in detecting and sensing applications as well as in molecular electronics.

Keywords DNA, DNA self-assembly, DNA origami, TX tile construct, quantum dot, dielectrophoresis, nanoelectrodes, atomic force microscopy, impedance spectroscopy, immobilization, conductivity, pattern transfer, polymerase chain reaction

Author's address Veikko Linko
Nanoscience Center
Department of Physics
University of Jyväskylä
Jyväskylä
Finland

Supervisor Docent Jussi Toppari
Academy Research Fellow
Nanoscience Center
Department of Physics
University of Jyväskylä
Jyväskylä
Finland

Reviewers Doctor Wolfgang Fritzsche
Head of the Department
Nanobiophotonics Department
Institute of Photonic Technology (IPHT)
Jena
Germany

Docent Emppu Salonen
Academy Research Fellow
Department of Applied Physics
Aalto University School of Science and Technology
Espoo
Finland

Opponent Professor Hendrik Dietz
Laboratory for Biomolecular Nanotechnology
Physics Department
Technical University of Munich
Munich
Germany

List of Abbreviations

3′ end of ssDNA	phosphate end -group linked to 3rd carbon in the sugar
5′ end of ssDNA	hydroxyl end -group linked to 5th carbon in the sugar
AC	alternating current
AC-IS	alternating current impedance spectroscopy
A-DNA	double helical DNA in A-form
AFM	atomic force microscopy
B-DNA	double helical DNA in B-form (the most stable form)
bp	base pair(s)
CNLS	complex nonlinear least squares
CNT	carbon nanotube
CPE	constant phase element
CT	charge transfer
CVD	chemical vapor deposition
Cy3	fluorescent cyanine dye, emission maximum $\sim$ 570 nm
Cy5	fluorescent cyanine dye, emission maximum $\sim$ 650-670 nm
DAC	digital-to-analog converter
DAQ	data aquisition
DC	direct current
DEP	dielectrophoresis
DI	de-ionized
DNA	deoxyribonucleic acid
DX tile	DNA double-crossover tile
dsDNA	double-stranded DNA
EBL	electron beam lithography
EDTA	ethylenediaminetetraacetic acid
EEC	equivalent electric circuit
EIS	electrochemical impedance spectroscopy
EMS	electromagnetically shielded
FEM	finite element method
FINAL	field-induced nanolithography
GPIB	general-purpose interface bus

G-wire	quadruple helical DNA structure containing guanine tetrad motifs
HAc	acetic acid
H-DNA	triplex DNA, third strand attached to dsDNA via Hoogsteen bond
Hepes	4-(2-hydroxyethyl)-1-piperazineethanesulfonic acid
IPA	isopropanol / 2-propanol
I-V	current-voltage
LPCVD	low-pressure chemical vapor deposition
μCP	microcontact printing
MgAc	magnesium acetate
MIBK	methyl isobutyl ketone
NIL	nanoimprint lithography
nt	nucleotide(s)
oligo	DNA oligonucleotide, i.e., short ssDNA molecule
PBS	phosphate buffered saline
PCR	polymerase chain reaction
PDACMAC	poly(diallyldimethylammonium chloride)
PDMS	polydimethyl siloxane
PEG	polyethylene glycol
PMMA	polymethylmethacrylate
pp	peak-to-peak
QD	quantum dot
RF	radio frequency
RH	relative humidity
RIE	reactive-ion etcher
rms	root mean square
sccm	standard cubic centimeters per minute
SEM	scanning electron microscope
SPP	surface plasmon polariton
ssDNA	single-stranded DNA
TAE	Tris-acetate-EDTA
Taq	DNA polymerase from the bacterium *Thermus aquaticus*
TEG	triethylene glycol
TEM	transmission electron microscope
Tris	2-amino-2-hydroxymethyl-propane-1,3-diol
Tween 20	polyoxyethylene (20) sorbitan monolaurate
TX tile	DNA triple-crossover tile
UHV	ultra-high vacuum
Z-DNA	double helical DNA in left-handed Z-form

List of Publications

The main results of this thesis have been reported in the following articles:

A.I A. KUZYK, B. YURKE, J. J. TOPPARI, V. LINKO AND P. TÖRMÄ, *Dielectrophoretic Trapping of DNA Origami*. Small **4** (2008) 447–450.

A.II V. LINKO, S.-T. PAASONEN, A. KUZYK, P. TÖRMÄ AND J. J. TOPPARI, *Characterization of the Conductance Mechanisms of DNA Origami by AC Impedance Spectroscopy*. Small **5** (2009) 2382–2386.

A.III V. LINKO, J. LEPPINIEMI, S.-T. PAASONEN, V. P. HYTÖNEN AND J. J. TOPPARI, *Defined-sized DNA triple crossover construct for molecular electronics: modification, positioning and conductance properties*. Manuscript, submitted for publication.

A.IV T. K. HAKALA, V. LINKO, A.-P. ESKELINEN, J. J. TOPPARI, A. KUZYK AND P. TÖRMÄ, *Field-Induced Nanolithography for High-Throughput Pattern Transfer*. Small **5** (2009) 2683–2686.

A.V V. LINKO, J. LEPPINIEMI, B. SHEN, E. NISKANEN, V. P. HYTÖNEN AND J. J. TOPPARI, *Programmable Immobilized PCR in Nanoscale: Bridging Nanoelectrodes with Single dsDNA Molecules*. Manuscript, submitted for publication. arXiv:1102.4594v1.

Author's contribution

In A.I the author participated in the sample fabrication, trapping experiments and data analysis.
In A.II the author fabricated the majority of the samples, carried out all the reported trapping experiments and electrical measurements, and participated both in data analysis and writing the publication.
In A.III the author participated in the designing of the DNA structure, sample fabrication, trapping experiments, AFM imaging, electrical measurements and data analysis, and was the main writer of the manuscript.

In A.IV the author participated in the optimization of the method and also in the experiments and data analysis.
In A.V the author carried out all the reported experiments, except the fabrication of the electrode structures, and was the main writer of the manuscript.

Other work to which the author has contributed:

L. J. ANTILA, M. J. HEIKKILÄ, V. MÄKINEN, N. HUMALAMÄKI, M. LAITINEN, V. LINKO, P. JALKANEN, J. J. TOPPARI, V. AUMANEN, M. KEMELL, P. MYLLYPERKIÖ, K. HONKALA, H. HÄKKINEN, M. LESKELÄ AND J. E. I. KORPPI-TOMMOLA, *Atomistic Description of the Effect of Atomic Layer Deposited Aluminum Oxide Barriers on Interfacial Electron Transfer and Performance of Dye-Sensitized Solar Cells.* Manuscript, submitted for publication.

Contents

Introduction

In 1959, Richard P. Feynman stated in his famous talk - 'There is Plenty of Room at the Bottom' - that fundamentally, there exists nothing in the laws of physics that restricts from making the components of the computers enormously smaller than they were at that moment [45]. This talk can be considered to be the starting point of the field of nanotechnology. Miniaturization is often related to efficiency and the continuous scaling-down of the components and circuits has followed the Moore's law, until now at least [102]. However, the scaling-down poses lots of new challenges, because operational principles of electronic nanoscale devices can be totally different compared to the macroscopic level. In addition, at this moment, the packing density of components is about to reach the resolution limit of standard 'top-down' processes and the nanometer scale is an intractable problem for the present-day manufacturing. Due to this, other methods to create functional components such as wires, memories, switches etc. in nanoscale are needed. Therefore, another way to realize nanoscale fabrication is the 'bottom-up' approach often based on the self-assembly of molecules [177]; molecules can form patterns via a programmable self-assembly, and on the other hand, even functional devices can be made out of individual molecules.

Feynman also ingeniously proposed in his talk that one could learn something important from the biological systems [45]: "The biological example of writing information on a small scale has inspired me to think of something that should be possible. Biology is not simply writing information; it is doing something about it." Now, 50 years later, various biomolecules and biochemical systems are exceedingly investigated and some of them have already been adopted for nanoscale fabrication; one could mimic behavior of evolution-optimized biosystems or even directly exploit them in order to create constructs and devices with small dimensions. One of the most promising molecule candidates in building from the bottom-up is deoxyribonucleic acid (DNA), largely due to its superior self-assembly charactreristics. However, using DNA and other biomolecules as nanoscale components and functional devices is very complicated because of their sensitivity to environment, e.g. the surrounding solution, temperature and pH, and also the uncertainty about their electrical properties.

The self-assembly, the small size and the exceptional mechanical properties of DNA enable the fabrication of diverse nanoscale DNA constructs, even functional

ones [138]. One of the main goals of this approach is to produce different types of DNA structures and utilize them as building frameworks to which biomolecules or other nanoscale components can be attached. For instance, nanoscale patterns and electronic devices can be built by combining molecular components and e.g. metallic nanoparticles, or structures of biomolecules may be studied when they are located on the DNA platforms [5, 137].

The fabrication of DNA structures was previously largely based on diverse DNA building blocks, i.e. contructs consisting of branched junctions or double (DX) and triple-crossover (TX) tiles with 'sticky ends' [138]. These methods provide only a periodic modification of structures and often the overall size of the assembled constructs is hard to control. In 2006, Paul W. K. Rothemund introduced how to create two-dimensional DNA constructs, 'DNA origamis', by folding a long single-stranded DNA with the help of short DNA strands into a desired shape [134]. This is a totally different way to assemble DNA constructs compared to the building block approach, and most importantly, it enables non-periodic patterning. Each of the short folding strands in the construct, so-called 'staple strands', can be replaced with a functionalized one, meaning that it is possible to pattern arbitrarily-shaped DNA templates with the scale of just a few nanometers. The patterning of origami is demonstrated e.g. with proteins [87] and carbon nanotubes (CNT) [111]. Recently, the method has been extended to 3D fabrication [38], and there already exist various designs and applications of DNA origamis (reviewed in Ref. [86]) providing a toolbox for the next generation of DNA-based nanodevices. But alas, exploiting DNA constructs as molecular scale circuit boards and studying the potential electronic applications are not readily available, since the field of electrical conductivity of DNA molecules and constructs is still highly controversial (experimental results and theoretical models reviewed in Refs. [42, 126, 152]). In addition, the controlled positioning of molecules and structures on a chip is one of the major challenges.

Actually, there is both scientific and commercial interest to spatially control individual objects in nanoscale, i.e. to form patterns of nano-objects and also to study the properties (e.g. electrical conductivity and functionalization) of various objects, single molecules and larger assemblies. For these purposes, several techniques to manipulate individual nanoscale objects in a controllable way have been demonstrated: fluidics and magnetic fields [146], as well as methods based on electric fields, including optical tweezers [69], surface plasmon polaritons [132], electrophoresis [32], light-induced electrophoresis [60] and dielectrophoresis (DEP), which is also exploited in this work to anchor a set of individual nano-objects. Dielectrophoresis can be adapted to manipulation of almost any kind of objects, since it is based on an inhomogenous electric field inducing a driving force on any polarizable particle, neutral or charged [123, 124]. Its applicability for small scale manipulation makes it very efficient method for directing and immobilizing various objects to certain locations on a substrate for the use of nanotechnology.

This thesis focuses on DNA-based applications in particular in the field of molecular electronics. First, dielectrophoresis of individual DNA molecules, DNA origamis, DNA triple-crossover constructs and semiconducting quantum dots is studied. Second, the DEP trapping technique used enables investigation of properties of DNA constructs, and also provides direct applications. Here, electrical conductivity measurements of single DNA constructs, which are trapped and immobilized between nanoscale electrodes by means of DEP, are carried out. The alternating current impedance spectroscopy (AC-IS) measurements and analysis give information about the conductance of DNA templates and DNA molecules in general, also taking into account the environmental factors such as humidity and the ions surrounding the DNA. In addition, two DEP-based applications, i.e. a high throughput pattern transfer technique for nanoscale objects and growing of single DNA molecules locally on a chip, are presented.

Part I of this thesis is mainly theoretical. Chapter 1 gives background information about DNA nanotechnology including the structure and properties of DNA, DNA constructs and fundamentals of the electrical conductivity of DNA. A principle of dielectrophoresis and methods for estimating the polarizabilities of DEP-trapped objects are presented in Chapter 2. Chapter 3 deals with the basics of the impedance spectroscopy utilized in the electrical measurements and in the characterization of electrical properties of the DNA constructs.

Part II presents all the experiments and results obtained in this work. Chapter 4 introduces the DNA constructs investigated in this thesis, their design and fabrication, as well as the functionalization of DNA triple-crossover tiles. In Chapter 5 all the data obtained from DEP trapping experiments is pulled together. The DEP trapping is realized by applying AC voltage to lithographically fabricated narrow nanoscale electrodes. This creates high electric field gradients resulting in the dielectrophoretic force which overcomes the thermal motion of the nano-objects and thus enables the efficient trapping. The last three chapters are about the applications. The results from the electrical measurements of the DNA constructs are explained in detail in Chapter 6. The high throughput pattern transfer method, field-induced nanolithography (FINAL), which is demonstrated in a proof-of-principle experiment using quantum dots, is introduced in Chapter 7. Chapter 8 describes a technique of growing single double-stranded DNA molecules at certain locations on a substrate. The method involves the elongation of DEP-immobilized single-stranded DNA molecules and the further hybridization of the extended strands by exploiting polymerase chain reaction, one of the common tools in molecular biology. Finally, the conclusions and future aspects have been briefly discussed.

Part I

Theory

Chapter 1

Structure and properties of DNA

1.1 DNA structure

1.1.1 Deoxyribonucleic acid

The deoxyribonucleic acid (DNA) is a polynucleotide, which contains a sequence of deoxyribonucleotide units, i.e. nucleotides. In each unit there is a phosphate group and an aromatic nitrogenous base attached to a 2′-deoxyribose (monosaccharide i.e. sugar). There are four different types of nucleotides in a DNA molecule depending on which of the following bases the unit contains: thymine (T), cytosine (C), adenine (A) or guanine (G). The nucleotides are covalently joined through 3′, 5′ -phosphodiester bonds thus forming a single DNA strand, i.e. a sugar-phosphate backbone with alternating bases (Fig. 1.1). The order of the bases in a DNA strand plays a vital role in living cells, because the base sequence encodes the genetic information.

1.1.2 DNA double-helix

Two single DNA strands having base sequences complementary to each other, can form a secondary structure of DNA, the DNA double-helix. In this conformation the strands are attached to each other via hydrogen bonds between the complementary bases. The complementary bases form so-called Watson-Crick base pairs, adenine-thymine (A-T, two hydrogen bonds between bases) and cytosine-guanine (C-G, three hydrogen bonds) (see Fig. 1.1), and these two types of base pairs constitute the double-stranded DNA (dsDNA). The double-stranded DNA has an antiparallel configuration since the 3′, 5′ -phosphodiester bonds of the two single DNA strands run in the opposite directions in the helix. The hydrogen bonds and also the base-stacking interactions, i.e., van der Waals and dipole-dipole interactions between the bases, contribute to the coherence and the stability of the double-helix [116].

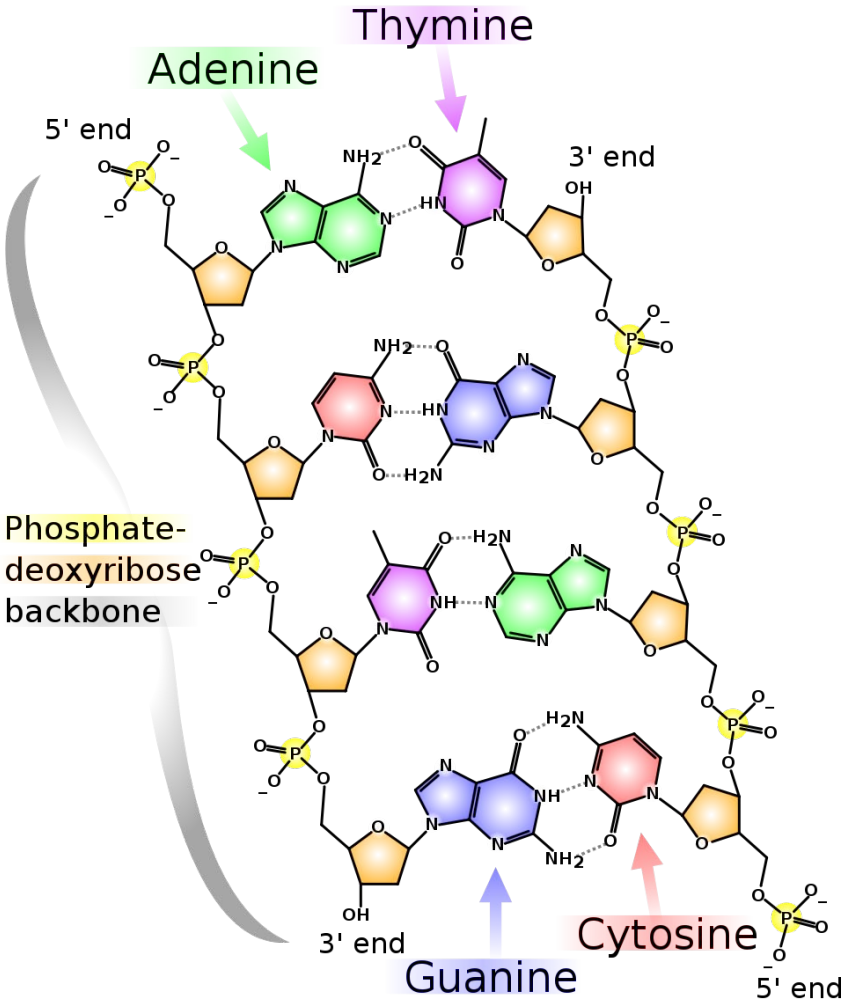

FIGURE 1.1 A schematic view of a DNA double-helix structure. Two single DNA strands comprised of the sugar-phosphate backbone and the alternating bases are linked together via Watson-Crick base pairing.

1.1.3 DNA conformations

Depending on the environment, the DNA double-helix can have different 3D forms, from which B-DNA is the most stable structure for a DNA molecule with an arbitrary sequence under physiological conditions, and actually it was the first discovered DNA-form (postulated by Watson and Crick in 1953 [165]). The other well-known types of the helix structures are A- and Z-DNA which can also be found in living organisms. The B-form is a right-handed helix and its helix diameter is approximately 2 nm. It has on average 10.5 base pairs (bp) per helical turn and the helix rise per bp is about 0.34 nm. A-DNA is also a right-handed form, but it has slightly different structural parameters compared to the B-DNA: diameter 2.6 nm, 11 bp per turn and helix rise per bp 0.26 nm. The plane of the base pairs respect to the helix

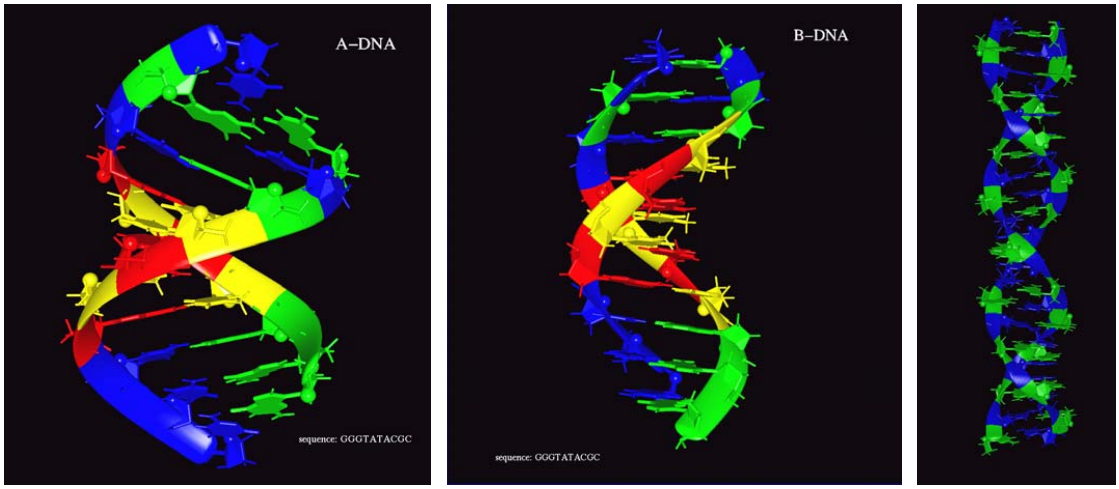

FIGURE 1.2 Models of A-, B- and Z-DNA [1]. The plane of the base pairs respect to the helix axis is tilted most in the A-form.

axis is tilted more in the A-form (20°) than in the B-form (6°). This structural difference explains their diverse stabilities in solutions and their electronic properties [42]. For example, to stabilize the B-DNA at least 13 water molecules per nucleotide are needed, but the A-form can be stable even if each of its nucleotide is surrounded only by 5-10 water molecules [162]. In contrast to the A- and B-DNA the Z-form is left-handed and more elongated (12 bp per turn, helix rise 0.37 nm per bp) and its backbone has a zigzag configuration. The structures of A-, B- and Z-form are presented in Fig. 1.2 and Fig. 1.3.

There also exist several exotic DNA structures, and here, two special cases should be mentioned. The triplex DNA, H-DNA, is formed when an additional DNA strand links up with B-DNA via Hoogsteen bonds [64]. In H-DNA, a base of the third strand can attach to the Watson-Crick base pair in such a way that A or T binds to a T-A base pair and G or C^+ (protonated C) to a C-G pair [112]. The Hoogsteen pairing also enables four guanine-rich DNA strands to form a so-called G tetraplex. In the presence of metal cations (e.g. K^+, Na^+ or Mg^{2+}) the G tetraplexes can form very stable and long superstructures, G-wires, via a self-assembly process [108, 109]. These structures are interesting in the field of nanoelectronics due to their capability to serve as molecular nanowires or switches [24, 113].

1.1.4 DNA fabrication

By means of the methods of molecular biology and chemistry, it is relatively easy to fabricate a desired DNA molecule with a specific length and base sequence. A short single-stranded DNA (oligonucleotide) can be produced by exploiting a chemical synthesis of single nucleotides. This method also offers a chance to add various

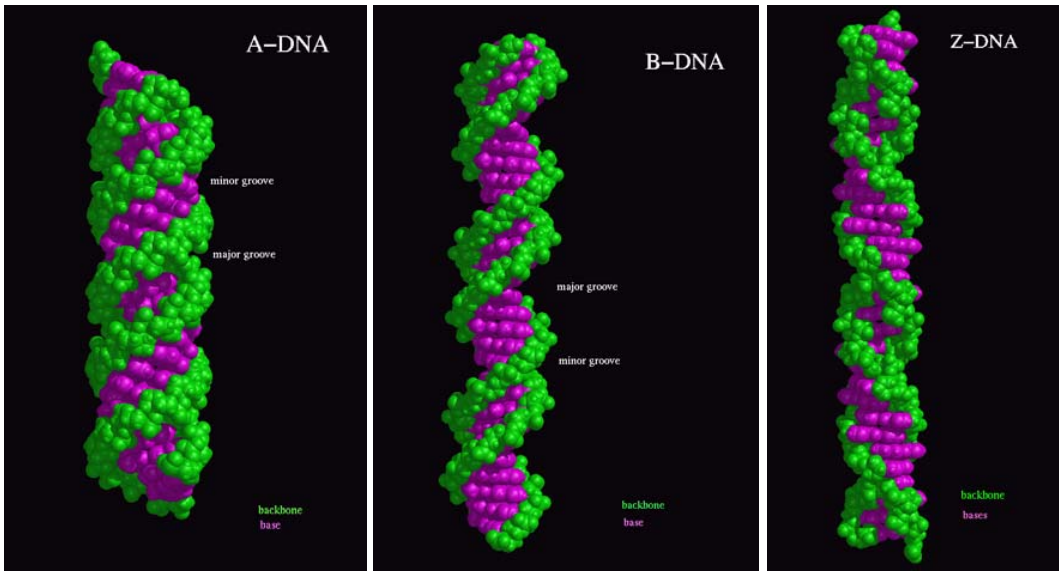

FIGURE 1.3 Ball models of A-, B- and Z-DNA [1]. A- and B-DNA have right-handed helical sense and Z-DNA is a left handed helix (the backbone is green, bases are violet).

functional groups to the oligonucleotide. Secondly, DNA fragments can be made by cutting a long natural DNA molecule with restriction enzymes. With this method a DNA molecule can be cut in a controllable way from the certain place by a restriction enzyme (sequence-specific enzyme). Polymerase chain reaction (PCR) is a third and very efficient method to fabricate DNA fragments. The main idea in using PCR instead of the above-mentioned ways is to fabricate large amounts of dsDNA with a certain base sequence from a DNA template, for example plasmid DNA. PCR exponentially amplifies a chosen sequence via enzymatic replication, and so it yields a huge amount of dsDNA with the desired base sequence [115].

1.2 DNA constructs

Due to the small size (diameter of dsDNA $\sim$ 2 nm), mechanical properties (ssDNA is flexible, but dsDNA is rigid in the length scale of 50 nm under normal physiological conditions) and superior self-assembly characteristics (specific base pairing), DNA is one of the most interesting molecules in nanotechnology and in the 'bottom-up' fabrication [138]. It is possible to produce different 1D, 2D and 3D constructs, even functional ones, out of DNA molecules by exploiting several building block methods (for example TX tiles [88]), or alternatively, a folding technique (DNA origami [134]). Some of the discovered constructs are presented in this section (for extensive reviews, see e.g. Refs. [138, 140]).

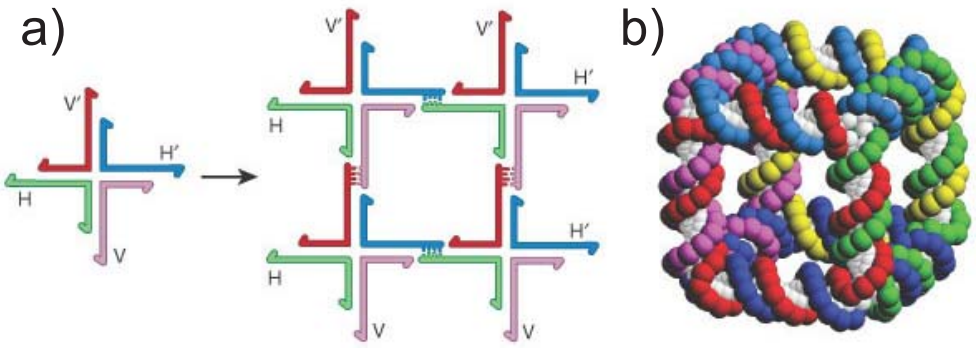

FIGURE 1.4 a) A branched DNA building block with four distinct arms is consisted of four oligonucleotides connected through the crossover junction. The blocks can attach to each other via complementary sticky-end pairs H - H′ and V - V′ thus forming a 2D crystal. b) A 3D cube construct formed of branched DNA molecules. Adapted with permission from Ref. [138].

1.2.1 'Building block' approach

The starting point of making DNA structures has previously been the 'sticky ends' approach [71, 137]. The so-called 'sticky end' is a short single-stranded DNA overhang in the end of a double-stranded molecule. If two dsDNA molecules have complementary overhangs, molecules can combine via the base-pairing of sticky ends. By joining many dsDNAs together via sticky ends one can fabricate 1D constructs, chains and rings, which are in fact double-helix structures. To further extend the structures from 1D to 2D, a crossover junction was introduced [71] (a junction is illustrated in Fig. 1.4). In general, the synthetic branched DNA which can act as a building block, includes from three to twelve ssDNAs linked together through the crossover point. The blocks can be attached to each other via sticky ends, similarly as in 1D constructs (Fig. 1.4a). The main idea in utilizing branched DNA molecules with certain sticky ends, for example building blocks with four double-helical arms connected via a crossover junction (analogous to a Holliday-junction intermediate appearing in nature during meiosis), is to create more sophisticated DNA structures such as a 2D lattice or a 3D cube [138] (see Fig. 1.4b).

The branched DNA building block mentioned above is not very stiff and thus, in order to produce more stable DNA constructs, one can utilize more rigid 2D structures with sticky ends. One example of such component is so-called 'double-crossover' (DX) molecule [94], which is comprised of two parallel dsDNAs, which have joined together through two Holliday-junctions. DX tiles can be exploited in the fabrication of 2D lattices, if they just have suitable sticky ends to join each other in a desired way [166].

There also exist 'triple-crossover' (TX) molecules (see also Ch. 4), which are similar to DX blocks, but literally they consist of three dsDNAs (two crossovers in

both inter-helix gaps). By means of the DX and TX tiles and their combinations, various planar structures and 3D objects have been produced, e.g. arrays [88], 'barcode-patterns' [170], triangulars [98], 'crossbar' lattices [171], 'DNA nanotubes' [135] and even a regular 3D DNA lattice [122]. In general, it is conventional that available low-dimensional patterns are exploited in the fabrication of many 3D structures. For example, the DNA nanotubes can be based on either DX [135] or TX tiles [97] and a DNA tetrahedron can be formed by utilizing 2D triangular building blocks [49,50]. For a review of 3D DNA nanoconstruction, see Ref. [148].

1.2.2 DNA origami

As mentioned above, various 2D and 3D DNA patterns can be formed by building blocks, but these approaches are often ineffective; the amount of successful structures in fabrication processes can be very small and the yield can vary a lot between successive syntheses. Also, a more fundamental restriction is, that it is hard to limit the overall size of the 2D constructs. In many cases, due to interactions between the ssDNAs in solution, a synthesis is highly sensitive to the stoichiometrical ratios of the strands.

Besides the building block approach, there exists another way to assemble DNA constructs, that is, folding linear DNA scaffolds into complex structures. The first demonstration of this kind of approach was a DNA octahedron assembled by folding a long ssDNA with additional short strands [145], and later on, a method based on similar technique, called 'DNA origami', was introduced [134]. The fabrication of DNA origami is based on the folding of a long 7.3 kb viral ssDNA into a definitive pattern with a help of directing short oligonucleotides (staple strands), which can not bind to each other (Fig. 1.5a). With this method, one can create almost arbitrary 2D shapes with a high yield and controlled size in a 'one-pot' experiment (Fig. 1.5b) (see also Ch. 4). DNA origamis may be used in several applications, they can serve as sophisticated scaffolds for non-periodic patterning in nanoscale by virtue of the small pixel size defined by the length of staple strands in question (for example in Fig. 1.5c DNA hairpin patterning is used) and on the other hand, individual origamis can be programmed to form larger structures via combining; even 20,000 features could be included in a micrometre-size origami.

Recently, the conventional fabrication method of DNA origami, based on the certain viral genome (M13mp18) serving as a scaffold strand, has been generalized for any kind of single strand available from dsDNA molecules [62, 127]. Thus, the size of a DNA origami is no more restricted by the length of the original M13 scaffold strand. Also, the origami method has been extended to the field of 3D DNA nanofabrication: a tetrahedral molecular cage [74], a functional nanoscale box [6], topological reconfigurable architechtures, such as a Möbius DNA strip [59], tensegrity structures [95] and a method with an open-source software to fabricate custom

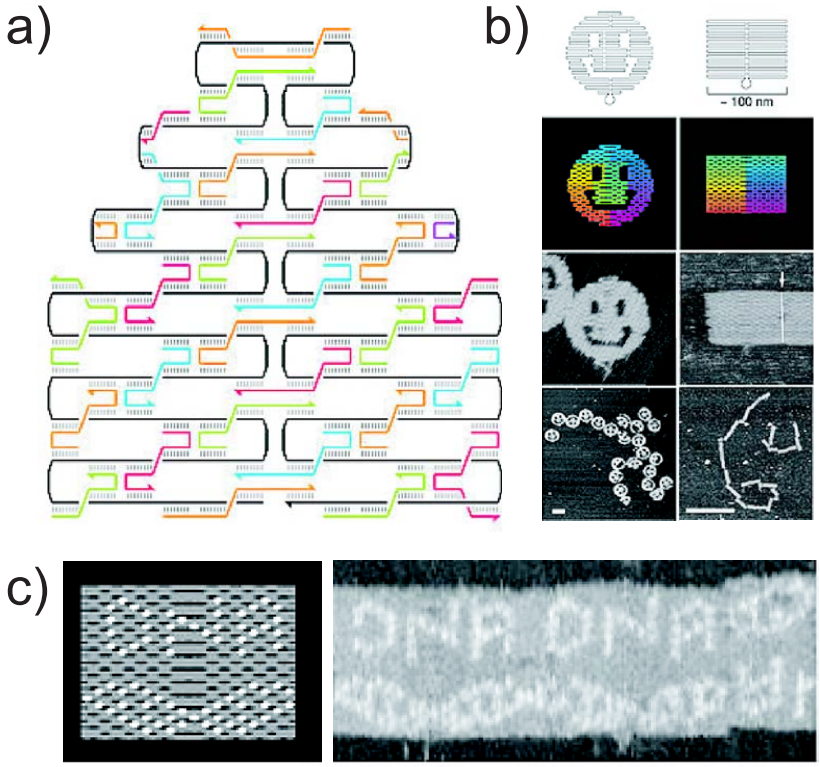

FIGURE 1.5 DNA origami. a) DNA origami method: A long viral single-stranded scaffold strand (black strand) is folded into a 2D object with the help of short oligonucleotides, i.e. staple strands (orange, green, blue and purple strands). b) Models of a so-called smiley origami and a rectangular origami, and the atomic force microscope (AFM) images of the fabricated structures. The scale bars are 100 nm (smiley) and 1 μm (rectangular). c) DNA hairpin patterning of a rectangular origami. Adapted with permission from Ref. [134].

3D shapes [36,38,39] have been presented. For a review of basic designs and applications of DNA origami, see Ref. [86].

1.2.3 Applications of DNA constructs

DNA constructs as templates

As described briefly in the Sec. 1.1.4, DNA can be modified with different chemical groups. These functionalizations can act as binding sites for other materials, and therefore DNA molecules and self-assembled DNA constructs can be utilized as scaffolds in the assembly of nanocomponents (reviewed in Refs. [3,52]). Linear DNA molecules have been used as templates for proteins [78], nanoparticles [163], carbon nanotubes (CNT-DNA transistor) [77] and in fabrication of conducting nanowires [55].

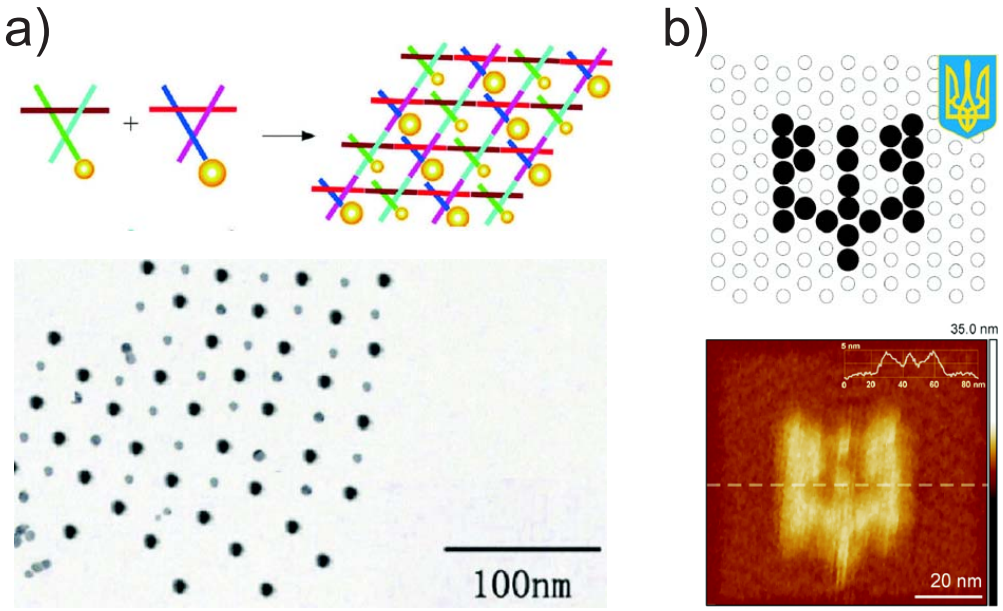

FIGURE 1.6 DNA constructs as templates. a) Periodic organization of gold nanoparticles using 2D DNA construct motifs, i.e. building blocks, and a transmission electron microscope (TEM) image of a fabricated 2D lattice. b) Non-periodic assembly of proteins on a rectangular DNA origami. Upper image: Black staple strands are replaced with biotinylated strands to which streptavidin can attach. Lower image: An AFM image of streptavidin decorated origami. Adapted with permission from Refs. [178] (a) and [87] (b).

These methods can be extended to the patterning of periodic 2D lattices (Fig. 1.6a) and tiles with e.g. proteins [171] (also article **A.III**), metallic nanoparticles [90, 178] and semiconducting quantum dots [142]. In addition, there exist various types of 3D DNA cages with site-specific incorporation of a range of metals [173]. Due to the great interest of non-periodic patterning provided by DNA origami technique, several examples of assembling materials with origami-based templates have been demonstrated (see also Fig. 1.6b): attachment of proteins [28, 85, 87, 143], gold nanoparticles [37, 141] and carbon nanotubes [111] to 2D origamis and quantum dots to DNA origami nanotubes [22] have been performed, and also single-molecule chemical reactions have been carried out on a DNA origami [158].

In summary, DNA self-assembly and especially DNA origami technique enables the controlled organization of wide range of materials. Since each of the staple strands of origami can be functionalized separately, the method allows one to use such a structure as a nanoscale circuit board and furthermore, to fabricate multicomponent devices and constructs for bionanotechnology, nanoelectronics and plasmonics.

Functional and dynamic DNA constructs

On top of the various DNA templates and assemblies listed in previous section, it is possible to fabricate artificial active constructs or scaffolds with functional structures, so-called DNA nanomachines. In biological approaches, both constructs that bind to specific target molecules (DNA aptamers and enzymes [20]) and protein-based molecular machines can be realized. For example, a DNA nanomachine can be a switch based on the rotation of connected DX molecules [105], or a device, which is fuelled by ions or protons in order to produce a state transition or some sort of desired conversion [43, 96, 117]. Reversible structurally switchable 3D DNA objects, based on a small set of building blocks, have also been presented [4].

Most of the two-state devices are based on DNA hybridization and thus on a simple conformational transition of the construction, e.g. DNA tweezers [175] and a so-called PX-JX_2 device [172]. However, if the operational principles consist of several conformational transitions, devices could be used for quite advanced applications. For example, there also exist 'walkers', which move along a simple track with suitable anchorages for the feet of the sophisticated device, and DNA-based molecular motors powered by (enzymatic) DNA or ATP hydrolysis [10,27,144,147,174]. In addition, DNA walkers containing cargo or 'molecular spiders' can move along on an appropriately designed track on a DNA origami [54,101]. Various DNA nanomachines have been reviewed in Ref. [11].

In addition, 3D DNA constructs may be used in loading and releasing cargo. For instance, a DNA origami box [6] and DNA-based nanotubes [99] can serve as capsules for molecules or nanoparticles, and futhermore, it is possible to open them in a controllable way by using specific additional DNA strands. These kinds of structures could be utilized in drug-delivery and biological sensing applications. As a final note to this section, one can exploit certain DNA constructs such as DNA tiles and 'origami seeds' also in algorithmic self-assembly and thus in DNA computing (see e.g. Ref. [8] and 'DNA-Based Computation and Algorithmic Assembly' in Ref. [139]).

1.3 Electrical conductivity of DNA

1.3.1 Background

In order to fully exploit DNA molecules and self-assembled DNA constructs as building blocks, functional components and templates for molecular electronics (i.e. conducting wires, memories, rectifiers, switches, transistors and nanoscale circuit boards [47]) their electrical properties, and more precisely, their charge transport / transfer mechanisms should be well known and understood at the single molecule or single construct level. In this thesis (Ch. 6) the electrical conductivities of two different DNA templates, DNA origamis (**A.II**) and TX tile constructs (**A.III**), which

could potentially be utilized in molecular electronics or in nanotechnological devices, are characterized by means of DC and AC techniques. Electrical properties of DNA are of great concern not only in molecular electronics, but also in medicine, in cancer therapy and in investigation of genetic mutations [131] as well as in biological sensing such as DNA detectors [34].

Already in 1962, it was first time proposed that dsDNA molecules could conduct electricity due to the overlapping π orbitals of the base pair stack [41]. Since then, and in particular during recent 20 years, huge amount of theoretical and experimental articles about DNA conductivity, based on either physical or chemical approaches, have been published with contradicting results: ohmic, e.g. Ref. [46], insulating, e.g. Ref. [19], semiconducting, e.g. Ref. [125], and even superconducting [73] properties have been reported. In addition, the electrical characterization has often been based only on direct current observations, although in many cases also an alternating current measurements should have been performed in order to fully analyze the conductivity of DNA. Extensive reviews about DNA conductivity and the suggested conductance mechanisms can be found from Refs. [42, 126, 152].

However, it starts to be quite clear that a long, unmodified DNA molecule itself can not serve as an electrical building block or wire for the purposes of nanoelectronics, since it does not have high enough conductance. Yet, the conductance mechanism of the DNA is unknown and the topic of DNA conductivity still remains highly controversial.

1.3.2 Possible conductance mechanisms of DNA

This section deals with possible, mainly theoretically suggested conductance mechanisms of a plain dsDNA molecule. In reality, there exist various factors that affect the conductivity of DNA and thus the experimentally obtained results. These kinds of charge transfer mechanisms are discussed in Sec. 1.3.3.

π-stacking

In the aromatic rings of the bases (see Fig. 1.1) the atomic orbitals perpendicular to the plane of the ring form delocalised π bonding and $\pi^\star$ antibonding orbitals [41]. These orbitals are parallel to the plane of the base, and if the electronic coupling between π orbitals of adjacent base pairs is strong enough, the energy level broadening reduces the energy gap between π and $\pi^\star$ states (π-$\pi^\star$ gap ~ 4 eV). Thus, depending on the coupling, the energy gap could either be totally vanished (ohmic behavior) or significantly reduced (semiconductor, the conductivity could be obtained by doping the DNA). [42]

In a natural DNA molecule the non-periodicity of the system (varying base sequence) makes the situation quite complicated: the strength of the electronic coupling between the highest occupied and the lowest unoccupied molecular orbitals

of the adjacent base pairs depends on the bases in question and thus, in principle homogeneous sequences should provide the best conditions for the π orbital overlap. In addition, both the backbone flexibility and water molecules with counter-ions surrounding the negatively charged DNA affect the electronic structure of the π stack.

Tunneling and thermal hopping

If an electron-hole pair is formed in a single base pair, the charge can migrate from a donor (usually hole in a guanine base) to an acceptor through adjacent base pairs. In the simplest model for the charge transfer (CT), a charge tunnels through the one-dimensional energy barrier and the rate of the transfer decays exponentially as a function of a donor-acceptor distance. In more detail, CT can either be a uni-step coherent tunneling from a donor to acceptor (so-called superexchange, i.e. excited donor and the acceptor have lower energies than the intermediate base pair bridge) or thermally induced hopping process (incoherent sequential tunneling), where charge migrates through intermediate sites by diffusion type of random walk. If the number of bases between donor and acceptor is low, meaning a short bridge for tunneling, the first mentioned mechanism dominates in the CT process. On the other hand, if the direct tunneling is prohibited due to a long bridge, the thermal hopping becomes a dominant mechanism. In reality, a long-range CT could be a parallel combination of these two mechanisms and it can occur over 30 nm, decaying exponentially with distance [16]. For a review of CT in DNA, see Ref. [18].

1.3.3 Factors affecting the conductivity results

It has been found out that in the experiments the contacts between electrodes and the molecules play a crucial role [61], and ideally these contacts should be ohmic and have low resistances. To ensure a proper electrical contact at a single molecule level is extremely difficult. And further, even if the proper contacts could be realized, various environmental factors, e.g. humidity, affects the conformation of DNA [154,162], and also the conductivity [12]. In addition, at the high humidity levels the adsorbed and ionized water molecules surrounding a DNA molecule can themselves act as charge carriers [80, 169], or the conductivity can be ascribed to relaxational losses of the surrounding water dipoles [21] (for water dependent conductivity, see also articles **A.II** and **A.III** of this thesis). On the other hand, if electrical measurements are performed in a vacuum chamber, a DNA molecule completely dehydrates and thus the conformation of DNA can not be verified.

Moreover, several other factors such as the type of counter-ions and the salt concentration have a large influence to the secondary structure of dsDNA, and on the other hand, ions can diffuse and migrate along DNA thus giving a raise to an ionic conductivity. In addition, the charge of DNA depends on the dissociation of the

phosphate groups and therefore on pH. Other significant factors affecting the conductivity results are e.g. the measurement geometry (DNA lying on the substrate vs. freely hanging geometry), and the type of the substrate used, since the conformation of DNA also depends on the interaction between DNA and the substrate [72].

In summary, it is very demanding to create such a measurent setup that takes into account all these above-mentioned issues. Thus, in order to directly observe a DC-conductivity of a single DNA molecule, a delicate consideration of electrical contacts and environmental factors are required.

Chapter 2

Dielectrophoresis

2.1 Basics of dielectrophoresis

Dielectrophoresis (DEP) means a translational motion of any polarizable particle, neutral or charged, caused by the polarization effect in an inhomogeneous electric field [123, 124]. In general, an electric field induces positive and negative surface charges on the opposite sides of a polarizable particle. The Coulomb interactions between these surface charges and the electric field induce forces on both sides of the object. In the case of a neutral polarizable particle and a homogeneous electric field the induced forces cancel out each other, but in an inhomogeneous field the electric field densities on the different sides are unequal thus resulting in a net force, a dielectrophoretic force, and thereby the translational motion of the particle. If the particle is charged, also an electrophoretic force is acting on it according to Coulomb's law. The principle of DEP is schematically illustrated in Fig. 2.1.

The DEP force is parallel to the gradient of the square of the electric field, but the direction of the force depends only on the polarizabilities of the surrounding medium and the particle. Usually, the permittivities of the particle and the medium are purely real. In this generalized case, if the permittivity of the particle is higher than the permittivity of the medium, the phenomenon is called positive DEP and the polarizable particle travels towards the electric field maximum. In negative DEP, for one, the order of magnitude of the permittivities is opposite to positive DEP and thus the object is pushed towards the field minimum.

2.2 Dielectrophoretic force and potential

2.2.1 Effective dipole and polarizability

In this section the consideration of dielectrophoretic force is based on the concept of an effective dipole [70], although there also exist general solutions for higher order multipoles and therefore more accurate approximations [164]. Here, a dielectric

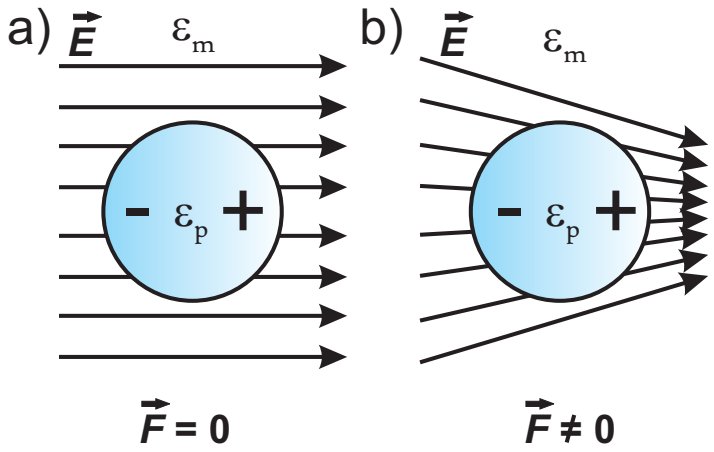

FIGURE 2.1 The main idea of the dielectrophoresis (DEP). A polarizable particle (permittivity ϵ_p) surrounded by the medium (permittivity ϵ_m) is in an electric field. a) In a homogeneous electric field the induced forces on the opposite sides of the particle cancel out each other and thus the object does not move. b) An electric field is nonuniform resulting in the dielectrophoretic force on the particle. The direction of the DEP force depends on the order of the (real) permittivities; $\epsilon_p > \epsilon_m$: positive DEP (force towards the field maximum) and $\epsilon_p < \epsilon_m$: negative DEP (force towards the field minimum).

particle and the surrounding medium, under an influence of the electic field $\vec{E}$, are treated as an effective dipole with dipole moment $\vec{p}$ in such a way that

$$\vec{p} = \alpha \vec{E}, \tag{2.1}$$

where α is the effective polarizability. For an ellipsoid particle with the permittivity ϵ_p, the polarizability component in the certain direction i can be written as

$$\alpha_i = 3V\epsilon_m \mathrm{Re}[K_i], \tag{2.2}$$

where V describes the volume of the particle, ϵ_m is the permittivity of the medium and $\mathrm{Re}[K_i]$ is real part of a Clausius-Mossotti factor [179]. This factor is a function of complex permittivities of both the particle and the medium. It includes also the depolarization factor N_i, which depends on the geometry of the object and the considered direction (see Sec. 2.4). The ellipsoid of revolution is the only shape for which the analytic expressions of N_i can be found, meaning that for other shapes the factors should be calculated numerically. The Clausius-Mossotti factor for an ellipsoid is given as

$$K_i = \frac{1}{3}\frac{\epsilon_p^* - \epsilon_m^*}{\epsilon_m^* + N_i(\epsilon_p^* - \epsilon_m^*)}. \tag{2.3}$$

Here, the complex permittivities for the particle and the medium have forms

$$\epsilon_p^* = \epsilon_p - j\frac{\sigma_p}{\omega} \tag{2.4}$$

and

$$\epsilon_m^* = \epsilon_m - j\frac{\sigma_m}{\omega}, \tag{2.5}$$

where j denotes the imaginary unit and ω is the angular frequency of the electric field $\vec{E}$. Conductivities of the particle and the medium are marked by σ_p and σ_m, respectively.

2.2.2 DEP force

A dielectrophoretic force caused by an inhomogeneous electric field can be written as

$$\vec{F}_{\mathrm{DEP}} = (\vec{p}\cdot\vec{\nabla})\vec{E}. \tag{2.6}$$

On the grounds of Eq. 2.1 and by noticing that the electric field is the negative of the gradient of the potential (magnetic field $\vec{B} = 0$) and accordingly $\vec{\nabla} \times \vec{E} = 0$, one can express Eq. 2.6 in an alternative way

$$\vec{F}_{\mathrm{DEP}} = \frac{\alpha}{2}\vec{\nabla}(E^2). \tag{2.7}$$

For a periodically alternating electric field, $E(t)$ (period T), the time-averaged DEP-force can be written as

$$\vec{F}_{\mathrm{DEP,t}} = \frac{1}{T}\int_0^T \frac{\alpha}{2}\vec{\nabla}[E(t)]^2 dt = \frac{\alpha}{2}\vec{\nabla}\left\{\frac{1}{T}\int_0^T [E(t)]^2 dt\right\} = \frac{\alpha}{2}\vec{\nabla}(E_{\mathrm{rms}}^2), \tag{2.8}$$

where E_{rms} is a root mean square value of an electric field. Therefore, for a sphere (radius r_p), which is the simplest example of an ellipsoid particle, i.e. $N_i = \frac{1}{3}$ for any i, the time-averaged DEP force within an AC electric field (also valid for a DC field) is

$$\vec{F}_{\mathrm{sphere,t}} = 2\pi\epsilon_m r_p^3 \mathrm{Re}\left[\frac{\epsilon_p^* - \epsilon_m^*}{\epsilon_p^* + 2\epsilon_m^*}\right]\vec{\nabla}(E_{\mathrm{rms}}^2). \tag{2.9}$$

Equation 2.7 implies that the DEP force is parallel to the gradient of the square of the electric field and the direction of the force does not depend on the direction of the field at all. For instance, if a sinusoidal AC voltage is the source of an inhomogeneous electric field, the direction of the DEP force always remains the same, although the sign of the field varies periodically in time.

According to Eqs. 2.2, 2.3 and 2.7, the Clausius-Mossotti factor and therefore also the DEP force are functions of the frequency of the field. The imaginary part of the Clausius-Mossotti factor is an essential term for electrorotation and traveling-

wave DEP [23, 70, 161], while the real part determines the sign of the DEP force; $\mathrm{Re}[K]$ can be positive (positive DEP) or negative (negative DEP). Consequently, the direction of the induced force can be changed by varying the frequency of the field, and this property can be utilized in manipulation of particles under a specific suspending medium.

One has seen above that the absolute value of the DEP force is proportional to the volume of the particle and this size-dependence complicates the manipulation of nanoscale objects. In general, previous equations may not be exactly accurate, because they have been derived using a classical approach. Here, conductivities as well as permittivities are approximated by bulk values, whereas in reality the distribution of atoms in nanoparticles or macromolecules is not homogeneous. A significant fraction of atoms lie on the surfaces and in addition, a charged particle, such as a DNA molecule, can be surrounded by a so-called counter-ion cloud within a medium [136,150]. Apparently, these nonidealities strongly affect the polarizability and DEP and thus the calculations based on this approach are only rough estimations (see Sec. 2.4).

2.2.3 Trapping by DEP and the Brownian motion

One can trap particles by taking advantage of DEP, if the preceding DEP force overcomes the Brownian motion. The Brownian motion can be considered as a random force, which is caused by the thermal motion of particles in a fluid. The maximum value of the force for a spherical particle is approximately [124]

$$F_{\mathrm{thermal}} = \frac{k_B T}{2 r_p}, \tag{2.10}$$

where k_B is the Boltzmann constant, T is temperature and r_p denotes the radius of the sphere. As seen from the expression, the thermal force increases with the decreasing particle size and as already mentioned, also the polarizability of the trapped object is proportional to its size. Accordingly, the smaller the particle the higher the thermal force and the smaller the DEP force, and thus, quite high gradients are needed to trap the particle successfully. In order to increase the magnitude of the gradient of the square of the electric field and therefore also the DEP force, one can reduce the dimensions of electrodes, by which the field is created. Higher voltages also improve trapping efficiency, but in practice, the medium surrounding the particles, for instance an aquatic solution, and the electrode structure can set restrictions for the voltage used. Moreover, there exist the motion of electrolytes in solutions (electro-convection) by virtue of the electric field, and also forces acting on the particles due to the motion of the solvent, e.g. electrothermal forces caused by the Joule heating [25].

2.2.4 DEP potential

Another way to describe the trapping of particles is based on a DEP potential. Universally, a force equals to the negative gradient of the potential energy and with Eq. 2.7 one can simply define the DEP potential for a polarizable uncharged particle in the electric field as

$$U_{\mathrm{DEP}} = -\frac{1}{2}\alpha E^2. \tag{2.11}$$

Combining the DEP potential with the thermal energy of a particle, i.e. the Brownian motion expressed in energy, one can write the total potential energy

$$U_{\mathrm{total}} = U_{\mathrm{thermal}} + U_{\mathrm{DEP}} = \frac{3}{2}k_B T - \frac{1}{2}\alpha E^2. \tag{2.12}$$

In general, this formula is derived for neutral objects, since it does not take the electrophoretic effects into account. However, it is also valid for charged particles in an AC electric field, since in this case the time-average of the electrophoretic forces is zero. The equation means that at a location where the absolute value of U_{DEP} is either higher than or equal to U_{thermal}, i.e. $U_{\mathrm{total}} \leq 0$, the particle is trapped in a 'DEP potential well'. The bottom of the well corresponds to the minimum of the total potential energy, which is the point towards which the DEP force pushes the particle.

2.3 Dielectrophoretic trapping of nanoscale objects

Manipulation, separation and trapping by dielectrophoresis have widely been applied in many fields and also for various objects in the micro- and nanometer scale. DEP has largely been used as an active and non-destructive manipulation method for trapping biological objects like eukaryotic cells, e.g. blood cells in Ref. [110], and prokaryotic cells e.g. in Ref. [107]. Although the Brownian motion poses challenges in trapping of the objects having all dimensions in nanoscale, successful experiments have been demonstrated for e.g. DNA [63] (also **A.I-A.III** and **A.V**), quantum dots (**A.IV)**, carbon nanotubes [31,157], semiconducting [84] and conducting nanoparticles [13], proteins [179], latex beads [66] and viruses [114]. DEP can also be utilized in pattern transfer, as seen in the article **A.IV** of this thesis and in Refs. [91, 149]. For extensive reviews on the dielectrophoresis and its applications, see Refs. [23, 65, 152, 176].

In Part II of this thesis the DEP trapping of DNA (DNA constructs in **A.I**-**A.III** and ssDNA molecules in **A.V**) is discussed, and therefore the DEP-trapping experiments for DNA carried out by Tuukkanen *et al.*, i.e. Refs. [152, 153, 154, 155], should especially be mentioned here. In these articles the techniques used for trapping and immobilization of individual thiol-modified DNA molecules to nanoelectrodes by means of alternating current dielectrophoresis (AC-DEP) are very similar to the approaches reported in the articles **A.I**-**A.V** of this thesis and in Chapter 5.

2.4 Calculations of polarizabilities

2.4.1 Motivation

In Chapter 5 the DEP trapping of two different types of DNA origamis (smiley and rectangular), TX tile constructs, DNA oligonucleotides and semiconducting quantum dots (QDs) are reported. Since the polarizability of the particle plays an essential role in the trapping process, the effective polarizabilities in different directions were calculated for above-mentioned objects. As stated in the previous section, in an aquatic solution DNA has the counter-ion cloud around the object, which polarizes under an electric field and significantly improves the trapping efficiency. In general, the volume and the shape of the ion cloud depends on the salt concentration, pH and the conformation of DNA. Here, the shape of the ion cloud is simply approximated by an ellipsoid and hence a few types of ellipsoids and their depolarization factors are considered. Furthermore, the magnitude of the effective polarizability components of a DNA - ion cloud hybrid in different directions can be deduced from the depolarization factors and the estimated volume of the ion cloud. The polarizability calculations are based on the equations represented in Sec. 2.2.

2.4.2 Depolarization factors of ellipsoid

The depolarization factor N_i, which is included in the Clausius-Mossotti factor (see Eq. 2.3), is a measure of how much the internal field within an ellipsoid is weakened by the polarization [156]. If the semi-axes of an ellipsoid in the three orthogonal directions are a_x, a_y and a_z, the depolarization factor in the direction of a certain semi-axis a_i can be described by [76, 89]

$$N_i = \frac{a_x a_y a_z}{2} \int_0^\infty \frac{ds}{(s + a_i^2)\sqrt{(s + a_x^2)(s + a_y^2)(s + a_z^2)}}, \tag{2.13}$$

where s is an integration variable (ellipsoidal coordinates). The three depolarization factors for any ellipsoid satisfy

$$N_x + N_y + N_z = 1, \text{ where } N_i \in [0,\ 1]. \tag{2.14}$$

The right hand side of Eq. 2.13 is an elliptic integral and it can be reduced into elementary functions, if the ellipsoid is a spheroid (an ellipsoid of revolution) [76, 89]. For a prolate spheroid, where $a_x > a_y = a_z$, the closed-form solutions are

$$N_x = \frac{1 - e^2}{2e^3} \left[\ln\left(\frac{1 + e}{1 - e} \right) - 2e \right] \tag{2.15}$$

and

$$N_y = N_z = \frac{1}{2}(1 - N_x), \tag{2.16}$$

where $e = \sqrt{1 - a_y^2/a_x^2}$ means the eccentricity of the ellipsoid. From this expression one can easily find also the factors for a spherical particle, such as a QD, as $e \to 0$. This consideration gives $N_x = N_y = N_z = \frac{1}{3}$, which is intuitively clear due to the rotational symmetry. For a rod-shaped object, such as a long DNA molecule and its counter-ion cloud, the factors can be determined as limit values, when $e \to 1$. In this case the depolarization factors are (0, $\frac{1}{2}$, $\frac{1}{2}$).

Another analytic solution for the integral 2.13 exists, when the equal axes are also major axes, i.e. the ellipsoid is an oblate ($a_x = a_y > a_z$). Now the depolarization factors are given by

$$N_z = \frac{1 + e^2}{e^3}(e - \arctan e) \tag{2.17}$$

and

$$N_x = N_y = \frac{1}{2}(1 - N_z), \tag{2.18}$$

where the eccentricity is defined as $e = \sqrt{a_x^2/a_z^2 - 1}$. If the eccentricity increases infinitely, the oblate converts into a disc at xy plane, with the depolarization factors (0, 0, 1).

2.4.3 Effective polarizability components

The expression of the effective polarizability component has been given in Sec. 2.2. Here, for a simplification the polarizability is described by

$$\alpha_i = \epsilon_m V \mathrm{Re}\left[\frac{\tau - 1}{1 + N_i(\tau - 1)}\right], \tag{2.19}$$

where a notation $\tau = \epsilon_p^*/\epsilon_m^*$ has been used. By using Eq. 2.19, one can calculate the depolarization factors and furthermore the polarizability components for all the DEP-trapped objects reported in this thesis. In order to estimate the volume of the object, one can assume that a counter-ion cloud covering a dsDNA (also DNA origami and TX tile construct) is about 20 nm thick [150]. This value is the estimated thickness of the cloud (Debye length) for long dsDNA molecules in the medium of which pH is close to 7 and the salt concentration is in the mM range, i.e. the conditions are similar to the ones in this work.

DNA oligonucleotide

In order to approximate the polarizability of a 40 nt (ca. 14 nm) long oligonucleotide, which has been trapped in **A.V**, one has to consider first a double-stranded DNA

molecule with the same length. One can approximate that a shape of the counter-ion cloud of the 40 bp dsDNA is a prolate ellipsoid with semi-axes a_x = 17 nm and $a_y = a_z$ = 11 nm (i.e. the thickness of the cloud is 10 nm). Because an oligonucleotide with the same length has half of the charges of the dsDNA, it can be estimated that its counter-ion cloud is roughly half of the volume of the cloud of the dsDNA, meaning that the thickness of the cloud for a 40 nt oligonucleotide is about 7.5 nm. Therefore semi-axes for the ellipsoid are a_x = 14.5 nm, $a_y = a_z$ = 8.5 nm and the volume is ca. $4.4 \cdot 10^{-24}$ m^3. With these parameters the depolarization factors can be easily determined by means of Eq. 2.15 and 2.16 yielding $N_x \approx 0.20$ and $N_y = N_z \approx 0.40$.

Now the dimensions and the depolarization factors of the particle are known, but the permittivity of the object has to be calculated. An estimation for the permittivity can be evaluated from the measured polarizabilities for dsDNA presented in [153], by applying additional simplifications. First, one has to reduce the complex permittivities into real ones and second, treat the medium simply as water ($\epsilon_m = \epsilon_{\text{water}} \approx 7.1 \cdot 10^{-10}$ F/m). Furthermore, if one chooses a dsDNA molecule, which is long enough to be a truly rod-shaped object (on the other hand, the longer the molecule, the more complex the tertiary structures can be), the calculation becomes easier, because the polarization is remarkable only in x-direction and the depolarization factors have the simple form of (0, $\frac{1}{2}$, $\frac{1}{2}$). Here, a 444 bp long dsDNA molecule in solution, with the polarizability ca. $8 \cdot 10^{-32}$ Fm^2, was chosen for the reference. After using Eq. (2.19) and some algebra, the permittivity of DNA and the surrounding ion cloud can be expressed as $\epsilon_p \approx 2.6 \cdot 10^{-9}$ F/m. With this result one obtains a handy formula for the polarizability

$$\alpha_i \approx \frac{\epsilon_{\text{water}} V}{0.38 + N_i}. \tag{2.20}$$

Substitution of the depolarization factors and the volume of the prolate in Eq. 2.20 yields the following effective polarizability components for a 40 nt oligonucleotide

$$\begin{cases} \alpha_x \approx 5.4 \cdot 10^{-33} \text{ Fm}^2 \\ \alpha_y = \alpha_z \approx 4.0 \cdot 10^{-33} \text{ Fm}^2. \end{cases}$$

Smiley DNA origami

The smiley DNA origami trapped in **A.I** has a diameter of 105 nm and a height of about 2 nm. Since origamis can be treated as complexes of many parallel dsDNA molecules (see Sec. 1.2.2), one can use 10 nm for the thickness of the counter-ion cloud, and thus the object can be approximated by an oblate with semi-axes $a_x = a_y$ = 62 nm and a_z = 11 nm. According to Eq. 2.17 and 2.18 the depolarization factors are

$N_x = N_y \approx 0.11$ and $N_z \approx 0.77$. The polarizability components for a smiley origami can be calculated similarly as above from Eq. 2.20:

$$\begin{cases} \alpha_x = \alpha_y \approx 2.6 \cdot 10^{-31}\ \mathrm{Fm}^2 \\ \alpha_z \approx 1.1 \cdot 10^{-31}\ \mathrm{Fm}^2. \end{cases}$$

Rectangular DNA origami

The rectangular DNA origami (see **A.I** and **A.II**) with a surrounding ion cloud can also be approximated by an ellipsoid (scalene). The area of a rectangular is 98 nm $\times$ 71 nm and the height of the origami is 2 nm. Thus, a rough estimate for the shape of the object is an ellipsoid with semi-axes a_x = 59 nm, a_y = 45 nm, a_z = 11 nm and since all the axis lengths are different from each other, the depolarization factors have to be evaluated numerically. By substituting the obtained factors $N_x \approx 0.11$, $N_y \approx 0.16$ and $N_z \approx 0.74$ in Eq. 2.20, one gets the polarizability components for a rectangular origami

$$\begin{cases} \alpha_x \approx 1.8 \cdot 10^{-31}\ \mathrm{Fm}^2 \\ \alpha_y \approx 1.6 \cdot 10^{-31}\ \mathrm{Fm}^2 \\ \alpha_z \approx 7.8 \cdot 10^{-32}\ \mathrm{Fm}^2. \end{cases}$$

TX tile construct

This consideration is similar to above-mentioned origamis with the same assumptions. Now the dimensions of the DNA construct are $\sim$ 10 nm $\times$ 60 nm (see **A.III**), i.e. the semi-axes of the ellipsoid (scalene) are a_x = 40 nm, a_y = 15 nm, a_z = 11 nm. With these parameters one can obtain the following depolarization factors $N_x \approx 0.10$, $N_y \approx 0.37$ and $N_z \approx 0.52$ and therefore the polarizability components are

$$\begin{cases} \alpha_x \approx 4.1 \cdot 10^{-32}\ \mathrm{Fm}^2 \\ \alpha_y \approx 2.6 \cdot 10^{-32}\ \mathrm{Fm}^2 \\ \alpha_z \approx 2.2 \cdot 10^{-32}\ \mathrm{Fm}^2. \end{cases}$$

Quantum dot

For the CdSe/ZnS quantum dot with the core diameter of $\sim$ 10 nm in de-ionized (DI) water (see **A.IV**), one can simply use the estimation $\alpha_i/\epsilon_0 = 2.8 \cdot 10^{-23}$ m^3 determined from an optical trapping experiments of QDs [69]. Thus, by multiplying

the given value with the permittivity of vacuum, the polarizability components for a spherical QD are

$$\alpha_x = \alpha_y = \alpha_z \approx 2.5 \cdot 10^{-34}\ \mathrm{Fm}^2.$$

Discussion

As seen in the results calculated in this section, the volume of the particle significantly contributes to the magnitude of the polarizability. Compared to origamis, the polarizability component of an oligonucleotide is less than one tenth of any component of origamis (40-60 times lower), whereas the components for the TX tile constructs are only 3-6 times smaller. According to these estimations, the polarizability of a QD mentioned above is really low in contrast to origamis (700-1000 times smaller). In addition, the polarizability of a smiley DNA origami is a bit higher than for rectangular origami due to the slightly distinct dimensions of the structures. Both origamis and TX tile constructs have a substantial direction-dependence in their polarizabilities. For origamis the polarizability component in x and y direction is over two-fold compared to the one in z direction, and in the case of TX tile construct the polarizability component in x direction is almost two times as large as in y and z directions. The results of DEP trapping are presented and discussed in Chapter 5.

Chapter 3

Impedance Spectroscopy

3.1 Motivation and general aspects

Commonly, impedance spectroscopy (IS) is used in fundamental and applied electrochemistry and in materials science. It can be utilized in studying the dynamics of charge (mobile or bound) in bulk or interfacial regions of any kind of material (solid or liquid): ionic, semiconducting, electronic-ionic and insulators. This chapter deals with electrochemical impedance spectroscopy (EIS), focusing on alternating-current impedance spectroscopy (AC-IS) and its key elements relevant to the articles **A.II** and **A.III** of this thesis. In these articles AC-IS has been used in characterization of the conductivity mechanisms of DEP-trapped and immobilized DNA constructs. The discussion in this chapter is based on Ref. [9] unless otherwise mentioned.

In EIS measurement an investigated sample, typically located between two similar electrodes, is excited by a voltage/current signal and then a current/voltage response is detected. The basic idea is to measure the frequency dependent electrical impedance of the sample and model the response. The most common way to find out the impedance of the system is to feed a sample with a monochromatic voltage signal [$V = V_0 \sin(\omega t)$, where V_0 is an amplitude, ω is an angular frequency of a signal and t is time] and measure an amplitude (I_0) and a phase difference (θ) of a current [$I = I_0 \sin(\omega t + \theta)$] within a desired frequency range (possible range may extend over 12 orders of magnitude, i.e. from 10 μHz to 10 MHz or even higher frequencies [103]). This yields a complex impedance as a function of a frequency for linear, causal and stationary systems $Z(j\omega) = V(j\omega)/I(j\omega)$ (V is a complex voltage, I is a complex current and j denotes the imaginary unit). For systems without discrete components the impedance can be expressed by means of Fourier transforms ($\mathcal{F}$) of voltage (V) and current (I): $Z = \mathcal{F}\{V(\omega t)\}/\mathcal{F}\{I(\omega t)\}$.

With AC-IS one can separate influences of the individual components to the response from each other, i.e. the characteristics of the investigated material (conductivity, dielectricity, mobilities of the charge carriers etc.) and the properties of the electrode-material interfaces (capacitance, diffusion constants, chemical reaction

rates etc.) can be segregated. Therefore, AC-IS is precisely suitable for studying conductivity mechanisms of various molecules, such as DNA, since the method implicitely enables taking into account the crucial role of electrode-molecule contacts and the environmental factors.

3.2 Cole-Cole plot and equivalent circuit

As stated above, in AC-IS the measured data consists of a complex impedance as a function of frequency of the excitation signal, and thus the measurement yields a set of points in a three-dimensional space (ω, Re Z, Im Z): ω is an angular frequency of the signal and Re Z and Im Z are real and imaginary parts of the impedance, respectively. The data can be expressed as a 2D plot, so-called Cole-Cole plot (or Nyquist plot), where -Im Z is presented as a function of Re Z, and frequency is an implicit variable (also 3D perspective plotting can be used to illustrate the behavior of all three variables simultaneously [104]). Another common way to present the measured data is to use Bode plots: the absolute value of the impedance and a phase difference are plotted against logarithmic frequency.

An equivalent electric circuit (EEC) is a (theoretical) model/method, which is used for fitting the measured data by using CNLS-method (complex nonlinear least squares). A typical equivalent circuit model is comprised of linear components (ideal resistors, capacitors and coils) and also non-linear elements (the investigated system is often nonideal). For example, an ideal resistor can describe e.g. a step in a chemical reaction or ohmic charge transport through a channel, and capacitors / coils can model e.g. chemical layers or polarization and absorption phenomena. Non-linear components can be used to explain e.g. nonideal surfaces of the electrodes or a combination of various phenomena such as polarization and transport (diffusion). Usually the measured data can be fitted with several different EECs and thus, the physical interpretation of the components in a system is not straightforward, and frequently it is also quite demanding.

3.3 Constant phase element and Warburg impedance

Influences of microscopic nonidealities (surface roughness, local inhomogeneous charge distributions etc.), distributions of activation energies and time constants of parallel chemical reactions in a studied system can be described in macroscopic scale by a distributed element (averaged influence of all parallel microscopic phenomena). This element is called a constant phase element (CPE), and its impedance has a form

$$Z_{\mathrm{CPE}} = \frac{1}{Q_{\mathrm{CPE}}(j\omega)^{n},} \tag{3.1}$$

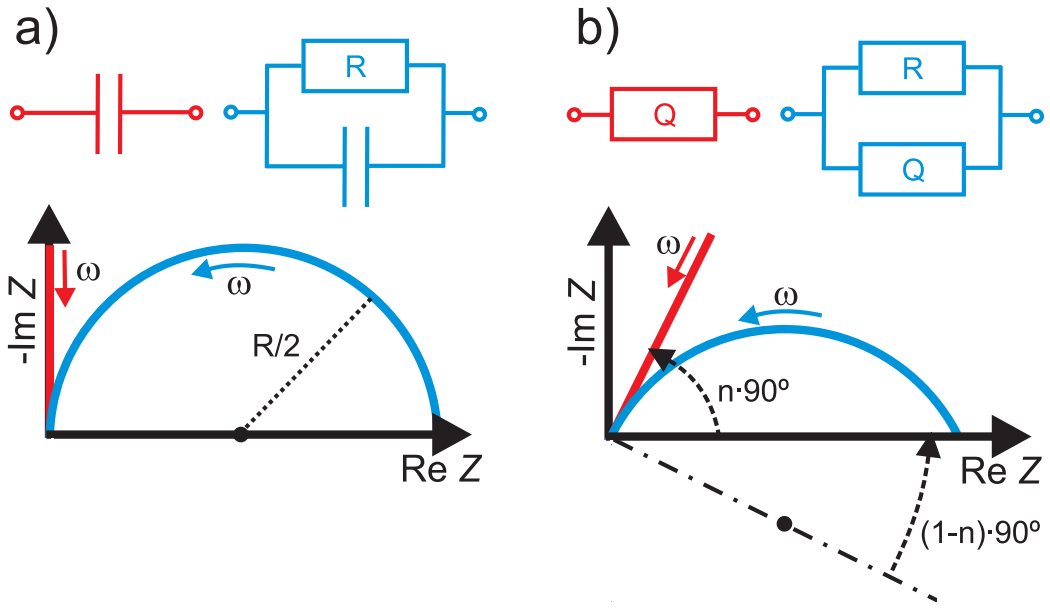

FIGURE 3.1 a) A schematic Cole-Cole plot of a plain capacitor (straight line) and a parallel combination of a resistor and a capacitor (semicircle with a radius of $R/2$). b) The impedance spectra change when a capacitor is replaced with a CPE. A Cole-Cole plot produced by a single CPE is a straight line at an angle of $n \cdot 90°$ with respect to the Re Z axis (n is an exponent of CPE, see Eq. 3.1). A combination of CPE and a resistor in parallel forms a semicircle, of which center lies on the axis tilted $(1-n) \cdot 90°$ with respect to the Re Z axis. Arrows indicate the direction of increasing frequency.

where Q_{CPE} is a constant and $n \in [-1,\ 1]$. If $n = 0$, CPE reduces to an ideal resistor, if $n = 1$, CPE is a capacitor, and if $n = -1$, CPE describes a coil, i.e. inductance. Schematic Cole-Cole plots of a single capacitor/CPE, and a capacitor/CPE in parallel with a resistor are illustrated in Fig. 3.1.

In electrochemistry, one special case of CPE is an infinite-length Warburg (one-dimensional diffusion of a particle in a semi-infinite space), which can be obtained from the solution of Fick's second law (diffusion in x-direction):

$$\frac{\partial c}{\partial t} = D\frac{\partial^2 c}{\partial x^2}, \tag{3.2}$$

where c denotes concentration and D a diffusion coefficient of diffused material. The infinite-length Warburg impedance (long diffusion lenght, low frequencies) can be written as

$$Z_{W,\infty} = \frac{1}{Q_W\sqrt{j\omega}} = \frac{1}{Q_W\sqrt{\omega}}(1-j), \tag{3.3}$$

where Q_W is a constant. Since the Warburg impedance is a special case of CPE with $n = \frac{1}{2}$, it produces a straight line in a complex plane pointing at an angle of 45° with respect to both impedance axes. Its influence can be distinguished usually in a Cole-

Cole plot as 'a low frequency tail', since in the most of the cases in high-frequency region the large particles can not follow the electric field due to the high inertia (see Fig. 3.3).

In this thesis the diffusive element is always assumed to have a form of infinite-length Warburg (long diffusion length), but there also exists a more general form of diffusion, which can be used to describe limited/restricted diffusion. When a diffusion length is short, the impedance of a so-called finite-length Warburg is given by

$$Z_W = \frac{1}{Q_W\sqrt{j\omega}}\tanh\left(C_W\sqrt{j\omega}\right), \tag{3.4}$$

where Q_W and C_W are constants. From this equation one can see that when C_W is large, Z_W simply yields the infinite-length impedance, $Z_{W,\infty}$ [if $A \to \infty$, $\tanh(A\sqrt{j})$ $\to 1$].

The form of the diffusion depends on several factors and it is often very hard to define exactly. For example, in the case of diffusion related redox reactions, Q_W is dependent on concentrations and diffusion constants of oxidized and reduced forms of materials, temperature and a surface area of an electrode used. Instead, C_W is proportional to a thickness of diffusion layer and inversely proportional to the average value of diffusion coefficients of diffused materials.

3.4 Randles circuit

3.4.1 Common model

A so-called Randles circuit [129] is one of the most common EECs exploited in the interpretation of electrochemical impedance spectra and it is usually a starting point in analysis of many complex systems. The basic form of the Randles circuit describes a charge transfer process occuring at an electrode-material interface (typically in solution). The interface is presented as a combination of a so-called double-layer capacitance, which is formed by ions surrounding the electrode in solution due to Coulomb attraction, and a charge transfer (CT) resistance denoting redox reaction(s) at the electrodes or direct charge transfer from the electrode to the material or solution. Furthermore, the model can also take into account diffusion of materials (reagents or products) to the electrodes, if a diffusive Warburg element is incorporated into the circuit in series with a CT resistance. A full block describing the interface is assembled by adding a capacitor (double-layer capacitance C_{dl}) in parallel to a resistor (charge transfer resistance R_{ct}) and a Warburg element (impedance Z_W). The actual circuit is formed by adding a resistor (R_{s}), denoting a resistance of an electrolyte / solution of the cell, in series with the interface block. The configuration of elements in the full Randles circuit is presented in Fig. 3.2 and a schematic Cole-Cole plot produced by the circuit is illustrated in Fig. 3.3.

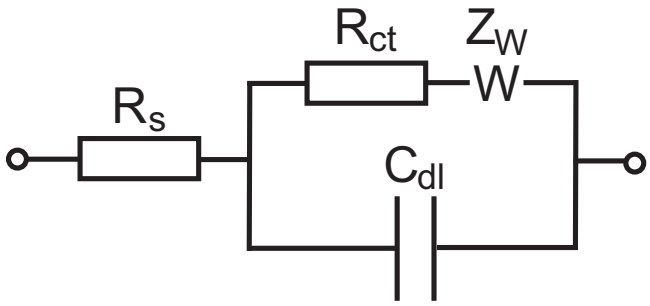

FIGURE 3.2 A full Randles equivalent circuit [129]. A solution can simply be described by the resistance of an electrolyte (R_{s}) and the electrode-material /electrode-electrolyte interface is comprised of capacitance of a double-layer (C_{dl}), the charge-transfer resistance (R_{ct}) and a Warburg element W (with the impedance Z_W). In some cases, a cell without a Warburg impedance is also called a Randles circuit.

In an ideal case, where the interface is simply expressed only in terms of a capacitor and a resistor, the time constant (τ) of a charge transfer can be calculated by multiplying obtained values of these elements with each other, i.e. $\tau = RC$. However, as already mentioned, the interface is rarely ideal, and thus the rates of chemical reactions at different locations of the electrode can diverge from each other significantly (i.e. an electrochemical activation energy might not have the same value at all points on an electrode surface). Accordingly, in a fitting procedure the capacitor and also the possible Warburg element of the Randles EEC are frequently replaced with more general CPEs due to the distribution of time constants in charge transfer processes. Then the averaged time constant can be calculated using a relation $\tau_{\mathrm{eff}} = (R_{\mathrm{eff}} Q_{\mathrm{CPE,eff}})^{\frac{1}{n}}$ [15], where R_{eff} and $Q_{\mathrm{CPE,eff}}$ are the effective components producing a truncated semicircle in a Cole-Cole plot (see Fig. 3.1b).

3.4.2 DNA conductivity / hybridization models

The Randles circuit is most often used in characterization of an electrolyte-electrode interface and its modifications in the redox-probe based experiments. These experiments are carried out in a three-electrode cell, where one electrode serves as a reference electrode (constant potential, lies in an electrolyte) and the other two act as a working electrode (e.g. investigated material on top of it) and a counter-electrode. This setup can be utilized for characterization of conductance related properties of DNA molecules on the working electrode, and therefore also for detecting the influence of DNA hybridization or metallization to the impedance spectrum (see e.g. Refs. [56,68,92,100,120]). The starting point of this kind of experiment is to measure the (control) impedance spectrum of a cell where a working-electrode is totally uncoated or coated with ssDNA molecules (DNA attached either via a self-assembled monolayer of linker molecules or directly via sulphur-modification). This step is

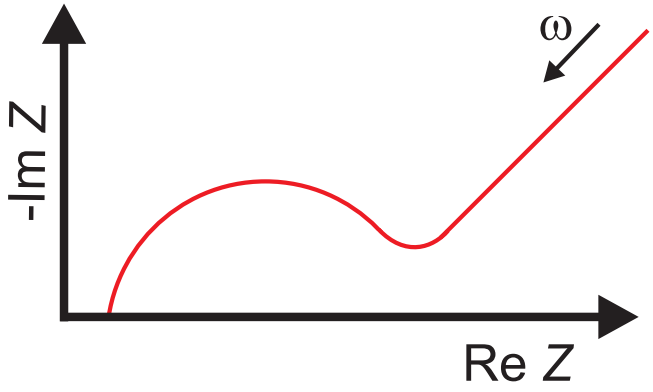

FIGURE 3.3 A schematic Cole-Cole plot produced by the full and ideal Randles circuit. The parallel combination of C_{dl} and R_{ct} forms a semi-circle, of which center is shifted along the Re Z axis by the amount of the resistance of an electrolyte, R_{s}. The Warburg impedance is dominating at low frequencies: the diffusion is seen as 'a low-frequency tail' at an angle of 45° with respect to Re Z axis. The arrow indicates the direction of increasing frequency.

followed by the measurement of the impedance spectrum after the immobilized ssDNA molecules have hybridized with fully or partially complementary DNA strands. Finally, the comparison of measured responses, i.e. comparison between control sample and after hybridization samples is carried out and consequently, data fitting with relevant EEC models (typically a simple or modified Randles circuit) including the analysis of the variation of key parameters between the samples is performed. For example, a value of a double-layer capacitance is different due to the variation of total amount of charges between samples, or charge transfer resistance can be changed, since the charge transport through/along hybridized dsDNA is different in contrast to the case of immobilized ssDNA molecules. It is conventional that influence of DNA is modeled as a parallel resistance beside the double-layer block.

In the articles **A.II** and **A.III** of this thesis, the conductivity mechanisms of a single DNA construct (DEP-directed and chemically immobilized between two opposite nanoelectrodes on a silicon oxide substrate) placed in a high humidity environment, were characterized by exploiting the AC-IS methods. The steps of exploring the model and the parameters of elements were analogous to the ones mentioned above, but here the measurement was carried out by utilizing a four-probe setup. The influence of the control sample, i.e. an empty sample containing only an electrode structure and ions (adsorbed water and salt from the DEP trapping buffer) to the AC-response was first characterized by adopting the Randles circuit presented above with a couple of modifications: the double-layer did not contain the Warburg element, but the additional Warburg impedance denoting the diffusion of ions along the substrate was added in parallel to the resistance R_{s} describing

the solution/electrolyte. In the sample used, both the electrodes were covered by a double-layer of ions and these 'electrolyte'-electrode interfaces (in series), i.e. parallel combinations of CT resistance and CPE, could be considered to be equivalent to each other. Thus, these both interfaces were described by only one interface block similarly as in a Randles circuit modeling. When the DNA construct was bridging the gap between the electrodes, the total resistance between electrodes was lowered, diffusion was enhanced, and obviously DNA also modified the double-layer part via a chemical connection to the electrodes (DNA-electrode interface formed at the electrodes). The results, EECs and the measurement setup used are discussed in more detail later in Chapter 6.

Part II

Results

Chapter 4

Design and fabrication of DNA constructs

4.1 DNA origami fabrication

In order to demonstrate DEP trapping and immobilization of DNA origamis (**A.I**) and furthermore characterize the electrical conductivity of a single origami (**A.II**), two types of origami shapes were fabricated: smiley (105 nm in diameter) and rectangular origami (98 nm $\times$ 71 nm). These designs were adapted from Ref. [134] and also fabricated similarly, i.e. by thermal annealing treatment (Bio-Rad MyCycler PCR machine) for 50 µl of solution containing 10 nM single-stranded viral DNA from the M13mp18 virus (New England Biolabs) as a scaffold and a 10-fold excess concentration of staple strands (purchased unpurified with 150 nM concentration from Integrated DNA Technologies). In addition, T4 Polynucleotide Kinase (New England Biolabs, M0201S) was used for adding phosphate to the 5' end of the staple strands to enable the subsequent ligation procedure (for the detailed components and their amounts, see Table 4.1). In the annealing procedure the solution was first heated up to 37 °C and kept at this temperature for one hour to activate the kinase enzyme reaction. Then the solution was heated to 90 °C and after that cooled to 20 °C at the rate of 1 °C/min. Staple strands along the edges of origamis were left out to prevent the aggregation due to the stacking interaction. Two thiol-modified oligonucleotides (5ThioMC6-D and 3ThioMC3-D, purchased unpurified at 100 nM scale from IDT DNA technology, see Materials and methods in Appendixes) were incorporated in the middle of each side of the origami to allow the attachment to the gold electrodes through sulphur-gold bonding.

After annealing, the origami samples were ligated at the room temperature (see Table 4.2) using T4 DNA Ligase enzyme (New England Biolabs, M0202S) in T4 DNA Ligase reaction buffer (New England Biolabs, B0202S) to catalyze the formation of phosphodiester bonds between adjacent 5'-phosphates and 3'-hydroxyl termini of the staple strands in a formed duplex DNA. This process is known to in-

TABLE 4.1 Amounts of components for the DNA origami fabrication in the order of mixing.

Component	Amount (rect.) [μl]	Amount (smiley) [μl]
10× TAE Mg++ buffer	5.0	5.0
Distilled water	19.7	18.5
10× T4 DNA Ligase reaction buffer	5.0	5.0
M13mp18 virus (0.93 nM)	5.4	5.4
Staple strand mix	(0.78 μM) 6.9	(0.67 μM) 8.1
Thiol-modified side strands (1 μM)	5.0	5.0
T4 Polynucleotide Kinase	3.0	3.0

TABLE 4.2 Amounts of components for the ligation procedure in the order of mixing.

Component	Amount [μl]
Distilled water	67.0
10× TAE Mg++ buffer	9.0
10× T4 DNA Ligase reaction buffer	9.0
Annealed DNA origami solution	10.0
T4 DNA Ligase	5.0

crease thermal and mechanical stability of the DNA structures [118]. As a final step of the origami solution preparation, the buffer used for origami annealing [Tris-Acetate-EDTA (TAE) with 12.5 mM magnesium acetate, pH 8.1 and conductivity about 3.5 mS/cm] was changed to a Hepes/NaOH-based buffer of lower conductivity (6.5 mM Hepes, 2 mM NaOH, 1 mM magnesium acetate; conductivity ca. 300 μS/cm) using spin-filtering (Millipore Microcon YM-100 filter with a cutoff of 100 kDa), which should also wash out excess T4 DNA Ligase and glycerol from the ligation procedure (for detailed description of spin-filtering, see Materials and methods in Appendixes). The spin-filtering process was crucial to the DEP experiments, since the conductivity of the solution has to be well below 1 mS/cm for a successful trapping [150]. After the spin-filtering, the final concentration of origamis was about 1 nM. Origamis were stable at least for a week in the low conductivity buffer when stored at room temperature. An AFM image (Veeco Dimension 3100, Nanoscope IV, liquid tapping mode) of the fabricated smiley and rectangular origami is presented in Fig. 4.1.

4.2 TX tile construct fabrication

For studying the conductivity properties of also smaller DNA templates and subsequently using these constructs as parts of potential nanodevices, a defined-sized TX tile -based construct was designed (**A.III**). The 14 different strands forming the tiles

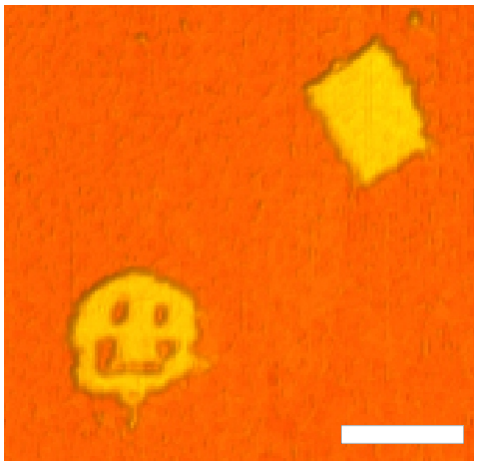

FIGURE 4.1 An AFM image of a smiley and a rectangular DNA origami on a mica surface. The image has been taken by using the liquid tapping mode (1× TAE Mg++ buffer as the imaging environment) after spin-filtering the origamis. The scale bar is 100 nm. Adapted with permission from **A.I**.

A and B were chosen in such a way that only a finite-size complex (length 167 bases) of tile B - tile A - tile B (see Fig. 4.2a and b) was able to assemble instead of infinite arrays of earlier designs [88, 93]. The majority of the DNA sequences were adopted from previously published structures [93, 121], and modified where necessary (e.g. the biotinylated hairpins were removed). The change of the sequence symmetry and undesired complementarity was minimized by using M-fold web server [2, 180].

To fabricate such a structure only three different kinds of 8 nt long sticky ends were symmetrically used in the tile A, i.e. a, b and c (see the color codes of sticky ends in Fig. 4.2a). This enables the rotation of 180 degrees of tile A, still having the sticky ends at the same orientation in the both ends. Accordingly, the tile B had complementary sticky ends a', b' and c' at one end. The sticky ends d (12 nt) at the other end of the tile B had identical sequences and therefore they could be assembled with complementary strands d' containing thiol-groups at the 5′ end. The thiol-modifications were added to the tile B for the purpose of the forthcoming DEP-immobilization of the constructs to the gold nanoelectrodes via sulphur-gold bonding [5′ Thiol Modifier C6 S-S (Disulfide) was incorporated into the one specific strand, purchased from Integrated DNA Technologies, IDT Coralville, Iowa, whereas other strands were ordered from Biomers GmbH, Ulm, Germany]. The construct was designed in such a way that the tiles B were enabled to assemble to the both ends of the tile A. For this, all the sticky ends were designed to have the specific distance from the nearest crossover point at the both ends, and the suitable space between the crossover-points (1.5 turns of double-helices) of adjacent tiles was taken into account to prevent twisting stresses at the junctions. The detailed sequences of the strands and the map of the design are presented in Appendixes (Materials and

TABLE 4.3 Amounts of components in 'a master mix' for the kinase treatment.

Component	Amount [μl]
40 mM Tris, 1 mM EDTA, 19 mM HAc, 500 mM MgAc	5.8
40 mM Tris, 1 mM EDTA, 19 mM HAc	0.8
10× T4 DNA Ligase reaction buffer	23.0
T4 Polynucleotide Kinase (10,000 U/ml)	0.5

TABLE 4.4 Amounts of components in the reaction solution.

Component	Amount [μl]
All B-A-B complex strands (pretreated with master mix)	(in total) 260.0
40 mM Tris, 1 mM EDTA, 19 mM HAc	7.0
40 mM Tris, 1 mM EDTA, 19 mM HAc, 500 mM MgAc	1.0
10× T4 DNA Ligase reaction buffer	30.0
T4 DNA Ligase (400,000 U/ml)	2.0

methods).

The stability of the complex was improved by modifying each strand of the complex (except the one with the thiol-modification) separately with T4 kinase followed by the ligation procedure (T4 DNA ligase) after annealing the complexes. In a kinase treatment procedure (37 °C), 10 μl of 'A-strand' solution (10 μM), i.e. the strands that form the tile A, was mixed with 1.5 μl of 'a master mix' (see Table 4.3). For the 'B strands', i.e. for the strands that form the tile B, the amounts were duplicated, and also the thiol-modified strand was diluted to the same final concentration. The fabrication procedure was similar to the origamis: the complexes were formed by heating the strand mixture (see Table 4.4) up to 90 °C and cooling it down to 20 °C at a rate of 0.01 °C/s in a PCR-machine (Biometra GmbH, Goettingen, Germany) (see Materials and methods in Appendixes). To achieve appropriate stoichiometric concentration of each tile, the T4 kinase modified strands were mixed by using two-fold amount of 'B strands' compared to 'A strands'. Furthermore, three-fold amount of 5' thiol-modified strands compared to B strands were used in order to hybridize them with each sticky end d. The theoretical concentration of obtained complexes was 0.29 μM of tile A (A strands) and 0.58 μM of tile B (B strands).

4.3 TX tile construct decoration

In order to show that the TX tiles can be used in assembling of materials and therefore as templates for nanofabrication, simple biotin functionalization (one biotin per TX tile) and a following streptavidin decoration of tiles was demonstrated (the method demonstrated here for a regular for TX tiles can easily be extended to the finite-sized TX tile constructs). Same kind of biotinylated TX tiles [93] and so-called

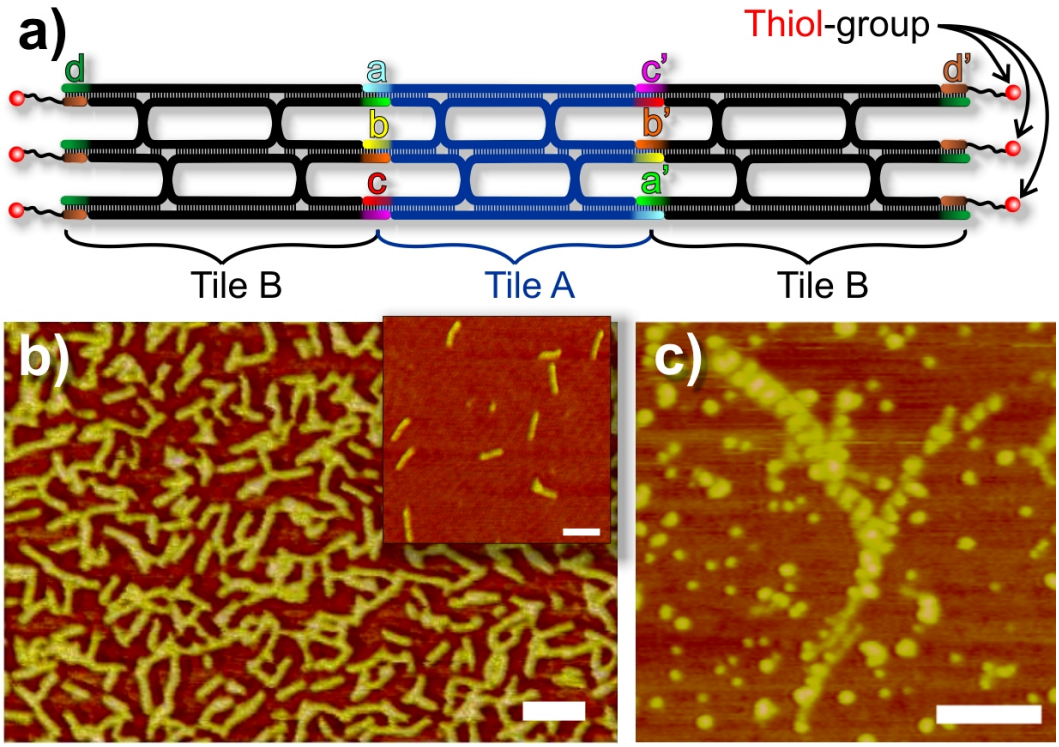

FIGURE 4.2 TX tile construct design and decoration. a) Schematic picture of the B-A-B -complex. The tiles are conjugated together via the sticky end pairing ($a - a'$, $b - b'$ and $c - c'$). The thiol-modified strands d' are paired to the B tiles via sticky ends d. b) AFM images of TX tile constructs dried on a mica surface. c) An AFM image of chained biotin-TEG functionalized TX tiles decorated with streptavidin. The scale bars are 100 nm. The image is adapted from **A.III**.

4 × 4 tiles [171] have previously been decorated with streptavidin, but with two biotins (per streptavidin) in each hairpin.

Here, TX tiles were fabricated by utilizing the same strands as in Ref. [93] (purchased from Biomers GmbH) with one strand containing a biotin attached to a 15-atom flexible triethylene glycol (TEG) spacer to optimize the streptavidin binding (strand 3, TAG Copenhagen, Copenhagen, Denmark) (see Materials and methods in Appendixes). This kind of linker was used for functionalization since the length of the linker/spacer is assumed to have an influence to tight biotin binding as reported in Refs. [53, 106]. TX tiles were formed (without ligation) by means of the heating and cooling procedure described above for the B-A-B complexes, and the full reaction mixture is presented in Table 4.5.

The final concentration of each strand (7 different strands), as well as TX tiles, were 1 μM. In the mixing of streptavidin with TX tiles, the concentration ratio 1 μM : 1 μM (TX tile : streptavidin) was used. After adding streptavidin to the TX tile solution, the mixture was incubated overnight at 4 °C. In order to verify the success in decoration a sample of 5 μl of streptavidin decorated TX tiles was pipetted onto

TABLE 4.5 Amounts of components in the reaction mix for biotin functionalization.

Component	Amount [μl]
TX tile strands 1-7 (10 μM each)	(in total) 140.0
20 mM Tris (pH 7.6), 2 mM EDTA	55.0
20 mM Tris (pH 7.6), 2 mM EDTA, 500 mM $MgCl_2$	5.0

a mica surface for 3 min (at the room temperature), gently dried under nitrogen stream followed by washing with 10 μl of deionized water and drying again with nitrogen, and finally the dry sample was imaged with AFM. An example of successful binding of streptavidin to TX tiles (TX tile chain) is shown in an AFM image in Fig. 4.2c. The result indicates that the designed structure could be utilized in arranging of proteins, and thus, also for other molecular scale patterning purposes efficiently.

Chapter 5

DEP studies

5.1 Sample preparation

5.1.1 Fabrication of nanoelectrode structures

In order to trap DNA constructs, ssDNA molecules and quantum dots by DEP, several different types of gold nanoelectrodes were utilized in the experiments. Most of the structures involved two opposing fingertip-type electrodes with varying widths (20-170 nm) and 50 - 140 nm constriction between them, but also samples with eight 20 - 30 nm wide electrodes were used (see Fig. 5.1). The fabrication of all electrode structures presented in this thesis is based on the standard electron beam lithography (EBL) technique.

The starting point for processing electrode structures in all the reported experiments is the fabrication of an insulating layer of silicon dioxide (SiO_2) on a slightly boron-doped (100)-silicon substrate by atmospheric pressure CVD with oxygen flow at 1100 °C (QD trapping in the article **A.IV** is the only exception, the substrate used in that work was silicon covered with LPCVD fabricated silicon nitride layer). For the lithography process, a 2 % solution of polymethyl methacrylate resist in anisole (Microchem A2 950 PMMA) was spin-coated on a SiO_2 surface with a rate of 2000 rpm followed by a 5 min baking on a hot plate (160 °C). The resist was exposed by an e-beam writer (Raith e-LiNE with Elphy Quantum 4.0 -lithography software) in order to pattern the desired electrode structure. The exposed resist was developed by immersion in a solution of methyl isobutyl ketone (MIBK) and isopropanol (IPA) (1:3 v/v) for 30 seconds at the room temperature (22 °C). The development was stopped by rinsing with IPA, and after that the sample was dried with a nitrogen flow.

The revealed SiO_2 surface was cleaned using a reactive ion etcher (Oxford Plasmalab 80 Plus RIE) before evaporation of metals. In the RIE cleaning, organic undeveloped resist residues from the mask openings were removed by a short oxygen plasma flash with the following parameters: oxygen flow 50 sccm, RF power 15 W

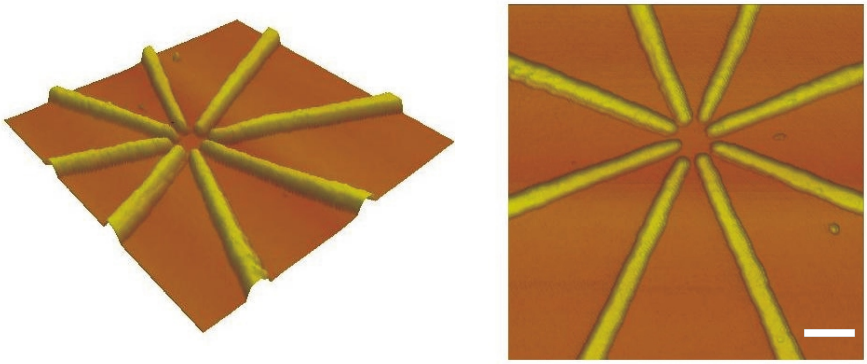

FIGURE 5.1 AFM images of a prepared electrode structure containing eight narrow gold nanoelectrodes. The area between the heads of the electrodes is ca. 95 nm $\times$ 80 nm. The scale bar is 100 nm.

and time 10 seconds. This step was crucial especially to the processing of narrow electrodes; the conductivity of 20 nm wide gold nanoelectrodes was increased by four orders of magnitude, while the patterned lines widened only about 5 nm. The evaporation of gold and titanium (titanium is assumed to improve the adhesion of gold) was performed in an ultra-high vacuum (UHV) chamber under the pressure of $\sim 10^{-8}$ mbar. The thickness of the evaporated layer of titanium was about 2 nm and it was topped with a 12-18 nm thick gold layer. After evaporation, the sample was immersed in hot acetone for an overnight lift-off procedure and finally shortly sonicated and rinsed with IPA. Just before the DEP experiments, the residues from the lift-off were removed by an oxygen plasma flash in the RIE process (50 sccm oxygen flow, 25 W RF power and 1 min time). This process also made the SiO_2 surface hydrophilic, which greatly helped in DEP experiments.

5.1.2 Electric field, DEP force and DEP potential simulations

To obtain some theoretical basis for the trapping, the electric fields and thereafter the DEP forces (the gradient of the square of the electric field) were simulated by the finite element method (FEM) (software COMSOL Multiphysics 3.3a) for the basic electrode structure geometries used in this work.

Geometry and physics of the modelling of the electric fields are based on the simulations done in Refs. [153, 155]. The substrate was simply treated as a 200 nm thick layer of SiO_2 with the relative permittivity of 3.6, under which there was a 800 nm thick silicon layer (relative permittivity 11.8). The buffer on top of the substrate was approximated to be a water layer with a thickness of 1 μm (relative permittivity 80), which is a good estimation for dilute Hepes/NaOH based buffer used in DEP trapping experiments. The electrodes in the water layer were considered as holes covered by equipotential surfaces. With the method used, the time-dependent

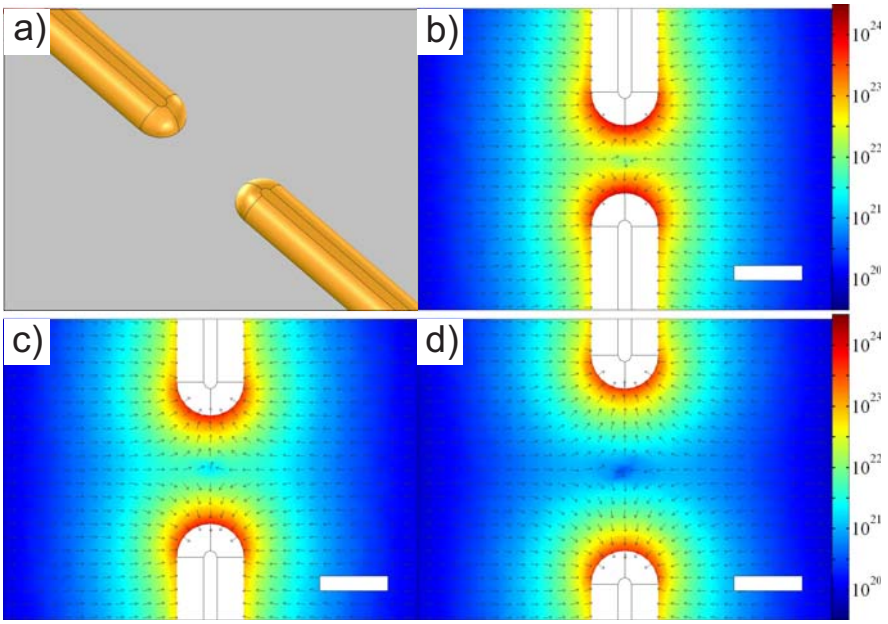

FIGURE 5.2 Simulated time-averaged DEP force, the gradient of the square of the electric field (SI-units: V^2/m^3) to be exact, for the narrow fingertip type electrodes with 2 V DC voltage. In a) the model of the electrodes is presented. b), c) and d) show the electrode configuration with the gap size of 50 nm, 80 nm and 120 nm, respectively. The scale bar in each figure is 50 nm. The simulations were carried out by Kimmo Laitinen.

simulations were not possible, and therefore only a constant voltage difference was applied to the electrodes. However, according to Eq. 2.8, by replacing a sinusoidal AC signal in question with its rms-value, the simulation yields the correct time-averaged DEP force. In the simulations, the potential was solved on the grounds of Poisson's equation and thereafter the electric field was calculated. In Fig. 5.2, the gradient of the square of the electric field (proportional to the DEP force) is simulated in the case of narrow electrodes (width 20 nm) (articles **A.I**-**A.III**), and in Fig. 5.3 the simulated trapping potential for 40 nt ssDNA molecules (**A.V**) is presented in the vicinity of the gap of the 100 nm wide fingertip-type electrodes. The polarizability of the oligonucleotide ($\alpha = 2 \cdot 10^{-33}$ Fm^2) was estimated from the measurements reported in Ref. [153].

The structure presented in Fig. 5.2 has two 20 nm wide and 20 nm high gold electrodes on the substrate. The edges of the electrodes were rounded to get a more realistic model for the lithographically fabricated electrodes. As seen from the images, the maximum of the electric field as well as the maximum of the DEP force occur at the end of the electrodes and the magnitudes of these maxima are not dependent on the gap size in this scale. However, the minimum value in the middle of the gap is the smaller the longer is the distance between the electrodes.

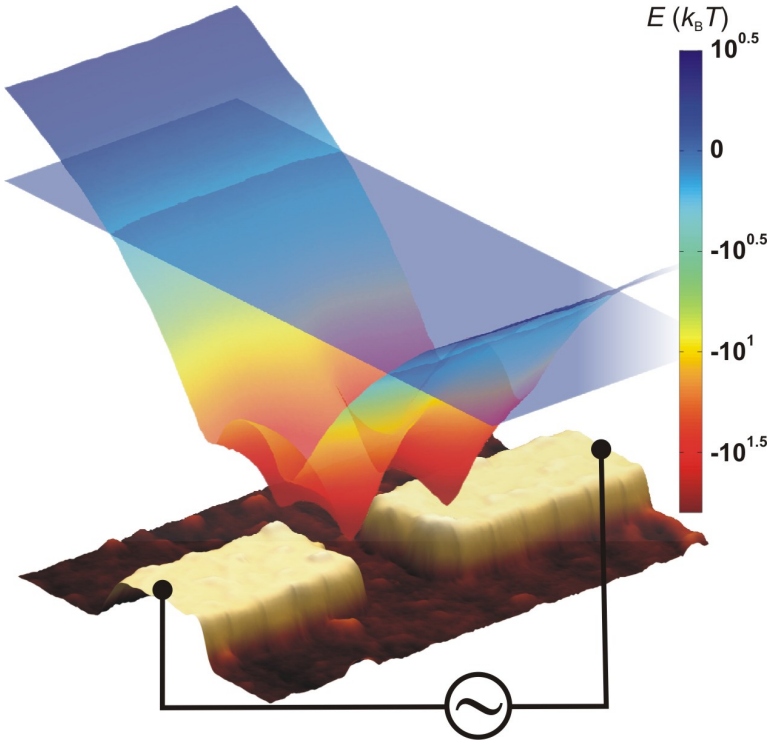

FIGURE 5.3 Simulated time-averaged DEP trapping potential, $U_{\mathrm{DEP}} = -\frac{1}{2}\alpha E^2$, (color coded surface) in the vicinity of 100 nm wide fingertip-type electrodes (shown as an AFM image) for 40 nt ssDNA molecules. Potential is calculated at the plane just above the electrodes, i.e., about 25 nm above the substrate. Trapping area is the region where the absolute value of the DEP potential is higher than the thermal energy of DNA, i.e., where the potential is below the flat horizontal surface, corresponding to the negative of thermal energy, $-\frac{3}{2}k_BT$ ($U_{\mathrm{DEP}} + U_{\mathrm{thermal}} = 0$). It can be seen that the strongest trapping spots lie at the end and the corners of the electrodes but trapping can also take place along the electrodes. The constant voltage used in the simulation (1.6 V) corresponds to the rms-value of an AC-signal of 4.5 V_{pp} (peak-to-peak). The image is adapted from **A.V**.

5.2 DEP results

5.2.1 DEP of DNA origamis

In order to demonstrate controlled anchoring of DNA origamis on a chip (**A.I**) and furthermore study their electrical properties (**A.II** and Ch. 6), origamis were directed and immobilized in between the conducting nanoelectrodes by utilizing DEP. The DEP experiments were performed by incubating a 8 µl drop of origami solution onto the hydrophilic surface of a nanoelectrode sample and keeping it in a moist chamber to prevent the drop from drying, while applying a sinusoidal AC voltage (Agilent 33120A waveform generator) to the electrodes for about 10 min. A schematic view of the DEP experiment is presented in Fig. 5.4a. After turning the voltage off, the

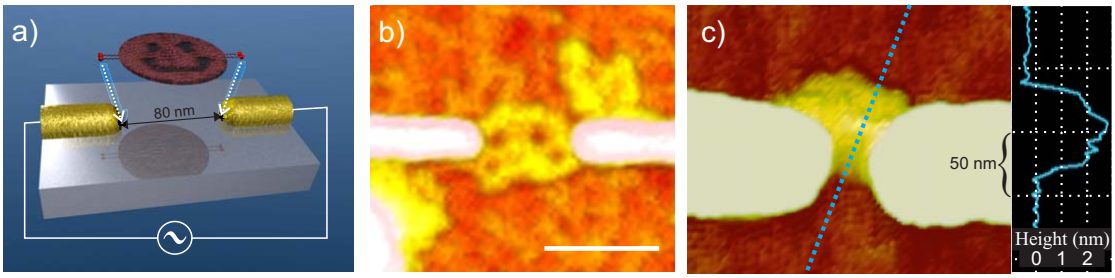

FIGURE 5.4 DEP trapping of origamis. a) A schematic view of trapping of a thiol-modified smiley DNA origami by using the AC-DEP and gold nanolectrodes. b) and c) are AFM images of an immobilized smiley origami (the 'chin' of the smiley is folded up) and a rectangular origami, respectively. The scale bar is 100 nm. The height of the origami construct lying on a substrate was typically 2 nm as seen from the cross-section shown in c. The images are adapted with permission from **A.I** (a-b) and **A.II** (c).

sample was gently rinsed with distilled water, dried with nitrogen flow and thereafter imaged with AFM (Veeco Dimension 3100, Nanoscope IV). As could be seen from AFM images (Fig. 5.4b and c), the origamis survived both the water washing and drying without losing their structure, although they were often folded, possibly because of the washing procedure or the DEP force, since the high force in the gap can fold origamis, and on the other hand, a folded shape can increase polarizability. Other explanation is that negative surface charges rebel the negatively charged origami and thus enhance the folding. To avoid this, one could improve the process by introducing a more suitable washing method or e.g. by attaching material to the origami that helps it to preserve its two-dimensional shape.

In the experiments DEP frequency was varied between 1-15 MHz, and the voltage from 0.6 V_{pp} to 2.4 V_{pp} (peak-to-peak values). Also, two types of buffers were used in the DEP experiments: A buffer with magnesium chloride (6.5 mM Hepes, 2 mM NaOH and 1 mM magnesium chloride, pH 7.2 and conductivity ca. 590 μS/cm) and a buffer with magnesium acetate (6.5 mM Hepes, 2 mM NaOH and 1 mM magnesium acetate, pH 7.2 and conductivity ca. 300 μS/cm). The best yield of trapping exactly a single origami between the electrodes was obtained using 12.5 MHz frequency and voltage of 1 V_{pp} for the buffer containing magnesium chloride and 0.8 V_{pp} for the buffer with magnesium acetate. It was observed that with the optimal voltage and frequency, the yield of trapping was dependent on the conductivity of the buffer: for the buffer with magnesium chloride the yield of trapping a single structure was about 5 % and for the magnesium acetate buffer ca. 10 %. This variance apparently comes from the difference in the conductivities of the buffers and thus, the higher yield could be caused by reduced fluid flows (electrothermal and AC-electro-osmotic) in the buffer of lower conductivity [25].

The yield of the trapping procedure significantly depends on the voltage and

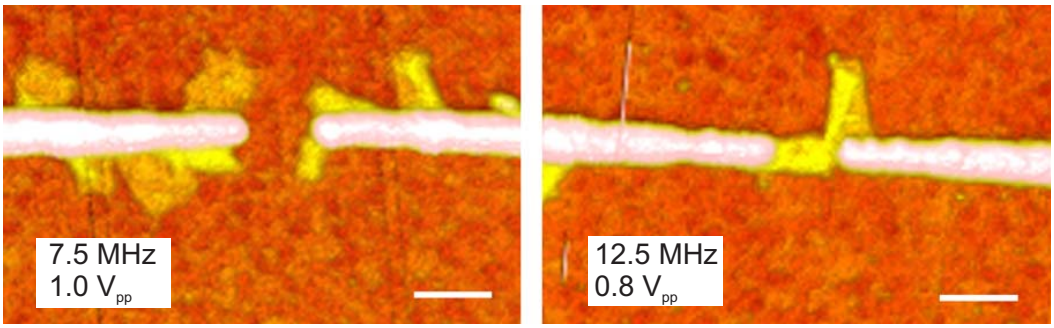

FIGURE 5.5 Influence of the DEP frequency to the trapping results. Left: When DEP frequency is below the optimal value, origamis are lying along the electrodes. Right: With the optimal frequency only two rectangular origamis are attached to the electrodes and strictly at the end of the electrodes. The scale bars are 100 nm. Adapted with permission from **A.I**.

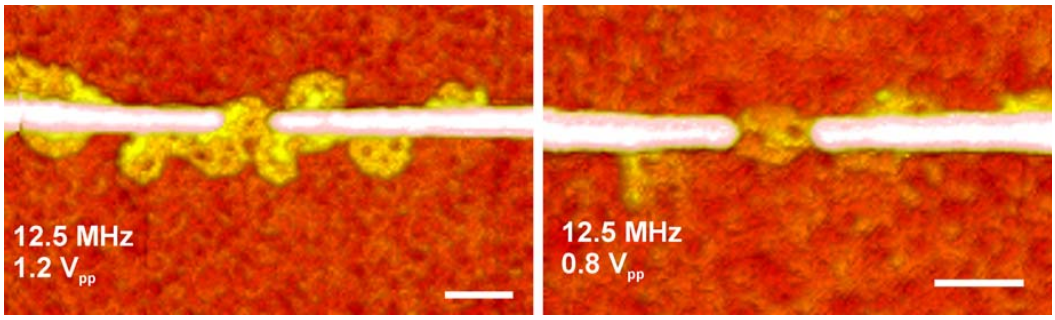

FIGURE 5.6 Influence of the DEP voltage to the trapping results. Left: When DEP voltage is only 0.4 V higher than the optimal value, origamis are trapped all along the electrodes. Right: When the optimal trapping voltage is applied to the electrodes, only one single origami is located precisely in the gap. The scale bars are 100 nm. Adapted with permission from **A.I**.

frequency parameters. In the case of a low frequency (under 12.5 MHz), trapped origamis laid along the electrodes, but not in the gap, whereas with the higher frequency (exactly 12.5 MHz) only a few origamis were attached to the electrodes, and in the best case only a single origami was precisely located in the gap. With frequencies below 10 MHz the yield of origamis trapped exactly in the gap was even less than 1 %. In addition, the amount of gathered origamis is remarkably sensitive to the applied voltage, and at the ideal frequency only about 0.2 V change in the amplitude significantly affects the efficiency of the trapping. The influence of the trapping parameters to the results is clearly seen in Figs. 5.5 and 5.6.

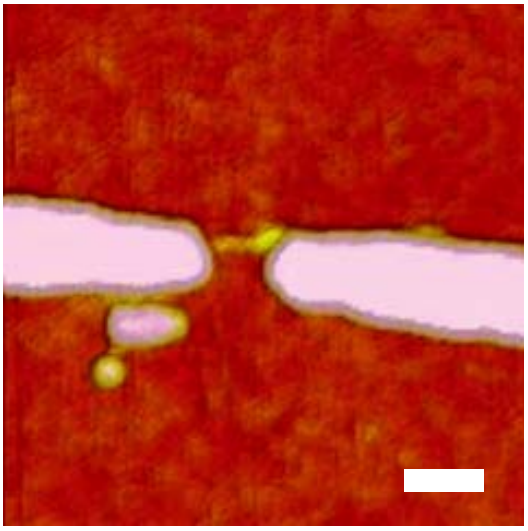

FIGURE 5.7 An AFM image of a trapped and immobilized single construct in between the gold nanoelectrodes. The scale bar is 50 nm. The image is adapted from **A.III**.

5.2.2 DEP of TX tile constructs

Besides origamis, the electrical conductivity of single defined-sized TX tile constructs, i.e. the complexes of tile B - tile A - tile B, was also investigated in this thesis (**A.III** and in Ch. 6). The measurement was realized similarly as for the origamis and thus, also the DEP experiments of the TX tile constructs resembled the trapping of origamis closely. The TX tile constructs also underwent similar spin-filtering after the annealing procedure (exchange to buffer of 6.5 mM Hepes, 1 mM MgAc, and $\sim$ 2 mM NaOH adjusting pH to 7). In addition, the trapping field was generated using similar narrow fingertip-type electrodes (widths of 30-50 nm and the gap between them of the size of 45-55 nm). However, the optimal trapping parameters were slightly different from the ones described for origamis. Here, the optimal result was achieved with an AC voltage of 1.2-1.5 V_{pp} at a frequency of 11 MHz applied to the electrodes for 3-5 minutes. The trapping results were verified by AFM imaging, and an example of a single B-A-B complex trapped and immobilized strictly in the gap is presented in Fig. 5.7.

5.2.3 DEP of quantum dots

The article **A.IV** of this thesis introduces a high-throughput pattern transfer method, which can be exploited for any polarizable nanoscale objects. The idea is to create a desired trapping pattern of nanoscale objects by DEP and then transfer the formed pattern to the specific target plate. In the article, a proof-of-principle experiment was demonstrated using quantum dots (QDs). The results of QD trapping are explained

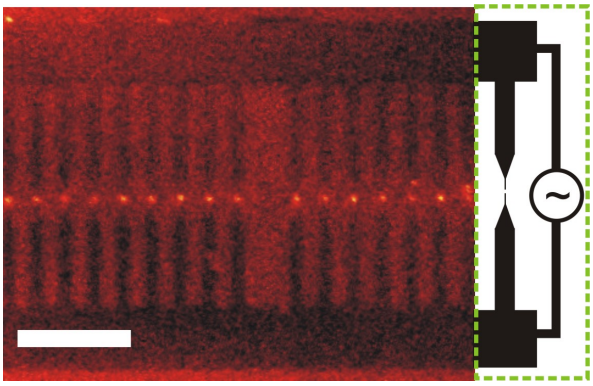

FIGURE 5.8 A confocal fluorescence image of QDs being trapped in between electrodes during dielectrophoresis. The scale bar is 50 μm. The image is adapted with permission from **A.IV**.

here and the actual pattern transfer method is presented in Chapter 7.

For creating a row of QD aggregates by DEP, the trapping template, a so-called master stamp, was designed to consist of an array of adjacent gold fingertip-type electrode pairs with widths of $\sim$ 170 nm (50 nm gap) lying on a Si/Si_3N_4 substrate (Fig. 5.8). Before trapping the electrode structure was incubated under SuperBlock blocking buffer (in phosphate buffered saline (PBS), Pierce) to prevent adhesion of QDs to the master stamp. A 10 μl droplet of 80 nM trapping solution, i.e. CdSe (core) / ZnS (shell) / polyethylene glycol (PEG) coated QDs (Invitrogen) in DI water, was injected onto a master stamp, and an AC-voltage (5.5-7.0 V_{pp}, 1 MHz) was applied to the electrodes for 10 minutes. During the optimization procedure of DEP parameters, the trapping of QDs with an emission wavelength of 655 nm was followed in real-time under a confocal microscope as seen in Fig. 5.8 (confocal microscope: Olympus FluoView 1000 with the software Olympus FluoView FV10-ASW 1.4, the lasers 405 nm and 543 nm were used to excite QDs).

The influence of the blocking solution and the efficiency of dynamic control of the trap were verified by detecting the time evolution of the system: after the trapping field was switched off, the trapped QDs escaped from the trapping spots due to the Brownian motion (Fig. 5.9). It was observed that the majority of QDs immediately vanished from the electrode gaps when the voltage was switched off, but after one minute waiting time some QDs were still attached to the electrodes indicating a non-specific binding of QDs. The escaped QDs were most probably aggregates as deduced from their high luminescence, but during the trapping the fluorescence intensity within the trap increased smoothly and continuously implying the majority of the trapped QDs being either smaller aggregates or individual dots. In addition, the FEM simulations of the system (see **A.IV**) confirmed that the DEP force was well above the thermal force of a single dot meaning that the used setup is also capable of trapping individual QDs (see also Sec. 5.3).

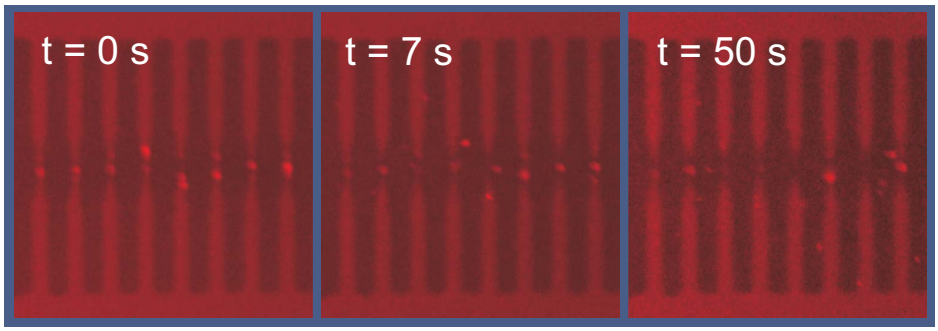

FIGURE 5.9 Confocal fluorescence images of the time-evolution of the system. The trap has been switched off at t = 3.5 s.

5.2.4 DEP of ssDNA/primers

In the paper **A.V** of this thesis, the DEP trapping and directing of ssDNAs to electrodes and the further utilization of these ssDNA molecules as immobilized primers in a PCR process is presented. The idea was to grow single dsDNA molecules locally on a chip and thus bridge the gap between neighboring electrodes with PCR-grown dsDNA. In order to realize that, firstly, 38 nt long ssDNA molecules (22 nt were complementary to terminal sequences of a 414 bp dsDNA template) were directed and immobilized to the ends of the opposite electrodes and secondly, they were elongated and subsequently hybridized by means of PCR yielding a dsDNA molecule in the gap region (see Ch. 8). In this section the optimization of the process of trapping of 22 nt and 40 nt oligonucleotides modified with fluorescent dye molecules (Cy3 and Cy5) is considered. In the actual PCR procedure the parameters optimized for 22 nt molecules were directly utilized for 38 nt ssDNAs. Therefore, the amount of trapped 38 nt molecules was simply controlled by adjusting the DEP trapping time. The PCR growing method is presented in detail in Chapter 8 and all the detailed sequences of oligonucleotides/primers are listed in Appendixes (Materials and methods).

Analogously to the QD trapping experiments, the confocal microscope was also exploited in the optimization of the ssDNA trapping (here, lasers 543 nm and 633 nm were used to excite Cy3 and Cy5 dyes, respectively). Firstly, 22 nt 3'-Cy3-labeled and 5'-hexanethiol-modified oligonucleotides (20 nM in 3 mM Hepes / 2 mM NaOH buffer) were DEP-trapped and immobilized in between fingertip-type electrodes similar to ones used in the QD trapping, i.e., the width of electrodes of 100-170 nm and the gap size of 100-140 nm. The optimal DEP trapping parameters for oligonucleotides were the following: voltage 4.5 V_{pp}, frequency 1 MHz and trapping time varied between 3-5 min.

Since the immobilized primers had to stay attached to the electrodes during

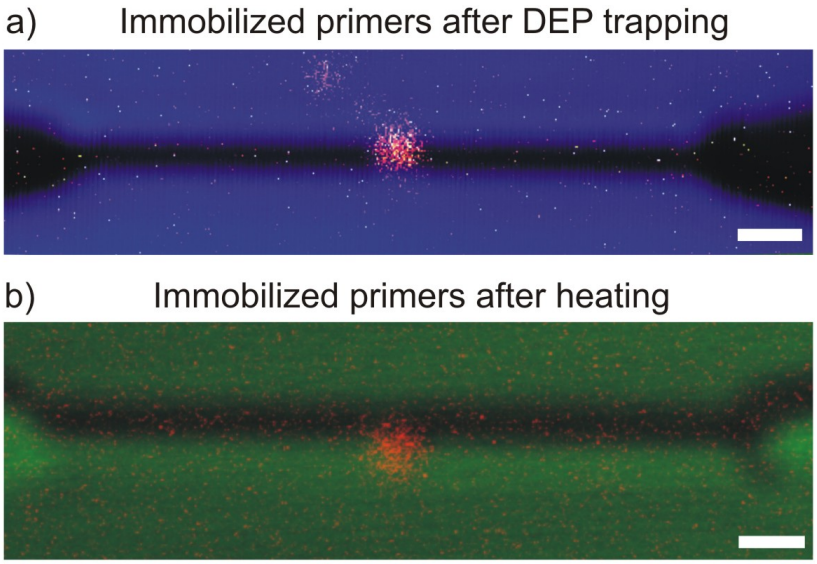

FIGURE 5.10 Confocal microscope images of 22 nt Cy3- and thiol-modified primers immobilized between the fingertip-type electrodes. a) A clear fluorescence spot in the gap means successful trapping and immobilization of the primers. The image is adapted from **A.V**. b) The fluorescence is still visible in the gap region after heating the sample in a PCR buffer to 95 °C, indicating covalent binding of the primers to the electrodes. The scale bars are ca. 500 nm.

the PCR run (repetitive heating and cooling cycles), the sample containing immobilized oligonucleotides was placed in the PCR buffer solution (distilled water, Taq buffer, $MgCl_2$, see Ch. 8), which was then heated up to 95 °C for several minutes to mimic the actual PCR process. After the heating cycle and the washing procedure the sample was imaged again with the confocal microscope. Although it is assumed that at least some part of the immobilized oligonucleotides, i.e. non-specifically bound strands, are detached during the heating, the fluorescence spot was still clearly visible after the procedure (e.g. Fig. 5.10). This observation means that at least part of the strands are properly attached to the electrodes, i.e., the binding between a sulphur-containing linker and a gold electrode is strong enough to last the actual PCR-experiments.

Secondly, in order to introduce a more sophisticated DNA-platform for potential applications, the multielectrode configuration was exploited in the trapping of oligos/primers. In addition, it was deduced that the electrode geometry presented in Fig. 5.1 could enable the electrode-specific trapping, and this was demonstrated with 40 nt long Cy3- and Cy5-modified ssDNA molecules. At first, Cy3-labeled oligonucleotides (0.3 μM in 3 mM Hepes / 2 mM NaOH buffer) were injected onto the sample, and only one of the eight electrodes of the structure was chosen to gather these oligonucleotides by connecting it to the waveform generator (AC-signal 5.0 V_{pp} and 1 MHz + DC-offset of 1.3 V), while all the other elec-

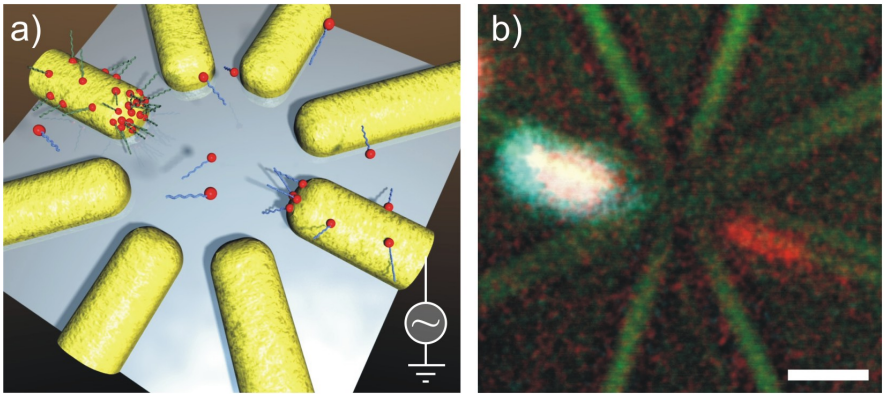

FIGURE 5.11 Trapping primers with the multielectrode geometry. a) A schematic view of the electrode-specific DEP trapping of different thiol-modified primers. An AC voltage signal (+ possible DC-offset) is applied one by one to the desired electrode gathering the primers to its end (also along the electrodes), while keeping the other electrodes grounded. b) A confocal microscope image of separately trapped and immobilized 40 nt long primers modified with different dye molecules [Cy3 (red) and Cy5 (blue)] and thiol-linkers. The scale bar is 1 μm. The image is adapted from **A.V**.

trodes were grounded. After the trapping, sample was rinsed with DI water and dried. Next, Cy5-labeled oligos were pipetted onto the substrate followed by applying the same AC signal with the DC-offset to the opposite electrode. As can be seen in Fig. 5.11, the two different oligonucleotides are clearly distinguishable in the confocal fluorescence image proving that the electrode-specific trapping and immobilization is realizable. This result will open up opportunities for more complex setups of growing DNA in a programmable way (see also Ch. 8) and also for other DEP-based systems.

5.3 Discussion

One can easily deduce from the results pulled together in this chapter that the controllable manipulation of almost any kind of objects in nanoscale is feasible, and that the trapping can be exploited for various purposes, as can also be seen in the following chapters. In addition, the calculated polarizabilities presented in Chapter 2 and also the estimated DEP potentials are in agreement with the observations indicating that even the simple theory is really advantageous to the experiments and interpretations of the results.

According to the calculations in Sec. 2.4, the effective polarizability component of a DNA origami is 3-6 fold compared to the corresponding component of a TX tile construct. On the other hand, it was noticed in the trapping experiments that 1.5-2 times higher voltages were needed to trap single TX tile constructs than

origamis, and since the DEP potential is proportional to the square of the electric field, 3-6 times lower polarizability is thus compensated by a factor 2-4 according to the raise in the optimal trapping voltage (the level of the DEP potential minimum has a quadratic dependence on the voltage as simulated in Ref. [153]). Actually, the compensation by the voltage raise is even higher than estimated above using the amplitude values directly, since a bit narrower gap was used for TX complexes than DNA origamis: the shorter gap enhances the electric field maximum and therefore also makes the DEP well a bit deeper as seen in Sec. 5.1.2 and in Ref. [153].

Trapping results of 38 and 40 nt ssDNA molecules and CdSe/ZnS QDs are not so straightforward to contrast with each other or the results of DNA constructs, since different buffers, concentrations and electrodes (electric fields) were used. However, if compared to DNA origamis, the estimated polarizabilities were 40-60 and 700-1000 -fold smaller, whereas 5-6 and 7-9 times higher voltages were applied to electrodes in order to trap ssDNA molecules and QDs, respectively. From these results one can see that the calculated polarizability for 40 nt ssDNA was quite a good approximation, since the lower polarizability is compensated by a factor of $\sim$ 25-40. Moreover, it was often observed that the short molecules were trapped and therefore also immobilized as bundles, i.e., non-specifically bound molecules were later detached at high temperatures. This observation should also be taken into account, since a bundle of molecules can have a totally different polarizability properties than just a single molecule surrounded by a counter-ion cloud. In the case of QDs, either the estimated polarizability is too low, e.g. due to the fact that the PEG coating of QD was not taken into account, or QDs were preferrable trapped as small aggregates, as speculated already in the context of time-evolution of the QD-trapping system in Sec. 5.2.3.

It was also noticed that quite high frequencies should be used in order to trap an individual origami and TX tile construct precisely between the electrodes. This is in agreement with the previous results from the DEP experiments for the double-stranded DNA [155]. However, in these experiments 1 MHz was already high enough frequency to yield an optimal result (the same frequency was also used in ssDNA and QD trapping). Surprisingly, smaller voltages were required at higher frequencies than at lower ones for the successful trapping, which is in contrast to the previous DEP observation for dsDNA [155].

An important result obtained was also that in the AFM images the height of the origamis were ca. 2 nm (see Fig. 5.4), whereas the typical height of a single double-stranded DNA on the SiO_2 surface is about 1-2 nm [73,152]. This perception suggests that a single double-stranded DNA molecule is more deformed due to the interactions with the SiO_2 surface than dsDNAs inside an origami. This is an interesting observation in perspective of studies of the DNA conductivity, where the conformation of DNA is expected to play a major role [73, 154] (see also Chapters 1 and 6).

While trapping and imaging the TX tile constructs, it was often found out that there were also fragments of constructs (tiles A and B). This might be due to the fact that designed structure was not as stable as an origami, although both of them were ligated. The stability problem of the structure could also have been a reason for rather low yield of single structure trapping. However, it was always verified by AFM imaging that the electrically measured TX tile constructs were intact and entire complexes.

Chapter 6

Electrical measurements of DNA constructs

6.1 Measurement setups

In order to characterize conductance mechanisms and properties of individual DNA constructs (rectangular DNA origami or TX tile complex), only the samples having just one construct bridging the nanoelectrodes after the DEP trapping were chosen for the electrical measurements. The measurements (both DC and AC characteristics) were performed inside an electromagnetically shielded (EMS) room, and the sample itself, i.e. EBL-fabricated electrodes and the immobilized DNA construct, was placed in a chamber containing a temperature and humidity sensor (Honeywell, HIH-3602-A). The humidity level (relative humidity (RH) 5-95 %) inside the chamber was controlled by adjusting nitrogen and water vapor flow rates into it. The majority of the electrical measurements were carried out at RH = 90 %, since this RH is just above the level, where dsDNA is in its natural form: RH = 90 % corresponds to $\sim$ 15 water molecules per nt in dsDNA [21, 44], and at least 13 water molecules are needed to stabilize the B-DNA [162]. On the other hand, one should avoid significant condensation of water on top of the sample, and thus, the chosen RH level for the measurements should not be too high.

DC measurements were realized by sweeping a battery-powered bias voltage between -0.3 V and 0.3 V [obtained via digital-to-analog converter (DAC) circuit], while measuring the current and voltage by a computer equipped with data aquisition (DAQ) card (National Instruments PXI-1031) via current pre-amplifier (DL-Instruments Model 1211) and a voltage pre-amplifier (DL-Instruments Model 1201) (see Fig. 6.1a).

For the AC-IS measurements, two lock-in amplifiers (Stanford Research 830) equipped with a general-purpose interface bus (GPIB) were connected to a computer running a specific home-made LabVIEW program (see Fig. 6.1b). The excitation voltage of $\sim$ 50 mV (rms) with a frequency of 0.01 Hz - 100 kHz and a constant

phase was obtained from one of the lock-in amplifiers and fed into the sample. The voltage across the sample was detected with the same amplifier, and in order to avoid excessive current division, the signals went through separate pre-amplifiers (HMS Electronics, Model 568), which had the input impedances much higher than the impedance of the sample, i.e. the current into the lock-in amplifier was negligible. By utilizing a feedback system, the excitation signal was adjusted in such a way that the voltage across the sample was always 50 mV (rms). The response (current) was measured with another lock-in amplifier, which was also fed with the reference signal. Thus, by dividing the complex voltage across the sample, i.e. the measured amplitude and the phase difference between the excitation voltage and the measured voltage, by the obtained complex current, i.e. the measured amplitude and the phase difference between the current and the excitation voltage, the measurement yielded the desired complex impedance as a function of frequency. Finally, the obtained data was fitted using CNLS-method by exploiting LEVMW 8.08 software [9].

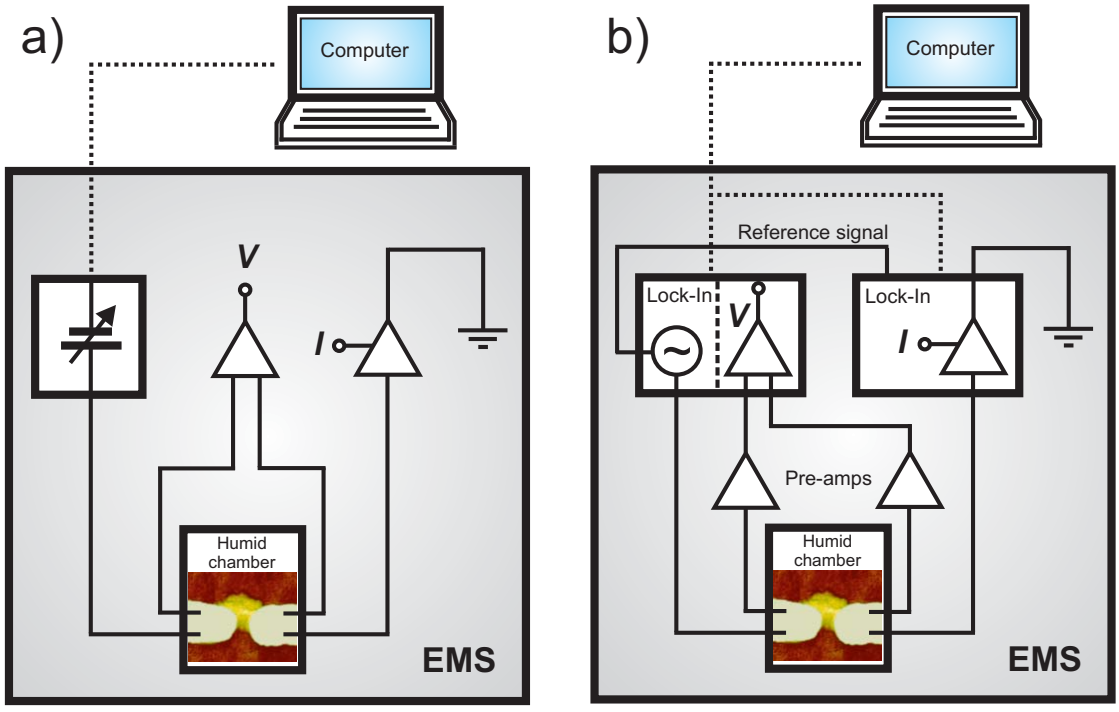

FIGURE 6.1 Schematic views of the measurement setups used to obtain a) *I-V* curves (DC) and b) AC impedance spectra from the DNA constructs.

6.2 Electrical conductivity of DNA origami

6.2.1 DC characteristics and the role of humidity

After the successful DEP trapping of origamis, the sample containing a single structure was placed into the measurement chamber and first, DC characteristics were investigated with variating RH levels. These results were compared to control samples, i.e. samples that also underwent the same DEP trapping and following washing procedures as origami samples, but without any DNA in the trapping buffer.

At low RH levels DNA origami was insulating with the resistance of the order of teraohms (similar resistance observed also for dry dsDNA [154]). At RH = 90 %, DC-sweeping from -0.3 V to 0.3 V produced non-linear *I-V* curves with a resistance of $\sim$ 10 GΩ between -0.2 V and 0.2 V, and about $\sim$ 2 GΩ outside this region, while the measurement of the control sample yielded a linear *I-V* curve with a typical resistance value of 10-30 GΩ (see Fig. 6.2a). Similar non-linear *I-V* characteristics have previously been reported also for dsDNA molecules, e.g. in Refs. [33, 128]. From this point on, all the discussions are based on the measurements carried out at RH = 90 % unless otherwise stated.

The low DC-conductivity of the origami may be explained by a high resistance of the linker groups consisting of a $(CT)_{16}$ single strand sequence as a spacer and either a 3'-propane- or a 5'-hexanethiol-modification at its end. The resistance of the hexanethiol has been reported to be 10 MΩ - 1 GΩ [167] and moreover, it has been observed that a ssDNA molecule is a poor conductor [80, 82] (also lack of overlapping π orbitals opposite to dsDNA [75, 151]). Thus, the only possible pathway for a DC current to flow is via the water layer on top of the single strand spacer, or direct tunneling or hopping between the bases in the origami and the electrode.

It was noticed that the humidity enhanced the conductivity of both the origami and the control samples, as seen from Fig. 6.2b. The dependence between the conductance and RH was determined by applying a constant voltage of 0.3 V to the sample and slowly varying RH value from 5 % to 95 %, while measuring the current through the sample. The conductance of a control sample increased exponentially as a function of RH, proving the DC-conductivity of the sample to be ionic and the main charge carriers to be adsorbed and ionized water molecules [7, 169]. The origami sample also obeyed the exponential relation when RH was below 55 % or above 80 % addressing the conductance to be water dominated as reported earlier, e.g. in Refs. [58, 80, 119, 169], whereas between 55-80 % the current almost saturated.

In general, a DC current through an origami was higher than through the control within the whole RH range most probably only due to the capability of an origami to bind water molecules more efficiently. The difference between currents was clear at low RH levels meaning that the origami might not have been completely dry when the measurement started, although the sample was dried with the nitrogen flow (dsDNAs within an origami sustain their form also in dry conditions

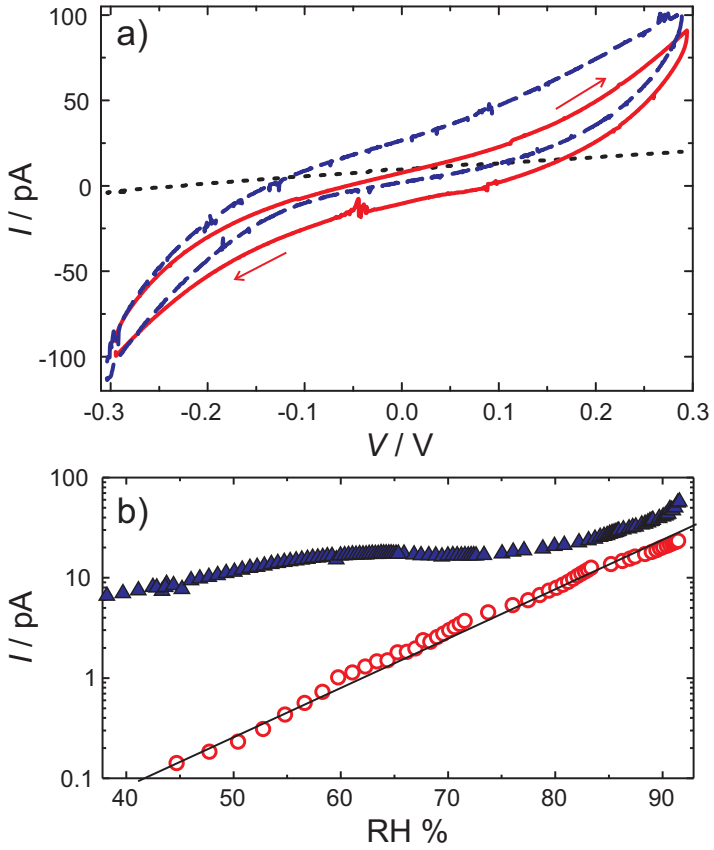

FIGURE 6.2 DC measurement of a rectangular DNA origami. a) *I-V* curves of two different origami samples (blue and red) and a control sample (black dashed line) measured at RH = 90 %. The arrow indicates the direction of the voltage sweep. The observed hysteresis is due to the high humidity. b) A current through an origami sample (blue triangles) and a control sample (red circles) vs. relative humidity. The current through the control sample increases exponentially as a function of RH. The image is adapted with permission from **A.II**.

as seen in AFM images presented in Ch. 5). These facts can explain the observed behavior, including the saturation of the current, since in dry conditions much more water molecules could have been bound to an origami than simply expected on the grounds of the RH value. However, since it was noticed that dsDNA inside the origami sustains the natural B-form even in the dry state, the excess conductivity at low RH, if compared to control, could be due to the electrical conductivity of the origami.

6.2.2 AC-IS measurement

As seen above, the DC measurements do not give any reliable information about the possible electronic conductivity of the DNA origami, or about the actual conductivity mechanisms (except the hint of the dominance of water molecules in the

conductivity), and thus, in order to characterize the conductance thoroughly, the AC-IS measurements were necessary.

Dry sample

Before measuring the AC-concutance of the control (described in previous section) and origami samples, the stray capacitances and the small leakage currents of the measurement setup were determined by recording the AC impedance spectrum of a dry and empty sample (only electrodes) followed by fitting the data with an equivalent circuit comprised of a resistor (leakage current) and a constant phase element (stray capacitances) in parallel. The fitting yielded a resistance R_{e} of 0.1 TΩ and proved CPE to be a pure capacitor (i.e. $n \approx 1$, see Eq. 3.1) with capacitance $C_{\mathrm{e}} \approx 9$ pF (fitting results are shown in Table 6.1).

Control sample

As the first step of the actual AC-IS measurements, performed also at RH = 90 %, a behavior of a control sample was studied (in total three control samples were measured). A typical Cole-Cole plot obtained from the control sample together with the fitting curve, is shown in Fig. 6.3a. The fitting of the data was carried out by exploiting a modified Randles circuit as an EEC model. As already introduced in Sec. 3.4 in addition to the common Randles circuit, the circuit used here included an additional Warburg impedance, with the parameter W_{diff} (denoting Q_W in Eq. 3.3 and also describing diffusion of the ions on the surface), which was placed in parallel to the resistance of the 'electrolyte', i.e. R_{s}, formed by the adsorbed water molecules and ions on the SiO_2 surface between the electrodes. This combination, denoted as Z_{s}, was in series with the simplified version of Randles double-layer impedance, Z_{dl}, consisting of a parallel combination of the double-layer impedance C_{dl} (ions and water molecules surrounding the electrode) and the resistance R_{ct}, i.e., the total charge moving through the double layer. The measured stray capacitance was then added in parallel to the above-mentioned blocks (and kept constant during the fitting) forming a circuit presented in Fig. 6.4a. In the circuit R_{e} is neglected due to its high value. Actually, during the fitting procedure, both W_{diff} and C_{dl} were replaced with more general CPEs, but the results always yielded $n \approx 0.5$ (i.e. the Warburg impedance) for W_{diff} and $n \approx 1$ (i.e. a pure capacitance) for C_{dl}. All these components and the corresponding values obtained from the fittings are shown in the Table 6.1.

In a Cole-Cole plot of a control sample, i.e. in Fig. 6.3a, two truncated semicircles are clearly distinguishable. The semicircle at the high frequencies is created by the combination of C_{e} and the rest of the circuit, whereas the low frequency semicircle is due to the parallel combination of capacitance and resistance in Z_{dl}. The effect

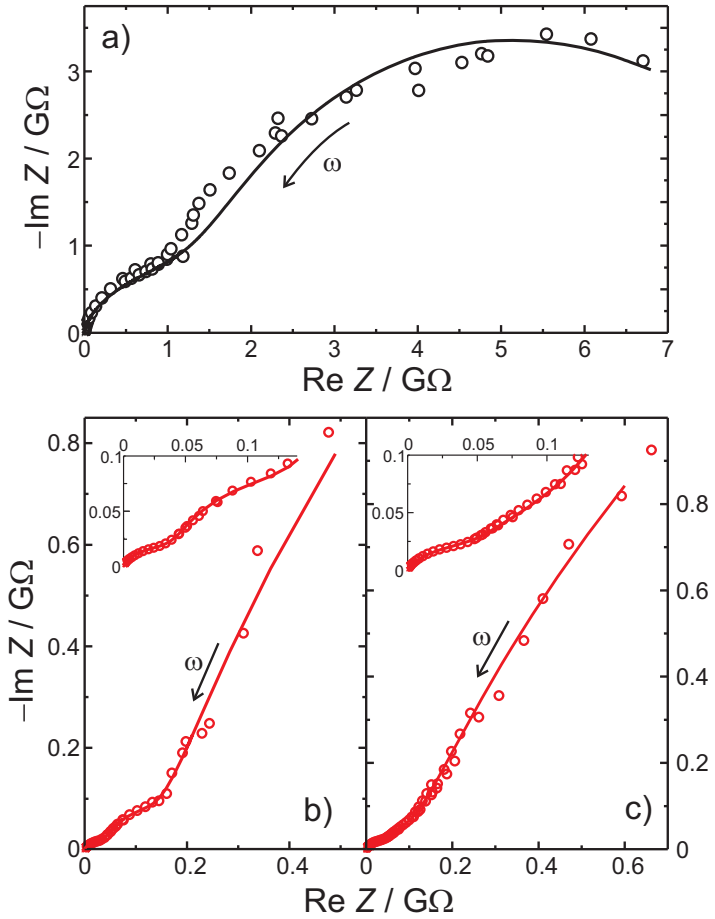

FIGURE 6.3 Cole-Cole plots and data fittings for a typical control sample (black circles and black curve in a) and two different samples containing a single rectangular DNA origami (red circles and red curves in b-c). The arrows indicate the direction of the increasing frequency and the insets in b and c are magnifications of the data near the origin. The fittings are based on the equivalent circuits presented in Fig. 6.4. The image is adapted with permission from **A.II**.

of the additional W_{diff} is to bend the semicircles down, resulting in the centers of the circles to fall below the Re Z axis.

DNA origami sample

As the second step, three separate samples (O1-O3) containing a single rectangular DNA origami precisely immobilized between the electrodes, were measured, subsequently fitted with EEC, and then compared to the results from the fittings for the control samples. The Cole-Cole plots obtained from the samples O1 and O2 and the data fittings based on the EEC model from Fig. 6.4b, are presented in Fig. 6.3b and c. Similarly to the control, two truncated semicircles are again clearly visible, but additionally, the low feaquency tail (i.e. the frequency approaches zero) is pointing

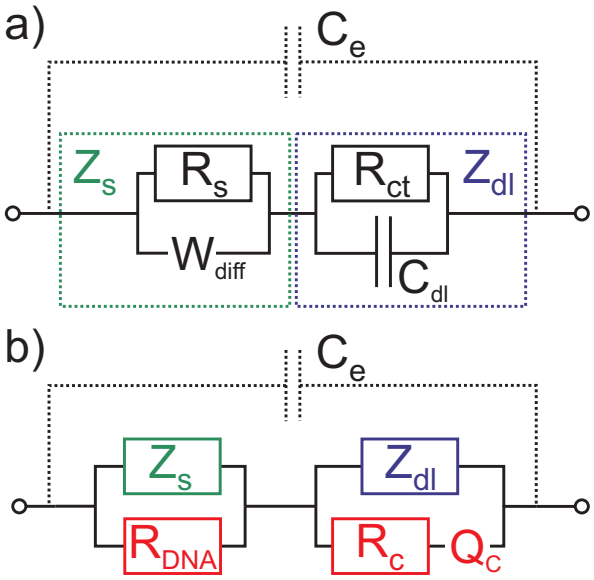

FIGURE 6.4 The equivalent circuits for a) a control sample and b) a sample containing a single rectangular DNA origami. The same circuits were also utilized in characterization of conductivity mechanisms of the TX tile construct. C_{e} is the measured stray capacitance of the electrodes. R_{s} represents the small current through the 'electrolyte' and W_{diff} describes the diffusion of the ions on the SiO_2 surface. Parallel combination of W_{diff} and R_{s} forms the impedance Z_{s} (green) and in series with this block, there is a double-layer impedance Z_{dl} (blue) comprised of the double-layer capacitance, C_{dl} and current through it, R_{ct}. When a DNA construct is present, R_{DNA} describes resistance of the construct, and R_{c} together with Q_{c} the contact impedances between the construct, linker and electrodes or in general the modification in the double-layer. The image is adapted with permission from **A.II**.

towards the direction of Re Z = -Im Z, which is a clear signature of an additional Warburg impedance (as described in Secs. 3.3 and 3.4).

The EEC model for the origami samples is similar to the control sample, except that there exist three additional components added to the control EEC: *1)* a resistance describing the origami, R_{DNA}, is added in parallel to the 'electrolyte' block, Z_{s}, *2)* a CPE, Q_{c}, and *3)* a resistance, R_{c}, in series had to be added in parallel to the double-layer impedance, Z_{dl}, in order to describe the modification in double-layer caused by the origami. Most probably, a very similar double layer, Z_{dl}, is again formed on the electrodes but since the origami is connected to the electrodes, either directly or via the linker, there exists a parallel route for CT through the double layer. The fittings indicate that the added CPE, including a constant, Q_{c}, and an exponent, n_Q, is neither the pure Warburg impedance nor the pure capacitor ($n_Q \approx 0.7$, see Table 6.1). Consequently, R_{c} and Q_{c} in series could be interpreted as a combination of sets of resistances and capacitances with different time constants in parallel, caused by the polarization of the DNA structure or the linkers, which are known to have a low

conductance as described in DC section. Another way to describe the exponent of the CPE is that if the two electrodes and contacts are dissimilar, their combination can not be modeled as an ideal element. In the fitting, the parallel resistances R_{s} and R_{DNA} are handled as a single resistance. All the results obtained from the fittings are shown in the Table 6.1.

Results and observations

In the origami equivalent circuit, the CT resistance R_{ct} is still present in the circuit but has a negligible contribution to the AC conductivity since it is large compared to other impedances parallel to it. However, at low frequencies, i.e. close to the DC limit, R_{ct} plays a significant role. Formally, the impedances of Q_{c} and C_{dl} are infinite at the DC limit, and thus they can not describe a possible small electronic DC current flowing directly from the DNA, or via the linker, to the electrode. The resistance describing such a small current would be parallel to R_{ct} and can be understood to be included therein. During the fittings, it was noticed that the value of R_{ct} was similar to the control sample, which implies that the resistance related to the direct electronic DC current from the DNA to the electrode is larger than the value of R_{ct} determined for the control sample. By adding R_{s} and R_{ct} from Table 6.1 together, one can estimate the DC resistance of the equivalent circuit to be roughly 10 GΩ, which agrees with the measured DC resistance near zero bias. Therefore, a simple DC measurement is not enough to characterize the conductivity, since the large resistances hide crucial information about other possible conductivity mechanisms.

However, by interpreting the results from the AC-IS measurement, it is possible to determine the conductivity related directly to the origami and also the influences of the immobilized origami to the other circuit. It can be seen from Table 6.1 that the resistance describing the parallel combination of R_{s} and R_{DNA} is significantly smaller than R_{s} of the control sample. If assumed that R_{s} is not changing remarkably due to the presence of the origami (the non-diffusive ionic conductivity due to salt ions is roughly proportional to the concentration of ions and it can be assumed to be similar to the control sample), the obtained result implies that the reduction is purely caused by R_{DNA} and that the influence of R_{s} is therefore negligible. According to this consideration and to Table 6.1, 60 MΩ for the sample O1 and 83 MΩ for the sample O2 can be deduced to be the resistances of the DNA origamis, i.e. the electronic conductivity of the origami or water-induced ohmic conductivity.

It was also noticed that the constant W_{diff} of O1 and O2 was about ten-fold compared to control indicating the enhancement of diffusion in the gap region. This result means that the ionic conductivity was increased due to the mobile counterions and adsorbed and ionized water molecules around the origami. Moreover, the observed change in C_{dl} can be ascribed to small changes in the double-layer structure.

In order to fully understand the EEC model and how it is related to DC measurements, the sample O2 was also measured with the 0.3 V DC-offset applied simultaneously to the system. As seen from Fig. 6.2, this bias voltage is within the higher-conductance region of the *I-V* curves, but still, the obtained AC response was very similar to the zero-bias AC spectrum, and it was fitted with almost the same parameters as the sample O2 without bias (see Table 6.1). Interestingly, by setting R_{ct} to be a free fitting parameter opposed to the samples O1 and O2 (in these cases R_{ct} is large and does not have a signficant contribution in the fittings, i.e. the fittings with free R_{ct} yielded either $R_{\mathrm{ct}} \to 0$ or $R_{\mathrm{ct}} \to \infty$), the fitting yielded a value of 2.8 GΩ, which is in agreement with the observed non-linearity in *I-V* curves (without bias R_{ct} was assumed to be in the order of 8 GΩ). This phenomenon can be addressed to some water-based redox-reaction(s) at the electrodes with the threshold voltage(s) above $\sim$ 0.2 V.

Finally, the influence of the amount of water to the AC spectrum was tested by measuring the sample O3 at RH = 95 %. This measurement revealed that the water is remarkably affecting the conductivity, since W_{diff} was drastically increased. In addition, the CPE in the double-layer was turned into the Warburg impedance, i.e. $n_Q \approx 0.5$, and the influence of the double-layer itself was almost vanished indicating that the adsorbed water molecules were dominating charge carriers covering the whole gap region including the double-layers. Despite the enhanced diffusion, the resistance of the origami was very similar to other samples, i.e. 67 MΩ for the sample O3 (here R_{ct} was set to be infinite, since its impedance was much higher than that of other components).

6.3 Electrical conductivity of TX tile construct

The methods in characterization of the conductivity of single TX tile constructs are analogous to the case of DNA origamis, and thus, only the main results obtained from the measurements are presented in this section. The TX tile constructs studied here are seamless structures unlike rectangular origamis, which had a seam in the middle of the structure, and they are much shorter and smaller than DNA origamis. Furthermore, compared to the origamis, ssDNA spacers were not included in the linkers, and the hexanethiols were directly attached to the TX tile complex. Due to these facts, the conductance properties between these constructs might be significantly different. Consequently, the results obtained from these measurements, contrasted with those obtained for DNA origamis (similar buffers and electrodes used), could reveal further information about the conductivity of DNA and DNA constructs in general. The differences between TX tile constructs and DNA origamis are discussed in detail in the next section, i.e. in Sec. 6.4.

The DC measurement was carried out at RH = 90 % similarly to origamis, and the samples yielded almost linear *I-V* curves with resistances of $\sim$ 15-20 GΩ as seen

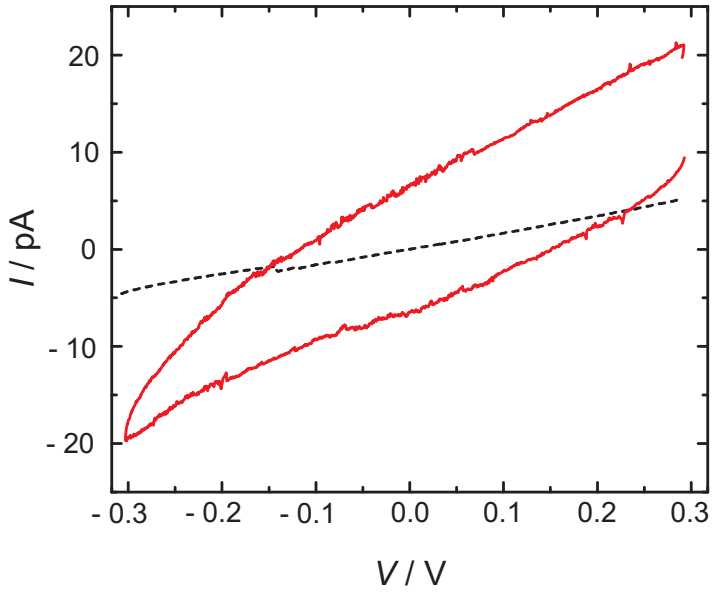

FIGURE 6.5 A typical *I-V* curve of a single TX tile complex (red) and a control sample (black dashed line) measured at RH = 90 %. The hysteretic behavior is due to the high humidity conditions (see Materials and methods in Appendixes). The image is adapted from **A.III**.

in Fig. 6.5. The control samples, instead, produced linear *I-V* curves with somewhat larger resistances, $\sim$ 30 GΩ or more.

The AC measurements were performed similarly as described above in the case of origamis i.e. first, the dry and empty sample was invetigated and second, both the control samples (three in total) and the TX tile construct samples (also three samples) were measured and consequently characterized by the same EEC models already introduced in the previous section.

The typical Cole-Cole plots and the data fittings (same EECs used as in Fig. 6.4 for origamis) for the control sample and the TX tile complex are shown in Fig. 6.6. According to the fittings (see typical values from Table 6.2), the resistance of the 'electrolyte' R_{s} for the control sample was $\sim$ 1-4 GΩ and the charge transfer resistance 20-30 GΩ. The sum of these two resistors roughly corresponds to the observed DC resistance, and apparently, the high resistance of the CT process through the double-layer can be considered to be the restricting factor in the DC conductivity, as observed in the DNA origami measurement also.

The Cole-Cole plot obtained from a typical TX tile construct is quite similar to the control, except the low frequency tail, which differs prominently (see Fig. 6.6). Results showed that for the TX tile complex the parallel combination of R_{s} and R_{DNA} is $\sim$ 1-2 GΩ, which is only about half of R_{s} of the control (see Table 6.2), indicating that the electronic conductivity through a single TX tile construct is very low. However, the factor W_{diff} was increased 2-3 times due to the presence of DNA indicating

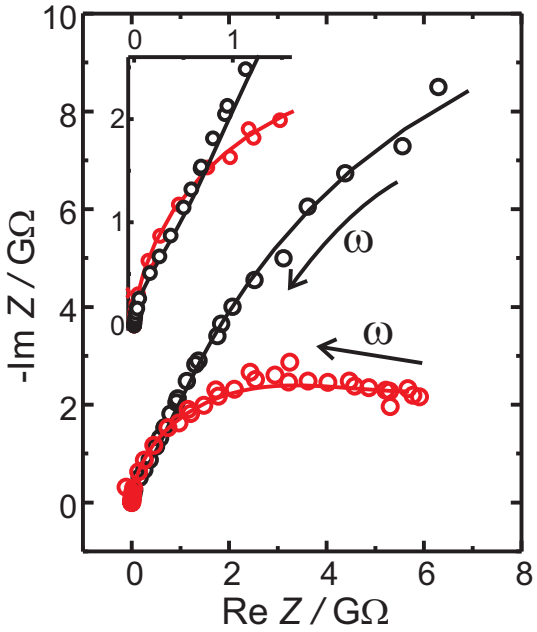

FIGURE 6.6 Cole-Cole plots and data fittings for a typical control sample (black circles and black curve) and a sample containing a single TX tile construct (red circles and red curve). The arrows indicate the direction of the increasing frequency. The fittings are based on the equivalent circuits presented in Fig. 6.4. The image is adapted from **A.III**.

enhanced diffusivity of ions due to the presence of the construct. Interestingly, the exponent n_Q was only about 0.3, resulting in the low frequency tail to turn towards the Re Z axis, just opposite to the origami samples. This could be due to the difference in the contacts (different linkers) between the construct and the electrodes.

6.4 Discussion

Analyzing the data and comparing the obtained results between the origamis and the TX tile constructs shows that the water indeed plays a crucial role in the CT processes at high humidity levels. Firstly, the difference between DC conductivites and the shapes of the *I-V* curves of origami and TX tiles can simply be explained by the dominance of water: *1)* a stretch of DNA nucleotides (nt) can adsorb only a certain number of water molecules at a given RH level [21], and *2)* the number of nucleotides is very different in TX tile construct ($\sim$ 1,000 nt) compared to the DNA origami ($\sim$ 14,000 nt). Thus, the total amount of adsorbed water molecules in a TX tile construct is much smaller than in a DNA origami meaning less conduction channels via the adsorbed water layer, and therefore, the higher DC resistance. Secondly, the presence of both the DNA origami and the TX tile complex increased the diffusion compared to the controls, but this effect was also more pronounced in the case

TABLE 6.1 Results from the fittings of the equivalent circuits for the dry sample, the control sample and the DNA origami samples O1-O3. The values in the parentheses are not fitted but fixed, based on the fitting of the dry or control sample or for other reasons (described in the text).

Sample (V_{DC}, RH)	$R_{s(\|DNA)}$ [MΩ]	W_{diff} $\left[ps^{\frac{1}{2}}/\Omega\right]$	C_{dl} [pF]	R_{ct} [GΩ]	R_c [MΩ]	Q_c $[ns^{n_Q}/\Omega]$	n_Q	R_e [TΩ]	C_e [pF]
Dry (5 %)	-	-	-	-	-	-	-	0.1	9.0
Control (90 %)	2200	110	290	7.4	-	-	-	(0.1)	(9.0)
O1 (0.0 V, 90 %)	60	1100	1100	(7.4)	120	5.3	0.79	(0.1)	(9.0)
O2 (0.0 V, 90 %)	83	1200	1800	(7.4)	73	4.6	0.71	(0.1)	(9.0)
O2 (0.3 V, 90 %)	69	1000	1500	2.8	66	3.7	0.77	(0.1)	(9.0)
O3 (0.0 V, 95 %)	67	2700	20	(∞)	41	3.7	0.77	(0.1)	(9.0)

TABLE 6.2 Results from the fittings of the equivalent circuits for the dry sample, the control sample and a typical sample containing a TX tile construct (TX). The values in the parentheses are not fitted but fixed, based on the fitting of the dry or control sample or for other reasons (described in the text).

Sample (RH)	$R_{s(\|DNA)}$ [MΩ]	W_{diff} $\left[ps^{\frac{1}{2}}/\Omega\right]$	C_{dl} [pF]	R_{ct} [GΩ]	R_c [MΩ]	Q_c $[ns^{n_Q}/\Omega]$	n_Q	R_e [TΩ]	C_e [pF]
Dry (5 %)	-	-	-	-	-	-	-	0.3	6.8
Control (90 %)	1300	13	26	26	-	-	-	(0.3)	(6.8)
TX (90 %)	900	29	1.8	(26)	1500	0.13	0.3	(0.3)	(6.8)

of DNA origami. The capability of DNA origami to bind more water molecules and ions than TX tile construct is seen from the diverse W_{diff} values, for the origami the Warburg impedance was 30 times smaller compared to B-A-B complexes (W_{diff} for origamis $\sim$ 1000 $ps^{\frac{1}{2}}/\Omega$ vs. W_{diff} for TX tile complexes $\sim$ 30 $ps^{\frac{1}{2}}/\Omega$). Thus, the observed ionic conductivity is strongly dependent on the size of the DNA structure in question.

The main structural difference between these structures is the smaller overall size and the seamlessness of the TX tile construct. In addition, the linker molecules (hexanethiols) of the designed B-A-B -complex have lower resistance [167] than the longer linkers used in the DNA origami design (propane- or hexanethiol and 32 nt ssDNA spacer). Preceding facts conclude that if the electronic conductivity through the bases was relevant, the TX tile complex should show higher conductivity than the DNA origami ($\sim$ 70 MΩ at RH = 90 %). However, our results clearly show that for the B-A-B complexes resistance is actually much larger, roughly 1-2 GΩ. This implies, that same way as the presence of DNA enhances diffusivity of ions along the construct via the gathered water molecules as described above, also the observed ohmic conductivity ($R_{s\|DNA} < R_s$), for both the TX tile construct and the origami, is just due to the enhancement of the conductivity of the 'electrolyte'.

A similar AC-IS approach as presented here, but without the detailed equiv-

alent circuits, has previously been used in measuring several but not a controllable number of B-DNA strands bridging a small gap [160]. The obtained resistance values roughly agree with the results obtained in the case of the DNA origami samples. AC-IS technique has also been utilized in the investigation of the electrical properties of triangular origamis in the buffer solution at the room temperature [17], and in this work the low frequency limit yielded similar results as seen in the experiments of the TX tile constructs in high humidity conditions. If one takes into account the fact that the conductivity is drastically reduced with the increasing length of the DNA, the results presented here (resistance $\sim$ 100 MΩ - 10 GΩ) somewhat agree with other earlier measured values for short DNA molecules, e.g. 8 MΩ for 8 bp ds-DNA in liquid [168], $\sim$ 1 MΩ for 15 bp dsDNA in liquid [57] and 80 MΩ for 12 bp dry dsDNA [40].

As a conclusion, AC impedance spectroscopy combined with the full EEC modeling makes determination of the processes that appear also along the DNA constructs possible. In addition, it gives information about the factors and the corresponding parameters related to the environment surrounding the measured construct. During the modeling and analysis, the conductivity of the DNA structures turned out to be rather low and mostly induced by the water molecules adsorbed to the DNA helices. The measurements were performed in a high humidity environment and thus, they yielded upper limits to the electrical conductance of such DNA structures. The results proved also that the direct electronic conductivity via base pairs is negligible in most practical constructs, and therefore, one can exploit plain, undoped DNA constructs as nanoscale templates also for electronic applications without having to take the possible small conductivity of the scaffold into account.

Chapter 7

Field-induced nanolithography

7.1 Background

As presented in the introductory chapter of this thesis, besides DEP there exist various methods to control nano-objects spatially and futhermore use them as components of functional devices. Many of these methods provide precise control of individual particles [32, 35, 69, 133], but are often limited in throughput. This is a restricting factor in most applications, in particular if considering mass production. On the contrary, there are also common limitations in the high throughput methods: they can either be restricted in spatial resolution [29, 60] or the objects are bound to the chip, which is used in the assembly of materials, making transferring of the formed pattern impossible [84, 132, 146, 157]. Although there are methods for controlling nanoparticles which can overcome all these issues, they are suitable only for certain type of particles, for example, the feasible pattern transfer method presented in Ref. [26] can be exploited only for charged particles.

In the field of pattern transfer, nanoimprint lithography (NIL) has been proven to be a very efficient low-cost method with high resolution and throughput. NIL is based on deforming a target surface, which is usually covered with a thin layer of resist, mechanically with a desired mold [30]. A similar method, microcontact printing (μCP), is also based on the mechanical pressing, but the material of the mold is flexible polymer (polydimethylsiloxane, PDMS), which enables direct pattern transfer of biomolecules or nanoparticles to the target surface [83]. The only hindrance of these methods is that each pattern needs a unique mold, which makes the multicomponent pattern transfer rather difficult. This is due to the requirement that the successive mold (master) pressings should always be aligned accurately with respect to the already formed pattern. Thus, in order to realize a practical multicomponent pattern transfer method, the stamp should enable transferring of any multicomponent pattern to the target surface without changing the master.

In this Chapter and in the article **A.IV** of this thesis, a versatile method, which is taking into account all the above-mentioned issues, is introduced. The method is

called field-induced nanolithography (FINAL) and it is based on the DEP manipulation of nano-objects into desired configurations on the master followed by a transfer of the pattern to another surface. The dynamic control over the trapping pattern by DEP enables usage of the same master stamp for successive transferring processes and thus also multicomponent patterning. The feasibility of the method is demonstrated using quantum dots as nano-objects (DEP of QDs is already presented in Sec. 5.2.3), also including the mechanical transfer of the created QD configuration to the target plate.

7.2 FINAL method

The experimental steps of the FINAL method for QDs (similarly to any polarizable nano-object) are the following (see also the corresponding schematics illustrated in Fig. 7.1):

1. An AC-voltage (7 V_{pp}, 1 MHz) is applied to the certain set of lithographically fabricated electrodes (electrode structure presented in Sec. 5.2.3) and a 10 µl drop of 80 nM quantum dot solution is pipetted onto the surface of the master, i.e. on top of the electrode structure. Before this step the master stamp was incubated with a SuperBlock blocking buffer in PBS (Pierce) in order to prevent non-specific binding of QDs to the electrodes and the substrate (Fig. 7.1a).

2. Waiting time of 10 minutes for the DEP trapping to take place (Fig. 5.8 and 7.1b). During the trapping one can reduce the concentration of freely moving, non-trapped QDs by washing a sample gently with DI water.

3. The target plate is brought in mechanical contact with the solution (Fig. 7.1b) and the trapped QDs (Fig. 7.1c). The target plate is a microscope cover slip, which was treated beforehand with poly(diallyldimethylammonium chloride) (PDACMAC) in order to enhance the adhesion of the QDs to the plate.

4. The target plate with QDs attached to it is removed and dried with nitrogen flow (Fig. 7.1d and 7.2a). The electrode structure is rinsed with DI water and dried enabling the reusage of the master (Fig. 7.2c).

By comparing the spacings between adjacent electrode pairs on the master stamp to the spacings between the high fluorescence intensity spots (QD aggregates) on the target plate (Fig. 7.2a) after the transfer and measuring the emission spectra from these spots, one can prove that the transfer pattern indeed consists of QDs originated from the DEP-traps. It can also be seen that the method is highly selective, since there is a huge difference in intensities between the QD-spots and the background. The 'signal-to-noise ratio', i.e. intensity of the high fluorescence spot

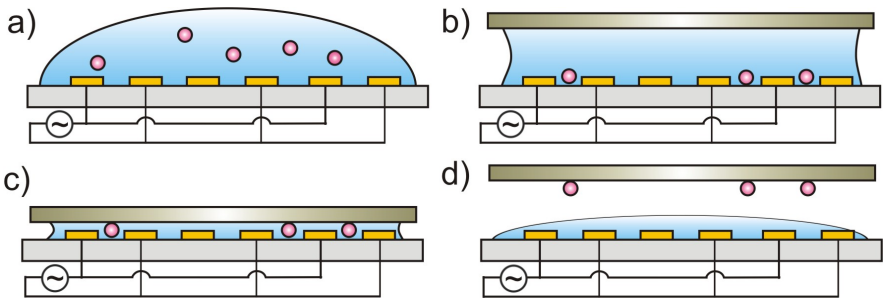

FIGURE 7.1 The principle of FINAL method. a) AC-voltage is applied to certain electrodes of a master stamp and the solution containing nano-objects is pipetted onto the surface. b) The nano-objects get trapped at the locations where the DEP force overcomes their Brownian motion resulting in the desired trapping pattern. c) The target plate is brought in mechanical contact with the trapped objects while the trapping field is on. d) The target plate is lifted with the nano-objects attached to it. The image is adapted with permission from **A.IV**.

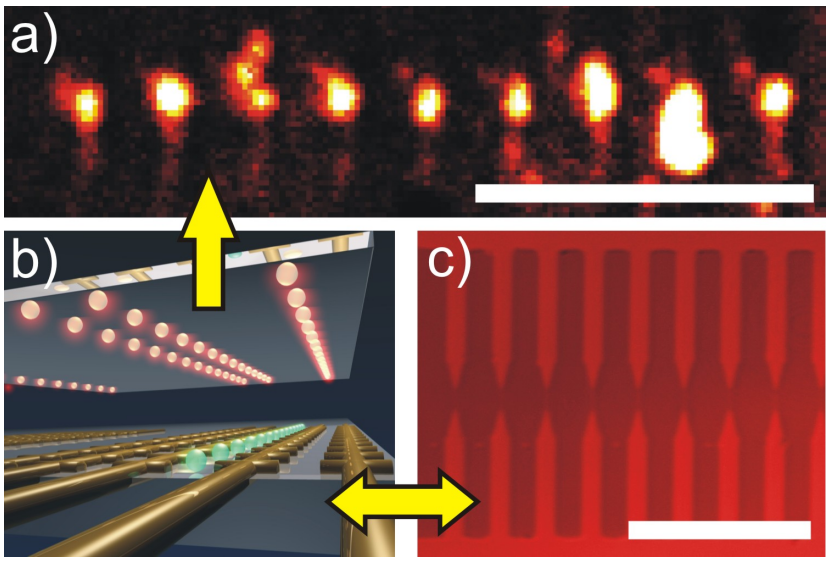

FIGURE 7.2 The dynamic control of the trap and the objects allows one to form multicomponent patterns. a) A desired pattern of QDs on the target plate after the transfer demonstrates the efficiency of the process (a confocal fluorescence micrograph). The image corresponds to the target plate shown in the schematic subfigure b. b) The second species of objects (green spheres) can be DEP-trapped on the master stamp after the first transfer (red spheres). c) The master stamp is empty and thus reusable after each transfer (a confocal fluorescence image after transferring the pattern shown in a). The scale bars are 50 μm. The image is adapted with permission from **A.IV** and slightly modified.

vs. intensity of the background emission, can be enhanced if the sample is washed with DI water during the step 2. It was observed that the signal-to-noise ratio was 5-50 fold higher compared to the reference sample, which was treated similarly but which did not undergo the washing procedure. The result indicates that the trapped QDs stay bound to the trap while washing, and that the background emission is due to the free, non-trapped QDs attached to the target plate during the step 3.

7.3 Discussion

Since the trap can be dynamically controlled as presented in Sec. 5.2.3 and the master stamp is universal and reusable, the method allows multicomponent patterning (see Fig. 7.2). In addition, the parallel fashion of trapping and and the pattern transfer could be exploited in the mass production.

The pattern is created by DEP trapping, meaning that the method is suitable for almost any kind of nano-objects. In a successful DEP trapping the only requirements are that the polarizability of the particle is larger than the polarizability of the medium and that the produced trapping force overcomes the thermal force of the objects. This can be achieved also in the case of nanoscale objects by applying the voltage to narrow electrodes, resulting in the high electric field gradients. Here, it was noticed that the FEM-simulated maximum gradient of the electric field squared in the vicinity of the nanoelectrodes ($\sim 10^{24}$ $\mathrm{V^2/m^3}$) was three and six orders of magnitude higher compared to the optical tweezers and surface plasmon polariton (SPP) based systems [69, 132], respectively.

DEP has also previously been exploited in the pattern transfer procedures [91, 149]. However, besides the high gradients, the advantage in using nanoelectrodes is to reduce the dimensions of the whole system: compared to Refs. [91, 149], one can achieve one tenth of the particle size and one fifth of the overall feature size with the demonstrated technique.

In addition, the power input needed for DEP trapping is assumed to be much lower than in the other systems. This is crucial in context of (temperature) sensitive materials such as many biomolecules, e.g. DNA. However, the mechanical pressing can damage very sensitive objects. Thus, one could improve the proposed setup by covering the surface of the target plate with a thin layer of PDMS as in μCP applications. This could enable a good mechanical contact with a relatively low pressing force and moreover, it has been reported that PDMS could also reduce a non-specific binding of objects to the target plate [83].

Chapter 8

Programmable immobilized PCR in nanoscale

8.1 Background

Polymerase chain reaction (PCR) is one of the basic tools in molecular biology (invented already in 1971 [81] and implemented to the laboratory work during 1990's - Nobel Prize was awarded to Kary B. Mullis in 1993) and it is widely used in production of DNA molecules with a desired sequence as mentioned in Sec. 1.1.4. It also enables applications in other fields such as diagnostics, juridical research and personal medicine. PCR allows exponential amplification of a target DNA sequence, i.e. a template, by using short synthetic DNA oligonucleotides as reaction primers, elongated by the polymerase. The method employs thermostable polymerase and temperature cycling enabling repetition of the amplification step and thus allowing one to detect and characterize small amounts - even a single copy - of DNA.

Usually, a PCR process is run in a solution. However, it is also possible to elongate DNA primers (used for amplification) even if they are immobilized on a substrate. The first reported 'immobilized PCR' reaction was based on detecting a virus by utilizing PCR with one of the primers covalently immobilized [130]. In addition, there exists a successful demonstration of the preparation of arrays of long DNA sequences by 'on-chip' elongation [159] as well as a so-called 'bridge amplification' method [14], where both primers are immobilized in large amounts to extensive surfaces, and then the extension product from one bound primer forms 'a bridge' to another.

In this Chapter and in the paper **A.V** of this thesis, it is shown that the concept of 'immobilized PCR' is realizable also in nanoscale. The method introduced here, a programmable immobilized PCR, provides controlled connection of gold nanoelectrodes with single dsDNA molecules by utilizing PCR. Potentially, it can find applications in the fields of detection and sensing, as well as in molecular electronics.

8.2 Bridging nanoelectrodes with dsDNA

The programmable immobilized PCR is based on trapping and immobilization of thiol-modified ssDNAs to the nanoelectrodes by AC-DEP (as described in Sec. 5.2.4) and consequently using them as primers and extending them in a PCR procedure. The elongated primers can either *1)* form a complete dsDNA bridging the gap between the electrodes (Fig. 8.1 4:upper and Fig. 8.2b) or *2)* pair with the complementary strands originated from a template (Fig. 8.1 4:lower and Fig. 8.2d). In principle, the method also allows more sophisticated wiring systems, if one uses multielectrode geometries for trapping primers in the electrode-specific manner as presented in Fig. 5.11. Here, multielectrode geometries were only exploited in order to demonstrate that primers can be trapped separately, but they were not used in the actual PCR experiment, since this kind of trapping procedure is a bit laborious method for studying the kinetics of extension of the primers in PCR due to an assumed low yield of the process. Moreover, the DNA molecules used in these experiments contained Cy3 and Cy5 dyes at the 3′ ends and thus, they were not suitable for being elongated.

The forward and reverse primers (see Materials and methods in Appendixes) used in the experiments were 5′-thiol-modified 38 nt ssDNA molecules (purchased from Integrated DNA Technologies as dual HPLC-purified), where the sequences downstream the $(CT)_8$-spacer matched to the terminal sequences of the complementary strands of the 414 bp template [partial complementary DNA of chicken avidin, sequence presented in Refs. [51, 154] and in Appendixes (Materials and methods)]. The role of the spacers is to facilitate the attachment of the template to the primers and also provide enough space for the polymerase to operate in the vicinity of the electrodes.

The trapping of the primers was carried out similarly as explained in Sec. 5.2.4, but now with similar array of adjacent fingertip type electrode pairs as in QD trapping in order to gain more data in a single PCR run. A gap between opposite electrodes in this electrode structure was $\sim$ 100-140 nm corresponding to the length of the template strand and thus the PCR product formed by the extended primers. The immobilization of the primers was carried out by exploiting AC-DEP: about 10 µl of ssDNA solution containing both the primers ($\sim$ 20 nM in the Hepes/NaOH buffer) was pipetted onto the chip and an AC voltage of 4.5 V_{pp} (V_{DC} = 0) was applied to the electrodes. The amount of immobilized primers was controlled by adjusting the trapping time, which was typically 1-2 minutes. Finally, the sample was gently rinsed with water and imaged with AFM (see Fig. 8.2a and c).

After the successful immobilization of the primers, the chip containing both the electrode structure and the primers was placed into a 0.2 ml tube with the reagents and components required for the PCR procedure (see the components and amounts from Table 8.1). The following thermal cycle (Biometra T3 Thermoblock, Biotron, Germany) was used: *1)* 94 °C, 5 min; *2)* 94 °C, 40 s; *3)* 50 °C, 3 min; *4)* 72 °C,

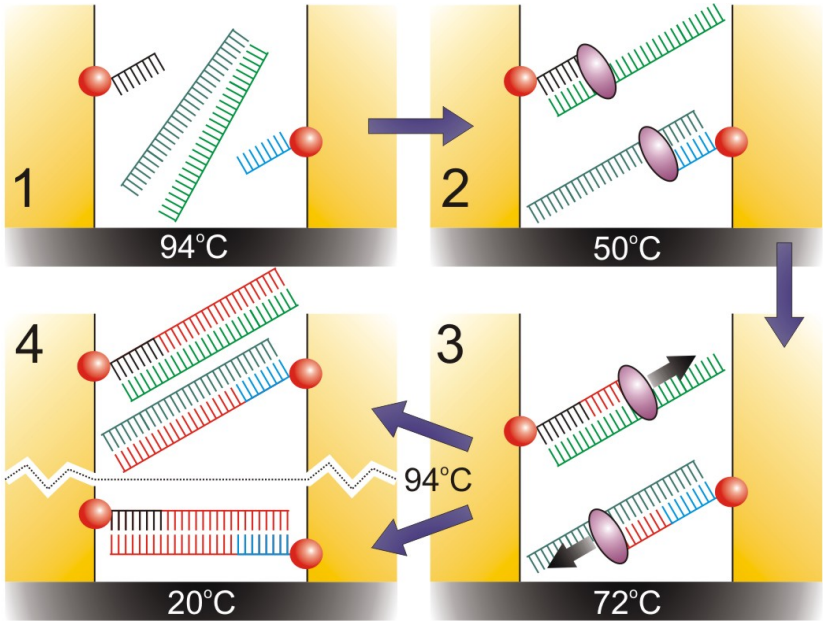

FIGURE 8.1 A schematic view of the PCR growing method. A sample, which contains two different types of primers (black and light blue) immobilized to the electrodes (yellow), is placed into a tube with required PCR reagents, such as dsDNA template (green strands), Taq DNA polymerase (violet) and nucleotides (red) (dNTP mix). *Step 1)* At the initialization / denaturation temperature the template dehybridizes. *Step 2)* In the annealing step the template strands pair with the primers (complementary sequences) and the polymerase binds to the primer-template hybrid. *Step 3)* The polymerase elongates the immobilized primers by building a complete strand nucleotide by nucleotide. During later cycles of the procedure the extended primer can act as a template strand for primers attached to the opposite electrode (in the steps 2 and 3). *Step 4)* After denaturation and annealing, the extended primers can bridge the gap between the electrodes via hybridization (lower image and Fig. 8.2b) or pair again with the complementary template strands (upper image and Fig. 8.2d). The image is adapted from **A.V**.

4 min; *5)* 4 °C, where the cycles 2-4 were repeated 25-50 times. As a final step, the chip was first removed from the tube and washed with distilled water, and second, the results, i.e. extended and consequently hybridized PCR products, were verified by AFM imaging. In Fig. 8.2b an AFM image of a single $\sim$ 150 nm long dsDNA molecule, grown during the PCR run and comprised of the extended primers attached to the opposite electrodes, is bridging the gap between the electrodes (compare to the Fig. 8.2b). Figure 8.2d presents an alternative result of the PCR growing process, where elongated primers are paired with template strands via hybridization during the annealing step, also forming $\sim$ 150 nm long dsDNA molecules at the edge of the electrode.

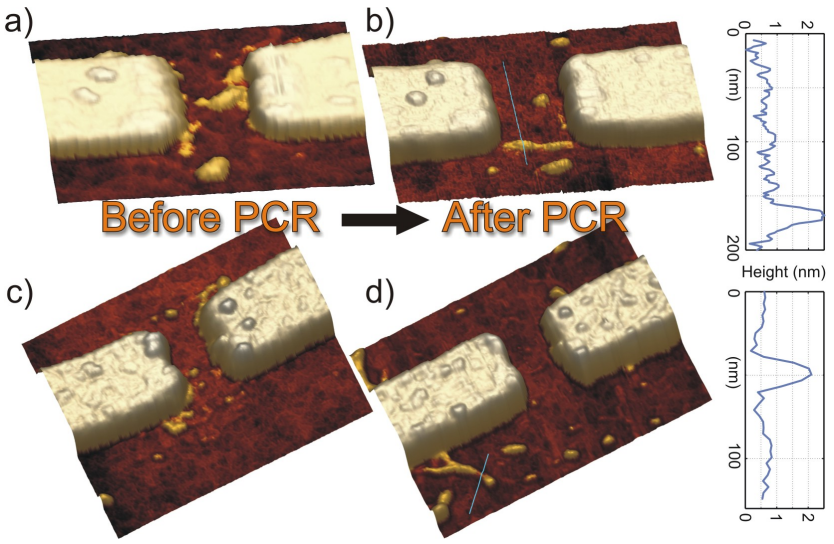

FIGURE 8.2 Growing dsDNA molecules by PCR. 'Before PCR' AFM images of 38 nt long primers immobilized to the electrodes (a and c) and 'after PCR' AFM images (b and d) of the same electrodes shown in subfigures a and c, respectively. After the PCR run, two different final results are possible: either a single grown dsDNA molecule, consisted of two elongated primers, bridges the gap between electrodes (see b) or a dsDNA molecule, i.e. a hybrid of an elongated primer and a template strand, is formed at the edge of the electrode (see d). The gap between the electrodes is ca. 120 nm in both samples. Height in the all images is presented in a logarithmic scale. The graphs on the right are cross-sections along the blue lines on b and d, showing the characteristic height of the dsDNA, i.e. ~ 2 nm. The image is adapted from **A.V**.

8.3 Discussion

In this particular experimental setup, AFM imaging was the only method to verify the PCR results. In principle, one could prove the successful bridging of the electrodes by measuring the electric current through the sample (this could be exploited in sensing applications assuming certain conditions), but here a quite long dsDNA was used and it is known to be a rather poor conductor according to the measurements reported in this thesis and e.g. in Refs. [126, 154]. In addition, almost insulating ssDNA spacers (see Sec. 6.2.1) were attached between a grown dsDNA molecule and an electrode resulting in the fact that the verification based on the electrical measurements was not practicable. Moreover, and most importantly, the electrical conductivity of DNA strongly depends on the environment (ions and water) as clearly seen already in Chapter 6. This forbids the direct comparison of the conductivity of the control sample (before PCR: Hepes/NaOH buffer) and the sample with bridged electrodes (after PCR: Taq buffer and $MgCl_2$). Also, the optical verification, i.e. labeling of a single grown DNA in the gap with dsDNA-specific fluorescent dye, is not realizable either, due to the detection limit of the confocal microscope contrasted

TABLE 8.1 PCR reagents and amounts in the order of mixing.

Component	Amount [µl]	Final concentration
Distilled water	69.9	-
10× Taq buffer [750 nM Tris-HCl (pH 8.8), 200 nM $(NH_4)_2SO_4$, 0.1 % Tween 20]	10.0	1×
$MgCl_2$ (25 mM)	8.0	2.0 mM
dsDNA template (51 ng/µl)	1.5	0.76 ng/µl
dNTP mix (2 mM)	10.0	0.2 mM
Taq DNA polymerase (5 U/µl)	0.6	1.5 U / 50 µl

with low number of molecules grown (and thus the amount of dye molecules attached).

In summary, by further optimizing the procedure and designing an electrode pattern suitable for the application in question, the developed technique could serve as a tool in exploiting PCR on a new level, in detecting molecules or molecule components, and in the fabrication of bottom-up based devices for nanoelectronics only at desired locations on a chip. This kind of device could be DNA-based multiswitching unit programmable to react on planned targets or DNA-programming platform, where identical electrode geometries are tailored by using different combinations of primers and template sequences. The simple concept of this kind of platform is presented in Fig. 8.3.

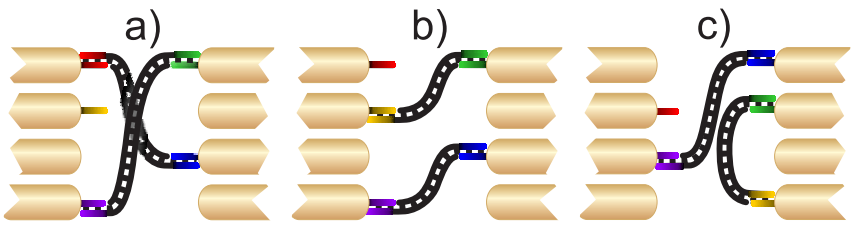

FIGURE 8.3 The proposed DNA programming technique and the potential of the demonstrated method. a) The chosen electrodes have been bridged by exploiting suitable templates and a configuration of the immobilized primers. b) The same configuration of the primers can be utilized to provide various connections by using different templates. c) Variation in the primer configuration enables numerous wiring options even with the same templates (identical templates in b and c).

Conclusions

DEP trapping studies. Dielectrophoresis was utilized for controlled positioning of nano-objects in between lithographically fabricated electrodes in all the papers **A.I** - **A.V** of this thesis, and the trapping results are discussed in detail in Chapter 5. It was shown that DEP is a very feasible tool for nanoscale manipulation and/or immobilization of DNA origamis (**A.I** and **A.II**), defined-sized TX tile constructs (**A.III**), quantum dots (**A.IV**) and single-stranded DNA molecules (**A.V**). In addition, the trapping results were in agreement with the simple estimations of polarizabilities of the DEP-trapped objects presented in Chapter 2. In most cases the method allows high yields (also for single object trapping) due to the high electric field gradients created by means of narrow nanoelectrodes. It was also demonstrated using single-stranded DNA molecules that the electrode-specific trapping of objects is possible with multielectrode geometries. DEP can also serve as a bridge between 'top-down' (lithography) and 'bottom-up' (self-assembly) fabrication approaches, and actually, the trapping of DNA origamis was the first reported demonstration of DEP manipulation of complex, self-assembled structures. By combining DEP or other possible anchoring mechanisms of DNA templates [48, 79] and the self-assemby properties of DNA with nanometer scale patterning possibilities (decorating demonstrated for TX tiles in paper **A.III** and in Chapter 4), one can fabricate devices with single components below 10 nm and all the dimensions of the complex below 100 nm, e.g. for the purposes of bionanotechnology, molecular electronics and plasmonics [67].

Electrical measurements. DEP trapping technique enables electrical measurements of single DNA constructs as described in articles **A.II** and **A.III** of this thesis and in Chapter 6. The electrical properties of DNA constructs were characterized by means of AC impedance spectroscopy with full equivalent circuit modeling combined with DC measurements. The developed equivalent circuit model quantitatively describes the processes contributing to the both DC and AC conductivity and indicates that the conductivities of the DNA structures contain both ohmic and diffusive contributions. The method reveals that the conductance of the DNA itself is poor and the main charge carriers in high humidity conditions are the adsorbed and ionized water molecules and thus, the conductivity is dependent on the size of the DNA construct in question. The electrical measurement of DNA origami was the first experiment where both the DC and AC conductivity mechanisms of DNA or any single complex self-assembled molecule construction have been fully ana-

lyzed using a detailed equivalent circuit. The obtained results showed clearly that the conductivity of DNA is strongly related to the surrounding environment, and thus, this study can also explain some controversy over the earlier results in the field of DNA conductivity. The results are essential information for the future development of DNA-based nanoelectronic assemblies, although the conductivities of the DNA templates investigated are quite low: in high humidity conditions (relative humidity $\sim$ 90 %) the resistance was of the order of 100 MΩ - 10 GΩ, and in the dry environment $\sim$ TΩ. Knowing the conductivity mechanisms of potential DNA templates allows their accurate manipulation, e.g. by electric fields and furthermore, one can find applications in the assembly of electrical nanodevices by making locally conducting parts in constructs by suitable doping.

Field-induced nanolithography. The article **A.IV** of this thesis and Chapter 7 deal with a novel method developed for high precision and high throughput pattern transfer of nano-objects from the master to the target plate simply by mechanical pressing. The technique is also based on DEP manipulation: it allows dynamic control over the trapped objects by electric fields on a universal master stamp (described in Chapter 5), and thereby it also makes multicomponent nanoscale patterns possible. The applicability of the technique was demonstrated using quantum dots, and such controllable arrays of QDs can be utilized e.g. in the context of solar cell fabrication and optical biosensors. But most importantly, it is readily extendable to other nano-objects as well. The method is robust and versatile meaning that it can be exploited in many potential applications in nanotechnology. The technique could also find commercial interest since even mass production is possible.

Programmable immobilized PCR in nanoscale. The paper **A.V** of this thesis and Chapter 8 introduce a method for bridging electrodes with double-stranded DNA molecules. This was done locally on a chip by utilizing polymerase chain reaction and single-stranded DNA molecules, i.e. reaction primers, immobilized to the opposite fingertip-type electrodes by means of DEP. The idea is to use a polymerase as a workhorse for elongating the immobilized primers, and thus to form a 'ds-DNA molecule bridge' over the gap of the nanoelectrodes via hybridization of the extended strands. This is the first time PCR has been used in nanoscale to produce molecular level nanotechnological structures or devices and it is an opportune example how one can exploit biological systems in nanoscale fabrication. However, in this particular experimental setup the yield was not very high, but further optimization could provide a tool to exploit PCR on a new level, and to design and realize sophisticated wiring systems and patterns out of DNA readily at certain spatial positions. Multielectrode geometries enable the electrode-specific trapping of primers as demonstrated in Chapter 5, and thus programmability of the method becomes possible, i.e. identical electrode geometries can be tailored by using different combinations of primers and template sequences. Therefore, the technique will open up opportunities for bionanotechnology, detecting and sensing applications as well as

for molecular electronics.

In summary, the work reported in this thesis provides crucial scientific information about the properties of DNA and potential DNA-based applications in nanotechnology. By combining the efficient and controllable DEP manipulation of single DNA molecules and complex self-assembled DNA constructs with the top-down techniques one can fabricate sophisticated and highly ordered circuits and functional devices truly in nanoscale. In general, the approaches based on exploiting evolution-optimized biosystems - in particular the exceptional self-assembly characteristics of DNA, also studied in this work - can serve as a toolbox for the next generation of device fabrication enabling the production of nanostructures made of materials relevant for electronics, optics and sensing.

Bibliography

[1] *IMB Jena Image Library of Biological Macromolecules, Institute of Molecular Biotechnology, Jena, Germany*, `http://www.imb-jena.de/image_library/DNA/DNA_models/`.

[2] *The mfold Web Server*, `http://mfold.rna.albany.edu/?q=mfold`.

[3] ALDAYE, F. A., PALMER, A. P., AND SLEIMAN, H. F., *Assembling Materials with DNA as the Guide*. Science **321** (2008) 1795.

[4] ALDAYE, F. A. AND SLEIMAN, H. F., *Modular Access to Structurally Switchable 3D Discrete DNA Assemblies*. J. Am. Chem. Soc. **129** (2007) 13376.

[5] ALIVISATOS, A. P., JOHNSON, K. P., PENG, X., WILSON, T. E., LOWETH, C. J., BRUNCHEZ JR., M. P., AND SCHULTZ, P. G., *Organization of 'nanocrystal molecules' using DNA*. Nature **382** (1996) 609.

[6] ANDERSEN, E. S., DONG, M., NIELSEN, M. M., JAHN, K., SUBRAMANI, R., MAMDOUH, W., GOLAS, M. M., SANDER, B., STARK, H., OLIVEIRA, C. L. P., SKOV PEDERSEN, J., BIRKEDA, V., BESENBACHER, F., GOTHELF, K. V., AND KJEMS, J., *Self-assembly of a nanoscale DNA box with a controllable lid*. Nature **459** (2009) 73.

[7] ANDERSON, J. H. AND PARKS, G. A., *Electrical conductivity of silica gel in the presence of adsorbed water*. J. Phys. Chem. **72** (1968) 3662.

[8] BARISH, R. D., SCHULMAN, R., ROTHEMUND, P. W. K., AND WINFREE, E., *An information-bearing seed for nucleating algorithmic self-assembly*. Proc. Nat. Acad. Sci. U.S.A. **106** (2009) 6054.

[9] BARSOUKOV, E. AND MACDONALD, J. R., *Impedance Spectroscopy: Theory, Experiment, and Applications, Second Edition*. Wiley, Hoboken, New Jersey (2005).

[10] BATH, J., GREEN, S. J., AND TURBERFIELD, A. J., *A free-running DNA motor powered by a nicking enzyme*. Angew. Chem. Int. Ed. **44** (2005) 4358.

[11] BATH, J. AND TURBERFIELD, A. J., *DNA nanomachines*. Nature Nanotech. **2** (2007) 275.

[12] BERASHEVICH, J. AND CHAKRABORTY, T., *How the Surrounding Water Changes the Electronic and Magnetic Properties of DNA*. J. Phys. Chem. B **112** (2008) 14083.

[13] BEZRYADIN, A., DEKKER, C., AND SCHMID, G., *Electrostatic trapping of single conducting nanoparticles between nanoelectrodes*. Appl. Phys. Lett. **71** (1997) 1273.

[14] BING, D. H., BOLES, C., REHMAN, F. N., AUDEH, M., BELMARSH, M., KELLEY, B., AND ADAMS, C. P., *Bridge Amplification: A Solid Phase PCR System for the Amplification and Detection of Allelic Differences in Single Copy Genes*, `http://www.promega.com/geneticidproc/ussymp7proc/0726.html`.

[15] BISQUERT, J., GARCIA-BELMONTE, G., FABREGAT-SANTIAGO, F., FERRIOLS, N. S., BOGDANOFF, P., AND PEREIRA, E. C., *Doubling Exponent Models for the Analysis of Porous Film Electrodes by Impedance. Relaxation of TiO_2 Nanoporous in Aqueous Solution*. J. Phys. Chem. B **104** (2000) 2287.

[16] BIXON, M. AND JORTNER, J., *Long-range and very long-range charge transport in DNA*. Chem. Phys. **281** (2002) 393.

[17] BOBADILLA, A. D., BELLIDO, E. P., RANGEL, N. L., ZHONG, H., NORTON, M. L., SINITSKII, A., AND SEMINARIO, J. M., *DNA origami impedance measurement at room temperature*. J. Chem. Phys. **130** (2009) 171101.

[18] BOON, E. M. AND BARTON, J. K., *Charge transport in DNA*. Curr. Opin. Struct. Biol. **12** (2002) 320.

[19] BRAUN, E., EICHEN, Y., SIVAN, U., AND BEN-YOSEPH, G., *DNA-templated assembly and electrode attachment of a conducting silver wire*. Nature **391** (1997) 775.

[20] BREAKER, R. R., *DNA aptamers and DNA enzymes*. Curr. Opin. Chem. Biol. **1** (1997) 26.

[21] BRIMAN, M., ARMITAGE, N. P., HELGREN, E., AND GRÜNER, G., *Dipole Relaxation Losses in DNA*. Nano Lett. **4** (2004) 733.

[22] BUI, H., ONODERA, C., KIDWELL, C., TAN, Y., GRAUGNARD, E., KUANG, W., LEE, J., KNOWLTON, W. B., YURKE, B., AND HUGHES, W. L., *Programmable Periodicity of Quantum Dot Arrays with DNA Origami Nanotubes*. Nano Lett. **10** (2010) 3367.

[23] BURKE, P. J., *Nanodielectrophoresis: Electronic Nanotweezers*. Encycl. Nanosci. Nanotechnol. **6** (2004) 623.

[24] CALZOLARI, A., DI FELICE, R., MOLINARI, E., AND GARBESI, A., *G-quartet biomolecular nanowires*. Appl. Phys. Lett. **80** (2002) 3331.

[25] CASTELLANOS, A., RAMOS, A., GONZÁLEZ, A., GREEN, N. G., AND MORGAN, H., *Electrodynamics and dielectrophoresis in microsystems: scaling laws*. J. Phys. D: Appl. Phys. **36** (2003) 2584.

[26] CHANG, Y., HUANG, S., AND CHEN, Y., *Biomolecular Nanopatterning by Electrophoretic Printing Lithography*. Small **5** (2009) 63.

[27] CHEN, Y., WANG, M., AND MAO, C., *An autonomous DNA nanomotor powered by a DNA enzyme*. Angew. Chem. Int. Ed. **43** (2004) 3554.

[28] CHHABRA, R., SHARMA, J., KE, Y., LIU, Y., RINKER, S., LINDSAY, S., AND YAN, H., *Spatially Addressable Multiprotein Nanoarrays Templated by Aptamer-Tagged DNA Nanoarchitectures*. J. Am. Chem. Soc. **129** (2007) 10304.

[29] CHIOU, P. Y. AND WU, M. C., *Manipulating Nanoparticles and Macromolecules with Light Patterned Microfluidic Flow*. Proc. IEEE Int. Conf. Nano/Micro Eng. Mol. Sys. (2008) 1204.

[30] CHOU, S. Y., KRAUSS, P. R., AND RENSTROM, P. J., *Imprint Lithography with 25-Nanometer Resolution*. Science **272** (1996) 85.

[31] CICORIA, R. AND SUN, Y., *Dielectrophoretically trapping semiconductive carbon nanotube networks*. Nanotechnology **19** (2008) 485303.

[32] COHEN, A. E., *Control of Nanoparticles with Arbitrary Two-Dimensional Force Fields*. Phys. Rev. Lett. **94** (2005) 118102.

[33] COHEN, H., NOGUES, C., NAAMAN, R., AND PORATH, D., *Direct measurement of electrical transport through single DNA molecules of complex sequence*. Proc. Natl. Acad. Sci. USA **102** (2005) 11589.

[34] DEKKER, C. AND RATNER, M., *Electronic properties of DNA*. Phys. World **14** (2001) 29.

[35] DIENEROWITZ, M., MAZILU, M., REECE, P. J., KRAUSS, T. F., AND DHOLAKIA, K., *Optical vortex trap for resonant confinement of metal nanoparticles*. Opt. Express **16** (2008) 4991.

[36] DIETZ, H., DOUGLAS, S. M., AND SHIH, W. M., *Folding DNA into Twisted and Curved Nanoscale Shapes*. Science **325** (2009) 725.

[37] DING, B., DENG, Z., YAN, H., CABRINI, S., ZUCKERMANN, R. N., AND BOKOR, J., *Gold Nanoparticle Self-Similar Chain Structure Organized by DNA Origami*. J. Am. Chem. Soc. **132** (2010) 3248.

[38] DOUGLAS, S. M., DIETZ, H., LIEDL, T., HÖGBERG, B., GRAF, F., AND SHIH, W. M., *Self-assembly of DNA into nanoscale three-dimensional shapes*. Nature **459** (2009) 414.

[39] DOUGLAS, S. M., MARBLESTONE, A. H., TEERAPITTAYANON, S., VAZQUEZ, A., CHURCH, G. M., AND SHIH, W. M., *Rapid prototyping of 3D DNA-origami shapes with caDNAno*. Nucleic Acids Res. **37** (2009) 5001.

[40] DULIĆ, D., TUUKKANEN, S., CHUNG, C. L., ISAMBERT, A., LAVIE, P., AND FILORAMO, A., *Direct conductance measurements of short single DNA molecules in dry conditions*. Nanotechnology **20** (2009) 115502.

[41] ELEY, D. D. AND SPIVEY, D. I., *Semiconductivity of organic substances. Nucleic acid in the dry state*. Trans. Faraday Soc. **58** (1962) 411.

[42] ENDRES, R. G., COX, D. L., AND SINGH, R. R. P., *The quest for high-conductance DNA*. Rev. Mod. Phys. **76** (2004) 195.

[43] FAHLMAN, R. P., HSING, M., SPORER-TUHTEN, C. S., AND SEN, D., *Duplex Pinching: A Structural Switch Suitable for Contractile DNA Nanoconstructions*. Nano Lett. **3** (2003) 1073.

[44] FALK, M., HARTMAN JR., K. A., AND LORD, R. C., *Hydration of Deoxyribonucleic Acid. I. a Gravimetric Study*. J. Am. Chem. Soc. **84** (1962) 3843.

[45] FEYNMAN, R. P., *There's Plenty of Room at the Bottom: A talk in the annual meeting of the American Physical Society at the California Institute of Technology (Caltech) on December 29th 1959.*, `http://www.its.caltech.edu/~feynman/plenty.html`.

[46] FINK, H.-W. AND SCHÖNENBERGER, C., *Electrical conduction through DNA molecules*. Nature **398** (1999) 407.

[47] FLOOD, A. H., STODDART, J. F., STEUERMAN, D. W., AND HEATH, J. R., *Chemistry. Whence molecular electronics?* Science **306** (2004) 2055.

[48] GERDON, A. E., OH, S. S., HSIEH, K., KE, Y., YAN, H., AND SOH, H. T., *Controlled Delivery of DNA Origami on Patterned Surfaces*. Small **5** (2009) 1942.

[49] GOODMAN, R. P., BERRY, R. M., AND TURBERFIELD, A. J., *The single-step synthesis of a DNA tetrahedron*. Chem. Commun. **2004** (2004) 1372.

[50] GOODMAN, R. P., SCHAAP, I. A. T., TARDIN, C. F., ERBEN, C. M., BERRY, R. M., SCHMIDT, C. M., AND TURBERFIELD, A. J., *Rapid Chiral Assembly of Rigid DNA Building Blocks for Molecular Nanofabrication*. Science **310** (2005) 1661.

[51] GOPE, M. L., KEINÄNEN, R. A., KRISTO, P. A., CONNEELY, O. M., BEATTIE, W. G., ZARUCKI-SCHULZ, T., O'MALLEY, B. W., AND KULOMAA, M. S., *Molecular cloning of the chicken avidin cDNA*. Nucleic Acids Res. **15** (1987) 3595.

[52] GOTHELF, K. V. AND LABEAN, T. H., *DNA-programmed assembly of nanostructures*. Org. Biomol. Chem. **3** (2005) 4023.

[53] GREEN, N. M., *Avidin*. Adv. Protein Chem. **29** (1975) 85.

[54] GU, H., CHAO, J., XIAO, S.-J., AND SEEMAN, N. C., *A proximity-based programmable DNA nanoscale assembly line*. Nature **465** (2010) 202.

[55] GU, Q., CHENG, C., AND HAYNIE, D. T., *Cobalt metallization of DNA: toward magnetic nanowires*. Nanotechnology **16** (2005) 1358.

[56] GUIDOTTI, C., MINUNNI, M., AND MONCELLI, M. R., *Probing DNA hybridization in thiolipid monolayers by means of impedance spectroscopy*. Electrochem. Comm. **9** (2007) 2380.

[57] GUO, X., GORODETSKY, A. A., HONE, J., BARTON, J. K., AND NUCKOLLS, C., *Conductivity of a single DNA duplex bridging a carbon nanotube gap*. Nature Nanotech. **3** (2008) 1632.

[58] HA, D. H., NHAM, H., YOO, K.-H., SO, H., LEE, H.-Y., AND KAWAI, T., *Humidity effects on the conductance of the assembly of DNA molecules*. Chem. Phys. Lett. **355** (2002) 405.

[59] HAN, D., PAL, S., LIU, Y., AND YAN, H., *Folding and cutting DNA into reconfigurable topological nanostructures*. Nature Nanotech. **5** (2010) 712.

[60] HAYWARD, R. C., SAVILLE, D. A., AND AKSAY, I. A., *Electrophoretic assembly of colloidal crystals with optically tunable micropatterns*. Nature **404** (2000) 56.

[61] HIPPS, K. W., *Molecular Electronics: It's All About Contacts*. Science **294** (2001) 536.

[62] HÖGBERG, B., LIEDL, T., AND SHIH, W. M., *Folding DNA Origami from a Double-Stranded Source of Scaffold*. J. Am. Chem. Soc. **131** (2009) 9154.

[63] HÖLZEL, R. AND BIER, F. F., *Dielectrophoretic manipulation of DNA*. IEE Proc. Nanobiotechnol. **150** (2003) 47.

[64] HOOGSTEEN, K., *The crystal and molecular structure of a hydrogen-bonded complex between 1-methylthymine and 9-methyladenine*. Acta Crystallogr. **16** (1963) 907.

[65] HUGHES, M. P., *AC electrokinetics: applications for nanotechnology*. Nanotechnology **11** (2000) 124.

[66] HUGHES, M. P. AND MORGAN, H., *Dielectrophoretic trapping of single submicrometre scale bioparticles*. J. Phys. D: Appl. Phys. **31** (1998) 2205.

[67] HUNG, A. M., NOH, H., AND CHA, J. N., *Recent advances in DNA-based directed assembly on surfaces*. Nanoscale **2** (2010) 2530.

[68] JANG JIAN, P.-C., LIU, T.-F., TSAI, C.-M., TSAI, M.-S., AND CHANG, C.-C., *Ni^{2+} doping DNA: a semiconducting biopolymer*. Nanotechnology **19** (2008) 355703.

[69] JAUFFRED, L., RICHARDSON, A. C., AND ODDERSHEDE, L. B., *Three-Dimensional Optical Control of Individual Quantum Dots*. Nano. Lett. **8** (2008) 3376.

[70] JONES, T. B., *Basic theory of dielectrophoresis and electrorotation*. IEEE EMBS Magazine **22** (2003) 33.

[71] KALLENBACH, N. R., MA, R.-I., AND SEEMAN, N. C., *An immobile nucleid acid junction constructed from oligonucleotides*. Nature **305** (1983) 829.

[72] KASUMOV, A. Y., KLINOV, D. V., ROCHE, P.-E., GUÉRON, S., AND BOUCHIAT, H., *Thickness and low-temperature conductivity of DNA molecules*. Appl. Phys. Lett. **84** (2004) 1007.

[73] KASUMOV, A. Y., KOCIAK, M., GUÉRON, S., REULET, B., VOLKOV, V. T., KLINOV, D. V., AND BOUCHIAT, H., *Proximity-Induced Superconductivity in DNA*. Science **291** (2001) 280.

[74] KE, Y., SHARMA, J., LIU, M., JAHN, K., LIU, Y., AND YAN, H., *Scaffolded DNA Origami of a DNA Tetrahedron Molecular Container*. Nano Lett. **9** (2009) 2445.

[75] KELLEY, S. O. AND BARTON, J. K., *Electron Transfer Between Bases in Double Helical DNA*. Science **283** (1999) 375.

[76] KELLOGG, O. D., *Foundations of Potential Theory, Reprinted Edition*. Springer-Verlag, Berlin, Germany (1967).

[77] KEREN, K., BERMAN, R. S., BUCHSTAB, E., SIVAN, U., AND BRAUN, E., *DNA-Templated Carbon Nanotube Field-Effect Transistor*. Science **302** (2003) 1380.

[78] KEREN, K., KRUEGER, M., GILAD, R., BEN-JOSEPH, G., SIVAN, U., AND BRAUN, E., *Sequence-Specific Molecular Lithography on Single DNA Molecules*. Science **9** (2002) 2445.

[79] KERSHNER, R. J., BOZANO, L. D., MICHEEL, C. M., HUNG, A. M., FORNOF, A. R., CHA, J. N., RETTNER, C. T., BERSANI, M., FROMMER, J., ROTHEMUND, P. W. K., AND WALLRAFF, G. M., *Placement and orientation of individual DNA shapes on lithographically patterned surfaces*. Nature Nanotech. **4** (2009) 557.

[80] KLEINE-OSTMANN, T., JÖRDENS, C., BAASKE, K., WEIMANN, T., HRABE DE ANGELIS, M., AND KOCH, M., *Conductivity of single-stranded and double-stranded deoxyribose nucleic acid under ambient conditions: The dominance of water*. Appl. Phys. Lett. **88** (2006) 102102.

[81] KLEPPE, K., OHTSUKA, E., KLEPPE, R., MOLINEUX, I., AND KHORANA, H. G., *Studies on polynucleotides: XCVI. Repair replications of short synthetic DNA's as catalyzed by DNA polymerases*. J. Mol. Biol. **56** (1971) 341.

[82] KRATOCHVÍLOVÁ, I., KRÁL, K., BUNČEK, M., VÍŠKOVÁ, A., NEŠPŮREK, S., KOCHALSKA, A., TODORCIUC, T., WEITER, M., AND SCHNEIDER, B., *Conductivity of natural and modified DNA measured by Scanning Tunneling Microscopy. The effect of sequence, charge and stacking*. Biophys. Chem. **138** (2008) 3.

[83] KRAUS, T., MALAQUIN, L., SCHMID, H., RIESS, W., SPENCER, N. D., AND WOLF, H., *Nanoparticle printing with single-particle resolution*. Nature Nanotech. **2** (2007) 570.

[84] KUMAR, S., SEO, Y.-K., AND KIM, G.-H., *Manipulation and trapping of semiconducting ZnO nanoparticles into nanogap electrodes by dielectrophoresis technique*. Appl. Phys. Lett. **94** (2009) 53104.

[85] KUZUYA, A., KIMURA, M., NUMAJIRI, K., KOSHI, N., OHNISHI, T., OKADA, F., AND KOMIYAMA, M., *Precisely Programmed and Robust 2D Streptavidin Nanoarrays by Using Periodical Nanometer-Scale Wells Embedded in DNA Origami Assembly*. ChemBioChem **10** (2009) 1811.

[86] KUZUYA, A. AND KOMIYAMA, M., *DNA origami: Fold, stick and beyond*. Nanoscale **2** (2010) 310.

[87] KUZYK, A., LAITINEN, K. T., AND TÖRMÄ, P., *DNA origami as a template for protein assembly*. Nanotechnology **20** (2009) 235305.

[88] LABEAN, T. H., YAN, H., KOPATSCH, J., LIU, F., WINFREE, E., REIF, J. H., AND SEEMAN, N. C., *Construction, Analysis, Ligation, and Self-Assembly of DNA Triple Crossover Complexes*. J. Am. Chem. Soc. **122** (2000) 1848.

[89] LANDAU, L. D. AND LIFSHITZ, E. M., *Electrodynamics of continuous media*. Pergamon Press, Oxford, UK (1960).

[90] LE, J. D., PINTO, Y., SEEMAN, N. C., MUSIER-FORSYTH, K., TATON, T. A., AND KIEHL, R. A., *DNA-Templated Self-Assembly of Metallic Nanocomponent Arrays on a Surface*. Nano Lett. **4** (2004) 2343.

[91] LEE, H. J., YASUKAWA, T., SUZUKI, M., TAKI, Y., TANAKA, A., KAMEYAMA, M., SHIKU, H., AND MATSUE, T., *Rapid fabrication of nanoparticles array on polycarbonate membrane based on positive dielectrophoresis*. Sens. Actuators B **131** (2008) 424.

[92] LI, A., YANG, F., MAA, Y., AND YANG, X., *Electrochemical impedance detection of DNA hybridization based on dendrimer modified electrode*. Biosens Bioelectron. **22** (2007) 1716.

[93] LI, H., PARK, S. H., REIF, J. H., LABEAN, T. H., AND YAN, H., *DNA Templated Self-Assembly Of Protein And Nanoparticle Linear Arrays*. J. Am. Chem. Soc. **126** (2004) 418.

[94] LI, X., YANG, X., QI, J., AND SEEMAN, N. C., *Antiparallel DNA double crossover molecules as components for nanoconstruction*. J. Am. Chem. Soc. **118** (1996) 6131.

[95] LIEDL, T., HÖGBERG, B., TYTELL, J., INGBER, D. E., AND SHIH, W. M., *Self-assembly of three-dimensional prestressed tensegrity structures from DNA*. Nature Nanotech. **5** (2010) 520.

[96] LIU, D. AND BALASUBRAMANIAN, S., *A Proton-Fuelled DNA Nanomachine*. Angew. Chem. Int. Ed. **42** (2003) 5734.

[97] LIU, D., PARK, S. H., REIF, J. H., AND LABEAN, T. H., *DNA nanotubes self-assembled from triple-crossover tiles as templates for conductive nanowires*. Proc. Nat. Acad. Sci. U.S.A. **101** (2004) 717.

[98] LIU, D., WANG, M. S., DENG, Z. X., WALULU, R., AND MAO, C. D., *Tensegrity: Construction of Rigid DNA Triangles with Flexible Four-Arm DNA Junctions*. J. Am. Chem. Soc. **126** (2004) 2324.

[99] LO, P. K., KARAM, P., ALDAYE, F. A., MCLAUGHLIN, C. K., HAMBLIN, G. D., COSA, G., AND SLEIMAN, H. F., *Loading and selective release of cargo in DNA nanotubes with longitudinal variation*. Nature Chem. **2** (2010) 319.

[100] LONG, Y.-T., LI, C.-Z., KRAATZ, H.-B., AND LEE, J. S., *AC Impedance Spectroscopy of Native DNA and M-DNA*. Biophys. J. **84** (2003) 3218.

[101] LUND, K., MANZO, A. J., DABBY, N., MICHELOTTI, N., JOHNSON-BUCK, A., NANGREAVE, J., TAYLOR, S., PEI, R., STOJANOVIC, M. N., WALTER, N. G., WINFREE, E., AND YAN, H., *Molecular robots guided by prescriptive landscapes*. Nature **465** (2010) 206.

[102] LUNDSTROM, M., *Moore's Law Forever?* Science **299** (2003) 210.

[103] MACDONALD, J. R., *Impedance Spectroscopy*. Ann. Biomed. Eng. **20** (1992) 289.

[104] MACDONALD, J. R., SHOONMAN, J., AND LEHNEN, A. P., *Three dimensional perspective plotting and fitting of immittance data*. Solid State Ion. **5** (1981) 137.

[105] MAO, C., SUN, W., SHEN, Z., AND SEEMAN, N. C., *A nanomechanical device based on the B-Z transition of DNA*. Nature **397** (1999) 144.

[106] MAREK, M., KAISER, K., AND GRUBER, H. J., *Biotin-Pyrene Conjugates with Poly(ethylene glycol) Spacers Are Convenient Fluorescent Probes for Avidin and Streptavidin*. Bioconjugate Chem. **8** (1997) 560.

[107] MARKX, G. H. AND PETHIG, R., *Dielectrophoretic Separation of Cells: Continuous Separation*. Biotechnol. Bioeng. **45** (1995) 337.

[108] MARSH, T. C. AND HENDERSON, E., *G-Wires: Self-assembly of a Telomeric Oligonucleotide, d(GGGGTTGGGG), into Large Superstructures*. Biochemistry **33** (1994) 10718.

[109] MARSH, T. C., VESENKA, J., AND HENDERSON, E., *A new DNA nanostructure, the G-wire, imaged by scanning probe microscopy*. Nucleid Acids Res. **23** (1995) 696.

[110] MASUDA, S., WASHIZU, M., AND KAWABATA, I., *Movement of blood cells in liquid by nonuniform traveling field*. IEEE Trans. Indust. Appl. **24** (1988) 217.

[111] MAUNE, H. T., HAN, S., BARISH, R. D., BOCKRATH, M., GODDARD III, W. A., ROTHEMUND, P. W. K., AND WINFREE, E., *Self-assembly of carbon nanotubes into two-dimensional geometries using DNA origami templates*. Nature Nanotech. **5** (2010) 61.

[112] MEDHI, C. AND PARAJULI, R., *Which base triplet stabilizes triple helix? Ab initio SCF and density functional methods of calculations on some base triplets*. J. Molec. Str. **717** (2005) 59.

[113] MIYOSHI, D., KARIMATA, H., WANG, Z. M., KOUMOTO, K., AND SUGIMOTO, N., *Artificial G-Wire Switch with 2,2'-Bipyridine Units Responsive to Divalent Metal Ions*. J. Am. Chem. Soc. **129** (2007) 5919.

[114] MORGAN, H., HUGHES, M. P., AND GREEN, N. G., *Separation of Submicron Bioparticles by Dielectrophoresis*. Biophys. J. **77** (1999) 516.

[115] MULLIS, K. B., FERRÉ, F., AND GIBBS, R. A., *The Polymerase Chain Reaction*. Birkhäuser, Boston, USA (1994).

[116] NELSON, D. L. AND COX, M. M., *Lehninger Principles of Biochemistry, Third Edition*. Worth Publishers, New York, USA (2000).

[117] NIEMEYER, C. M., ADLER, M., LENHERT, S., GAO, S., FUCHS, H., AND CHI, L., *Nucleic Acid Supercoiling as a Means for Ionic Switching of DNA-Nanoparticle Networks*. ChemBioChem **2** (2001) 260.

[118] O'NEILL, P., ROTHEMUND, P. W. K., KUMAR, A., AND FYGENSON, D. K., *Sturdier DNA Nanotubes via Ligation*. Nano Lett. **6** (2006) 1379.

[119] OTSUKA, Y., LEE, H.-Y., GU, J.-H., LEE, J.-O., YOO, K.-H., TANAKA, H., TABATA, H., AND KAWAI, T., *Influence of Humidity on the Electrical Conductivity of Synthesized DNA Film on Nanogap Electrode*. Jpn. J. Appl. Phys. **41** (2002) 891.

[120] PARK, J.-Y., KWON, S. H., PARK, J. W., AND PARK, S.-M., *Label-free detection of DNA molecules on the dendron based self-assembled monolayer by electrochemical impedance spectroscopy*. Anal. Chim. Acta **619** (2008) 37.

[121] PARK, S. H., BARISH, R., LI, H., REIF, J. H., FINKELSTEIN, G., YAN, H., AND LABEAN, T. H., *Three Helix Bundle DNA Tiles Self-assemble into 2D Lattice or 1D Templates for Silver Nanowires*. Nano Lett. **5** (2005) 693.

[122] PAUKSTELIS, P. J., NOWAKOWSKI, J., BIRKTOFT, J. J., AND SEEMAN, N. C., *Crystal Structure of a Continous Three-Dimensional DNA Lattice*. Chem. Biol. **11** (2004) 1119.

[123] POHL, H. A., *The Motion and Precipitation of Suspensoids in Divergent Electric Fields*. J. Appl. Phys. **22** (1951) 869.

[124] POHL, H. A., *Dielectrophoresis: The Behavior of Neutral Matter in Nonuniform Electric Fields*. Cambridge Univesity Press, Cambridge, UK (1978).

[125] PORATH, D., BEZRYADIN, A., DE VRIES, S., AND DEKKER, C., *Direct measurement of electrical transport through DNA molecules*. Nature **403** (1999) 635.

[126] PORATH, D., CUNIBERTI, G., AND DI FELICE, R., *Charge Transport in DNA-based Devices*. Top. Curr. Chem. **237** (2004) 183.

[127] POUND, E., ASHTON, J. R., BECERRIL, H. A., AND WOOLLEY, A. T., *Polymerase Chain Reaction Based Scaffold Preparation for the Production of Thin, Branched DNA Origami Nanostructures of Arbitrary Sizes*. Nano Lett. **9** (2009) 4302.

[128] RAKITIN, A., AICH, P., PAPADOPOULOS, C., KOBZAR, Y., VEDENEEV, A. S., LEE, J. S., AND XU, J. M., *Metallic Conduction through Engineered DNA: DNA Nanoelectronic Building Blocks*. Phys. Rev. Lett. **86** (2001) 3670.

[129] RANDLES, J. E. B., *Kinetics of Rapid Electrode Reactions*. Disc. Faraday. Soc. **1** (1947) 11.

[130] RASMUSSEN, S. R., RASMUSSEN, H. B., LARSEN, M. R., HOFF-JØRGENSEN, R., AND CANO, R. J., *Combined polymerase chain reaction-hybridization microplate assay used to detect bovine leukemia virus and Salmonella*. Clin Chem. **40** (1994) 200.

[131] RETÈL, J., HOEBEE, B., BRAUN, J. E., LUTGERINK, J. T., VAN DEN AKKER, E., WANAMARTA, A. H., JOENJE, H., AND LAFLEUR, M. V., *Mutational specificity of oxidative DNA damage*. Mutat. Res. **299** (1993) 165.

[132] RIGHINI, M., ZELENINA, A. S., GIRARD, C., AND QUIDANT, R., *Parallel and selective trapping in a patterned plasmonic landscape*. Nature Phys. **3** (2007) 477.

[133] RONDELEZ, Y., TRESSET, G., NAKASHIMA, T., KATO-YAMADA, Y., FUJITA, H., TAKEUCHI, S., AND NOJI, H., *Highly coupled ATP synthesis by F1-ATPase single molecules*. Nature **433** (2005) 7731.

[134] ROTHEMUND, P. W. K., *Folding DNA to create nanoscale shapes and patterns*. Nature **440** (2006) 297.

[135] ROTHEMUND, P. W. K., EKANI-NKODO, A., PAPADAKIS, N., KUMAR, A., FYGENSON, D. K., AND WINFREE, E., *Design and Characterization of Programmable DNA Nanotubes*. J. Am. Chem. Soc. **126** (2004) 16344.

[136] SCHWAN, H. P., SCHWARZ, G., MACZUK, J., AND PAULY, H., *On the low frequency dielectric dispersion of colloidal particles in electrolyte solution*. J. Phys. Chem. **66** (1962) 2626.

[137] SEEMAN, N. C., *Nucleid acid junctions and lattices*. J. Theor. Biol. **99** (1982) 237.

[138] SEEMAN, N. C., *DNA in a material world*. Nature **421** (2003) 427.

[139] SEEMAN, N. C., *An Overview of Structural DNA Nanotechnology*. Mol. Biotechnol. **37** (2007) 246.

[140] SEEMAN, N. C., *Structural DNA Nanotechnology: Growing Along with Nano Letters*. Nano Lett. **10** (2010) 1971.

[141] SHARMA, J., CHHABRA, R., ANDERSEN, C. S., GOTHELF, K. V., YAN, H., AND LIU, Y., *Toward Reliable Gold Nanoparticle Patterning On Self-Assembled DNA Nanoscaffold*. J. Am. Chem. Soc. **130** (2008) 7820.

[142] SHARMA, J., KE, Y., LIN, C., CHHABRA, R., WANG, Q., NANGREAVE, J., LIU, Y., AND YAN, H., *DNA-tile-directed self-assembly of quantum dots into two-dimensional nanopatterns*. Angew. Chem. Int. Ed. **47** (2008) 5157.

[143] SHEN, J., ZHONG, H., NEFF, D., AND NORTON, M. L., *NTA Directed Protein Nanopatterning on DNA Origami Nanoconstructs*. J. Am. Chem. Soc. **131** (2009) 6660.

[144] SHERMAN, W. B. AND SEEMAN, N. C., *A Precisely Controlled DNA Biped Walking Device*. Nano Lett. **4** (2004) 1203.

[145] SHIH, W. M., QUISPE, J. D., AND JOYCE, G. F., *A 1.7-kilobase single-stranded DNA that folds into a nanoscale octahedron*. Nature **427** (2004) 618.

[146] SHIM, J. S., YUN, Y.-H., RUST, M. J., DO, J., SHANOV, V., SCHULZ, M. J., AND AHN, C. H., *High precision fluidic alignment of carbon nanotubes using magnetic attraction on a metal catalyst*. MEMS 2008, Tucson, Az, USA, January 13-17 (2008) 729.

[147] SHIN, J.-S. AND PIERCE, N. A., *A Synthetic DNA Walker for Molecular Transport*. J. Am. Chem. Soc. **126** (2004) 10834.

[148] SIMMEL, F. C., *Three-dimensional nanoconstruction with DNA*. Angew. Chem. Int. Ed. **47** (2008) 5884.

[149] SUZUKI, M., YASUKAWA, T., SHIKU, H., AND MATSUE, T., *Negative Dielectrophoretic Patterning with Colloidal Particles and Encapsulation into a Hydrogel*. Langmuir **23** (2007) 4088.

[150] SUZUKI, S., YAMANASHI, T., TAZAWA, S., KUROSAWA, O., AND WASHIZU, M., *Quantitative Analysis of DNA Orientation in Stationary AC Electric Fields Using Fluorescence Anisotropy*. IEEE Trans. Ind. Appl. **34** (1998) 75.

[151] TREADWAY, C. R., HILL, M. G., AND BARTON, J. K., *Charge transport through a molecular π-stack: double helical DNA*. Chem. Phys. **281** (2002) 409.

[152] TUUKKANEN, S., *Dielectrophoresis as a tool for on-chip positioning of DNA and electrical characterization of nanoscale DNA*. Research report no. 13/2006, Department of Physics, University of Jyväskylä (2006).

[153] TUUKKANEN, S., KUZYK, A., TOPPARI, J. J., HÄKKINEN, H., HYTÖNEN, V. P., NISKANEN, E., RINKIÖ, M., AND TÖRMÄ, P., *Trapping of 27 bp - 8 kbp DNA and immobilization of thiol-modified DNA using dielectrophoresis*. Nanotechnology **18** (2007) 259204.

[154] TUUKKANEN, S., KUZYK, A., TOPPARI, J. J., HYTÖNEN, V. P., IHALAINEN, T., AND TÖRMÄ, P., *Dielectrophoresis of nanoscale double-stranded DNA and humidity effects on its electrical conductivity*. Appl. Phys. Lett. **87** (2005) 183102.

[155] TUUKKANEN, S., TOPPARI, J. J., KUZYK, A., HIRVINIEMI, L., HYTÖNEN, V. P., IHALAINEN, T., AND TÖRMÄ, P., *Carbon Nanotubes as Electrodes for Dielectrophoresis of DNA*. Nano Lett. **6** (2006) 1339.

[156] VENERMO, J. AND SIHVOLA, A., *Dielectric polarizability of circular cylinder*. J. Electrostat. **63** (2005) 101.

[157] VIJAYARAGHAVAN, A., BLATT, S., WEISSENBERGER, D., ORON-CARL, M., HENNRICH, F., GERTHSEN, D., HAHN, H., AND KRUPKE, R., *Ultra-Large-Scale Directed Assembly of Single-Walled Carbon Nanotube Devices*. Nano Lett. **7** (2007) 1556.

[158] VOIGT, N. V., TØRRING, T., ROTARU, A., JACOBSEN, M. F., RAVNSBÆK, J. B., SUBRAMANI, R., MAMDOUH, W., KJEMS, J., MOKHIR, A., BESENBACHER, F., AND GOTHELF, K. V., *Single-molecule chemical reactions on DNA origami*. Nature Nanotech. **5** (2010) 200.

[159] VON NICKISCH-ROSENEGK, M., MARSCHAN, X., ANDRESEN, D., ABRAHAM, A., HEISE, C., AND BIER, F. F., *On-chip PCR amplification of very long templates using immobilized primers on glassy surfaces*. Biosens Bioelectron. **20** (2005) 1491.

[160] WANG, J., *Electrical conductivity of double stranded DNA measured with ac impedance spectroscopy*. Phys. Rev. B. **78** (2008) 245304.

[161] WANG, X. B., HUANG, Y., BECKER, F. F., AND GASCOYNE, P. R. C., *A unified theory of dielectrophoresis and travelling wave dielectrophoresis*. J. Phys. D: Appl. Phys. **27** (1994) 1571.

[162] WARMAN, J. M., DEHAAS, M. P., AND RUPPRECHT, A., *DNA: a molecular wire?* Chem. Phys. Lett. **249** (1996) 319.

[163] WARNER, M. G. AND HUTCHISON, J. E., *Linear assemblies of nanoparticles electrostatically organized on DNA scaffolds*. Nature Mat. **2** (2003) 272.

[164] WASHIZU, M., *Equivalent multipole-moment theory for dielectrophoresis and electrorotation in electromagnetic field*. J. Electrostat. **62** (2004) 15.

[165] WATSON, J. D. AND CRICK, F. H., *Molecular structure of nucleid acid*. Nature **171** (1953) 737.

[166] WINFREE, E., LIU, F., WENZLER, L. A., AND SEEMAN, N. C., *Design and self-assembly of two-dimensional DNA crystals*. Nature **394** (1998) 539.

[167] XU, B. AND TAO, N. J., *Measurement of Single Molecule Conductance by Repeated Formation of Molecular Junctions*. Science **301** (2003) 1221. And references therein.

[168] XU, B., ZHANG, P., LI, X., AND TAO, N., *Direct Conductance Measurement of Single DNA Molecules in Aqueous Solution*. Nano Lett. **4** (2004) 1105.

[169] YAMAHATA, C., COLLARD, D., TAKEKAWA, T., KUMEMURA, M., HASHIGUCHI, G., AND FUJITA, H., *Humidity Dependence of Charge Transport through DNA Revealed by Silicon-Based Nanotweezers Manipulation*. Biophys. J. **94** (2008) 63.

[170] YAN, H., LABEAN, T. H., PENG, L., AND REIF, J. H., *Directed nucleation assembly of DNA tile complexes for barcode-patterned lattices*. Proc. Nat. Acad. Sci. U.S.A. **100** (2003) 8103.

[171] YAN, H., PARK, S. H., FINKELSTEIN, G., REIF, J. H., AND LABEAN, T. H., *DNA-Templated Self-Assembly of Protein Arrays and Highly Conductive Nanowires*. Science **301** (2003) 1882.

[172] YAN, H., ZHANG, X., SHEN, Z., AND SEEMAN, N. C., *A robust DNA mechanical device controlled by hybridization topology*. Nature **415** (2001) 62.

[173] YANG, H., MCLAUGHLIN, C. K., ALDAYE, F. A., HAMBLIN, G. D., RYS, A. Z., ROUILLER, I., AND SLEIMAN, H. F., *Metal-nucleic acid cages*. Nature Chem. **1** (2009) 390.

[174] YIN, P., TURBERFIELD, A. J., SAHU, S., AND REIF, J. H., *Designs for autonomous unidirectional walking DNA devices*. Lect. Notes Comput. Sc. **3384** (2005) 410.

[175] YURKE, B., TURBERFIELD, A. J., MILLS JR., A. P., SIMMEL, F. C., AND NEUMANN, J. L., *A DNA-fuelled molecular machine made of DNA*. Nature **406** (2000) 605.

[176] ZHANG, C., KHOSHMANESH, K., MITCHELL, A., AND KALANTAR-ZADEH, K., *Dielectrophoresis for manipulation of micro/nanoparticles in microfluidic systems*. Anal. Bioanal. Chem. **396** (2010) 401.

[177] ZHANG, S., *Buildind from the bottom up*. Materials Today **6** (2003) 20.

[178] ZHENG, J., CONSTANTINOU, P. E., MICHEEL, C., ALIVISATOS, A. P., KIEHL, R. A., AND SEEMAN, N. C., *Two-Dimensional Nanoparticle Arrays Show the Organizational Power of Robust DNA Motifs*. Nano Lett. **6** (2006) 1502.

[179] ZHENG, L., BRODY, J. P., AND BURKE, P. J., *Electronic manipulation of DNA, proteins, and nanoparticles for potential circuit assembly*. Biosensors and Bioelectronics **20** (2004) 606.

[180] ZUKER, M., *Mfold web server for nucleic acid folding and hybridization prediction*. Nucleic Acids Res. **31** (2003) 3406.

Part III

Appendixes

Materials and methods

Thiol-modified strands of DNA origami

Thiol-modified oligonucleotides were purchased unpurified at 100 nM scale from Integrated DNA Technologies (IDT). The sequences of the strands are the following:

For one end:

- 5′-AGCATAAAGCTAAATC$(CT)_{16}$-3ThioMC3-D-3′
- 5′-5ThioMC6-D-$(CT)_{16}$CTGTAGCTCAACATGT-3′

For another end:

- 5′-5ThioMC6-D-$(CT)_{16}$CGACAAAAGGTAAAGT-3′
- 5′-AAATCAGATATAGAAG$(CT)_{16}$-3ThioMC3-D-3′

16 bases of each strand are complementary with M13mp18 DNA sequence on the ends, and 32 bases long repetitive CT sequence is used as a spacer between the origami and the thiols.

Fabrication and design of TX tile construct

All the strands used in the design of the TX tile construct are presented in Table 1 and the sequence map of the tiles is illustrated in Fig. 1.

Strand 7 with 5′-thiol-modification [5′ Thiol Modifier C6 S-S (Disulfide)] was purchased as HPLC-purified from Integrated DNA Technologies, IDT (Coralville, Iowa, USA). All other oligonucleotides were purchased from Biomers GmbH (Ulm, Germany) purified either by PAGE or by HPLC. Strands were diluted to a concentration of 10 μM in 40 mM Tris (pH 8) buffer containing 1 mM EDTA and 19 mM acetic acid. Magnesium acetate was included in the final reaction mixture with concentration of 12.5 mM. Therefore, a buffer containing 40 mM Tris (pH 8), 1 mM EDTA, 19 mM acetic acid and 500 mM magnesium acetate was prepared and added to a master mix.

TABLE 1 Sequences of the strands used in tile A and tile B.

Strand	Sequence
1	5′-ATCGAGAGAC ATAACTGCTT GACCACGCTG TATCGGAACC TGACTCCTAA TCAGCA-3′
2	5′-AGGAGTCACT CTCGATGCCA GACG-3′
3	5′-GGTATAGTAT GCAACGTGAA TGAACAAGGT GAGGTGTCAA TGGAGATGAA TGTTC-3′
4	5′-ATCTCCATTG ACAGGTCAAG CAGTTATGTG GTTCTGCATA CTATACCGAA TGTTC-3′
5	5′-ATAGCACCAC TGCAAGGCCA GACG-3′
6	5′-CTTGCAGTCC TTGTTCATTC ACGTCGATAC AGCGTCCTCA GGTGCTATAA TCAGCA-3′
7	5′-5ThioMC6-D-TGGAGCGACA TG-3′
8	5′-AGATAACATA AGGACACTTA GGAATCCAGT ACTGACACAC AGTTGGAACA TTC-3′
9	5′-CAACTGTGTG AATGGGACTT TGCTGATT-3′
10	5′-AGCTGAACCT ACAGTCATAC GACTCGAACA CGTAGTATCA TCTAGCGTCT GGC-3′
11	5′-CTAGATGATA CTACGGCTAC TCAGTACTGG ATTCCTAAGT GAATTGGAC-3′
12	5′-GATCATGATG TTCGAGTCGT ATGACTGTAC TATCTCCTTA TGTTATCTCA TGTCGCTCCA-3′
13	5′-AAGTCCCATT GTAGCTCATG ATCGTCCAAT TGATAGCCCT GTTGACATGT CGCTCCA-3′
14	5′-TCAACAGGGG GTTCAGCTCA TGTCGCTCCA-3′

T4 Polynucleotide Kinase (New England Biolabs, Ipswich, MA, USA) was used to add phosphate groups to the 5′ end of each strand except the 5′-thiol-modified strand 7. Each strand was modified separately by adding 1.5 µl of master mix to tubes containing 10 µl of strands of tile A (10 µM) or by adding 3.0 µl of master mix to tubes containing 20 µl of strands of tile B (10 µM). This was followed by incubation for one hour at 37 °C. The strand 7 was diluted to the same concentration (8.7 µM) as the other strands had after incubation with T4 kinase. Then the kinase modified strands and strand 7 were mixed. To achieve appropriate concentration of each tile a two-fold amount (20 µl) of strands 8-14 of tile B were used compared to strands 1-6 of tile A (10 µl). In addition, three-fold amount (60 µl) of 5′-thiol-modified strands 7 compared to strands of tile B were used in order to hybridize them with each sticky end d of tile B. Complexes were formed by heating the mixture up to 90 °C and cooling it down to 20 °C at a rate 0.01 °C/s in a PCR-machine (Biometra GmbH, Goettingen, Germany). After annealing complexes were ligated using T4 DNA ligase (New England Biolabs) to make the complexes more stable for DEP. 800 units of T4 DNA ligase with T4 ligase buffer were added to the annealed complex described in Chapter 4. The reaction mixture was incubated for two hours in dark at room temperature and stored at 4 °C afterwards. The theoretical concentration of obtained complexes was 0.29 µM of strands 1-6 (tile A) and 0.58 µM of strands 8-14 (tile B).

Spin-filtering of DNA origamis and TX tile constructs

For filtering and buffer exchange Millipore Microcon YM-100 spin filters (molecular weight cutoff of 100 kDa) were used. The procedure was performed in the following way:

100 µl of annealed construct solution was mixed with 300 µl of Hepes/NaOH based

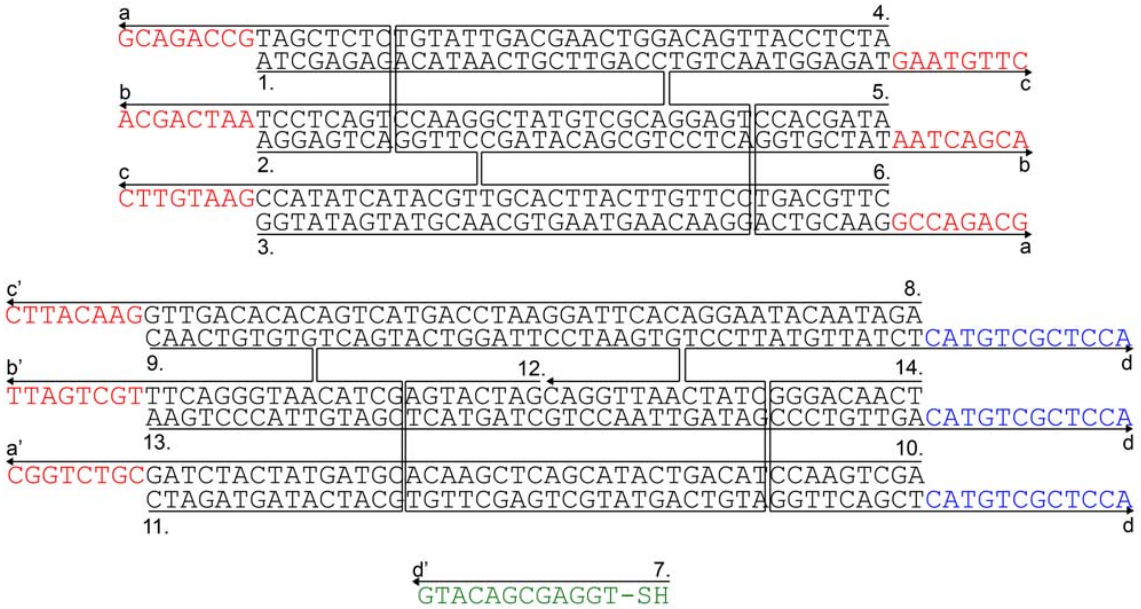

FIGURE 1 DNA strand structure and sequences of tile A and tile B. Sticky ends a, b and c are complementary to sticky ends a', b' and c'. Strand 7 is complementary to sticky ends d of tile B. To be accurate, the SH-group indicated in a figure contains also a protection group [5′ Thiol Modifier C6 S-S (Disulfide)] to avoid undesired S-S bonding between tiles.

buffer (6.5 mM Hepes, 1 mM MgAc and $\sim$ 2 mM NaOH). The sample was spun for 12 min at 1000 relative centrifugal force (rcf) at 4 °C. After centrifugation, the eluate was removed and 400 µl of the buffer was added to the sample. Then the sample was spun once more for 7 min with 1000 rcf at 4 °C. After this procedure $\sim$ 100 µl of the sample was retained in the spin filter. Finally, the spin filter was removed, placed upside down in a fresh tube and spun in a microcentrifuge for 2-3 min to collect the solution. It can be assumed that nearly all structures are recovered from the filter membrane, and thus filtering does not significantly change the concentration of constructs in the solution.

Design of biotinylated TX tiles

All the strands used in the design of the biotin-functionalized TX tiles are presented in Table 2 and the sequence map of the tile is illustrated in Fig. 2.

TABLE 2 Sequences of strands used in the biotinylated TX tiles. The location of nucleotide analog Biotin-TEG is indicated by an asterisk (∗).

Strand	Sequence
1	5′-GCAGACCGTA GAATCGCCTG CTCTGTATCA TAGATGTTTT CATCTATGTT TGCCGAACTG GACACTTACC TCTA-3′
2	5′-ACGACTAATC CGTCTTGTGG CGATTCTACG G-3′
3	5′-AAGCCATCTC CGAATGCCTG CGTTGCGGTA TCAGCGTT∗TT CGCTGATTTT ACTTGTTCCT GCCGTTCATT GT-3′
4	5′-ATGTCGCACC AGTTCGGCAA TACAGAGCAC CAGTGGCATT CGGAGAT-3′
5	5′-TCTGCTAGAG GTAAGTGTGG AGTGGAACAA GTAACCGCAA CGCACCAAGG CT-3′
6	5′-GTCGTTATCG TGGACTCCTG CGACATAGCC TTGGACTGGA CAAGACGGAT TA-3′
7	5′-GGCTTACAAT GAACGGCACC ACGATA-3′

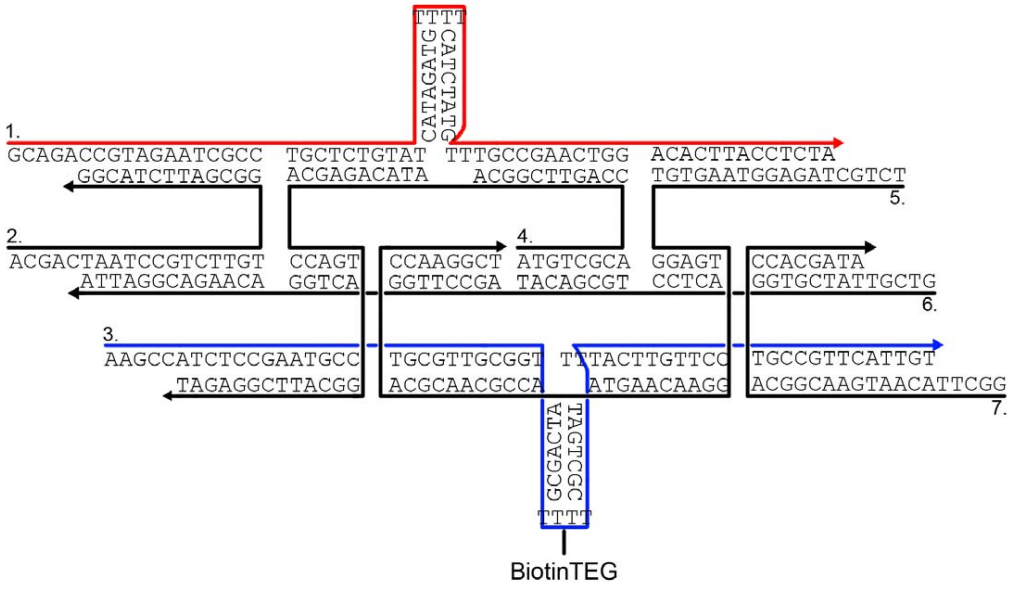

FIGURE 2 DNA strand structure of a TX tile functionalized with one biotin-TEG.

Charging induced hysteresis in DC measurements

The hysteretic behavior observed in the measurements of the *I-V* characteristics at high humidity conditions (see article **A.III**) is explained by currents due to charging of the total capacitance of the sample formed by the capacitance of the electrodes, parasitic stray capacitances and the capacitance of ions gathering on the electrodes. The polarization effect happens by the ions (ionized water molecules and counter-ions, i.e. Na+, Mg++) gathered on the electrode, and this process has a certain (quite slow) timescale. This effectively causes a parallel capacitance to the sample resistance, and is probably the main origin of the hysteresis seen in most of the DNA samples (capacitances measured for completely clean samples, i.e. no salt ions, lead to time constants that would not be visible as hysteresis in the results). The amount of hysteresis varies from sample to sample and this is likely to be due to the slightly

different salt concentrations and washing procedures applied from sample to sample. In addition, since the measurements are performed with very low DC voltages (0.3 V maximum), the reduction-oxidation processes of the ions at the electrodes are suppressed.

In the measurements, the DC bias voltage was changed in equal steps and after each step the sample was let to stabilize for $\tau_m \sim 0.5$ s before recording the current. In this case, one obtains for the measured current

$$I = \frac{V_n}{R} + I_0 \alpha \frac{1-\alpha^n}{1-\alpha}, \tag{1}$$

where n means the nth I-V point measured and V_n is the corresponding bias voltage. Other parameters are: R the resistance of the sample, I_0 the maximum charging current at bias voltage transients (depends on the resistances of the measurement instruments) and $\alpha = \exp(-\tau_m/\tau)$ the exponential of the ratio between the stabilization time, τ_m, and the time constant of charging, τ. Figure 3 of the article **A.III** shows this formula fitted to the measured data (the data without the fitting is also shown in Fig. 6.5). The obtained time constant, τ, was of the order of 70 s and the resistance of the TX tile construct sample was 20 GΩ.

Sequences of dye-labeled oligonucleotides

The sequences of the thiol-modified (5′ end) and either Cy3 or Cy5-labeled (3′ end) oligonucleotides used in the optimization procedure of the DEP-trapping were the following (strands purchased from Biomers as HPLC-purified):

40 nt long oligos:

- 5′-$(CT)_{16}$GATGGCTT-3′ with Cy3
- 5′-$(CT)_{16}$GAAAAAGC-3′ with Cy5

22 nt long ssDNA molecules:

- 5′-GCCAGAAAGTGCTCGCTGACTG-3′ with Cy3

Sequences of primers and 414 bp template for immobilized PCR

In the actual PCR-growing experiments the sequences of the 38 nt forward and reverse primers (without dye-molecules) were comprised of 22 nt long sequences complementary to the template DNA and the additional 16 nt spacer:

- 5′–$(CT)_8$GCCAGAAAGTGCTCGCTGACTG–3′
- 5′–$(CT)_8$TTCTCGACAAGCTTTGCGGGGC–3′

In these primers 5′ Thiol Modifier C6 S-S (Disulfide) was attached to 5′ end (ordered from Integrated DNA Technologies as dual HPLC-purified).

The sequence of the template (partial complementary DNA of chicken avidin) used in the PCR experiment (5′ → 3′):

```
1   GCCAGAAAGT GCTCGCTGAC TGGGAAATGG ACCAACGATC TGGGCTCCAA CATGACCATC
61  GGGGCTGTGA ACAGCAGAGG TGAATTCACA GGCACCTACA TCACAGCCGT AACAGCCACA
121 TCAAATGAGA TCAAAGAGTC ACCACTGCAT GGGACACAAA ACACCATCAA CAAGAGGACC
181 CAGCCCACCT TTGGCTTCAC CGTCAATTGG AAGTTTTCAG AGTCCACCAC TGTCTTCACG
241 GGCCAGTGCT TCATAGACAG GAATGGGAAG GAGGTCCTGA AGACCATGTG GCTGCTGCGG
301 TCAAGTGTTA ATGACATTGG TGATGACTGG AAAGCTACCA GGGTCGGCAT CAACATCTTC
361 ACTCGCCTGC GCACACAGAA GGAGTGAGGA TGGCCCCGCA AAGCTTGTCG AGAA
```